University of Cyprus

Department of Electrical and Computer Engineering

Electronic Particle Manipulation: Numerical Simulation and Device Design

Neophytos Loucaides

Dissertation submitted as part of the requirements for the degree of Doctor of Philosophy at the University of Cyprus

August 2009

ΣΕΛΙΔΑ ΕΓΚΥΡΟΤΗΤΑΣ

Υποψήφιος Διδάκτορας: Νεόφυτος Λουκαΐδης

Τίτλος Διατριβής: **Electronic Particle Manipulation: Numerical Simulation and Device Design**

Η παρούσα Διδακτορική Διατριβή εκπονήθηκε στο πλαίσιο των σπουδών για απόκτηση Διδακτορικού Διπλώματος στο Τμήμα Ηλεκτρολόγων Μηχανικών και Μηχανικών Υπολογιστών και εγκρίθηκε στις 21/08/2009 από τα μέλη της Εξεταστικής Επιτροπής.

Εξεταστική Επιτροπή:

Ερευνητικός Σύμβουλος:

Δρ. Γεώργιος Η. Γεωργίου
Επίκουρος Καθηγητής,
Πανεπιστήμιο Κύπρου, Τμήμα Ηλεκτρολόγων Μηχανικών και Μηχανικών Υπολογιστών

Άλλα Μέλη:

1. Δρ. Χαράλαμπος Χαραλάμπους, Αναπληρωτής Καθηγητής, Πανεπιστήμιο Κύπρου, Τμήμα Ηλεκτρολόγων Μηχανικών και Μηχανικών Υπολογιστών
2. Δρ. Κώστας Πίτρης, Επίκουρος Καθηγητής, Πανεπιστήμιο Κύπρου, Τμήμα Ηλεκτρολόγων Μηχανικών και Μηχανικών Υπολογιστών
3. Δρ. Ανδρούλα Νασιοπούλου, Διευθύντρια Ινστιτούτου Μικροηλεκτρονικής Ερευνητικού Κέντρου 'Δημόκριτος'
4. Δρ. Στάυρος Κάσσινος, Αναπληρωτής Καθηγητής, Πανεπιστήμιο Κύπρου, Τμήμα Μηχανολόγων Μηχανικών και Μηχανικών Παραγωγής

To my wife and daughter.

Acknowledgements

I would like to express my deep and sincere gratitude to my supervisor, Dr. George Georghiou, Assistant Professor at the Department of Electrical and Computer Engineering, University of Cyprus, for all his help and guidance during the course of this work.

I would like to thank Prof. Antonio Ramos, Associate Professor of Electromagnetism at the Department of Electronics and Electromagnetism, Faculty of Physics, University of Seville, for all the invaluable help and advice.

I am grateful to Prof. Charalambos Charalambous, Associate Professor at the Department of Electrical and Computer Engineering, University of Cyprus, for the useful discussions and guidance.

I also wish to thank my family, for their support and patience during all this time.

This research was supported by the Cyprus Research Promotion Foundation, Grant Number: PENEK 0505/24.

Abstract

This thesis deals with the simulation of devices utilising AC Electrokinetics (ACEK) for the manipulation of micro- and nano-particles. Such simulations are necessary in order to better understand and design AC Electrokinetics devices, that behave in a more predictable manner. A fundamental step towards the better understanding of ACEK methods is the development of a physical model that can describe the dynamics of such devices. Using such a physical model, numerical simulations of the devices' operation are performed. The simulations can be used as an aid in the analysis of devices and as a fast and cheap method for the design of novel systems, due to the low cost associated with the design process.

First of all, a physical model for the dynamics of a micro- or nano-particle subject to the Dielectrophoretic (DEP) force suspended in a fluid is introduced. Physical models are also introduced for other forces on the particle, such as drag, buoyancy and gravity, and the method of finite elements is used in order to solve the resulting system of equations.

In the next step, the Electrohydrodynamic (EHD) phenomena associated with DEP are investigated. The first of these is the AC Electroosmotic (ACEO) motion of the fluid, which is caused by the interaction of the fluid ions in the electrical double layer over the electrode surface with the AC electric field. A linear physical model for the double layer potential is used in order to simulate the ACEO fluid motion. These simulations enable the analysis of existing ACEO pumping systems and the design of novel systems. Using numerical simulation, a novel system for configurable ACEO pumping is proposed and analysed.

The second EHD phenomenon investigated is the AC Electrothermal (ACET) fluid motion. ACET is caused by the non-uniform heating of the fluid, due to the non-uniform electric field used for DEP. The physical model describing ACET fluid motion is also used in order to provide numerical simulations for the device operation. Using both the ACET and ACEO models, a device is analysed that utilises both phenomena for biosensor enhancement.

The following part investigates the dynamics of a DEP manipulation system using a velocity field analysis, in order to study the trapping of particles in

different occasions when both DEP and ACEO are significant. This study is extended by introducing the Smoluchowski equation in order to study the particle concentration evolution. It is found that the effect of ACEO is detrimental in the particle concentration dynamics and therefore its inclusion in any future study is considered essential.

The model used for the evolution of the particle concentration is further expanded in the subsequent part by introducing modifications in order to account for the finite particle dimensions. These modifications are necessary in order to enable the model to simulate the particle collection dynamics for larger particles, for which otherwise the concentration would reach unrealistic levels, due to the low diffusivity associated with such particles. It is found that the introduction of these modifications alters the simulated device dynamics significantly. The simulated dynamics using the steric particle model are more realistic and therefore the modifications are considered an improvement of the existing model.

Particle steric modifications are then applied to the Navier-Stokes equations for the suspension, so that joint DEP and ACEO can be investigated using the particle steric model. The results from the simulation of a real device for DNA manipulation are then compared with available experimental data and exhibit a more realistic behaviour than the previous model. Also, the ability to extract data from the simulation with and without the inclusion of the ACEO fluid motion allows the interpretation of observations previously unexplained, such as the non-linearity of the initial rate of increase of the particle collection with the particle polarisability. What is even more important in the results produced is that it can be deduced that the non-linearity of the relationship is actually due to enhancement of the initial rate of increase of the particle collection.

The modified model also allows the investigation of many design parameters that are important for the device operation, such as the particle size and the electrode height. The behaviour of devices with a range of different characteristics can therefore be investigated using simulations that can be performed with a relatively much lower cost and at reduced computation time compared to purely experimental methods.

Περίληψη

Αυτή η Διατριβή ασχολείται με την προσομοίωση συσκευών οι οποίες χρησιμοποιούν τεχνικές Ηλεκτροκινητικής Εναλλασσόμενου Ρεύματος (ΗΕΡ) για τη διαχείριση μικρο- και νανο-σωματιδίων. Οι προσομοιώσεις αυτές είναι αναγκαίες για την καλύτερη κατανόηση και το σχεδιασμό συσκευών ΗΕΡ οι οποίες συμπεριφέρονται με πιο προβλεπτό τρόπο. Βασικό βήμα προς την κατεύθυνση αυτή είναι η ανάπτυξη ενός φυσικού μοντέλου το οποίο να περιγράφει τη δυναμική τέτοιων συσκευών. Χρησιμοποιώντας το φυσικό μοντέλο, παρουσιάζονται αριθμητικές προσομοιώσεις της λειτουργίας των συσκευών. Οι προσομοιώσεις μπορούν να χρησιμοποιηθούν για να βοηθήσουν στην ανάλυση των συσκευών και σαν μια γρήγορη και χαμηλού κόστους μέθοδος για τον σχεδιασμό καινοτόμων συσκευών.

Κατ'αρχήν, παρουσιάζεται ένα φυσικό μοντέλο για τη δυναμική ενός μικρο- ή νανο-σωματιδίου αναρτημένου σε υγρό και το οποίο βρίσκεται υπό την επίδραση της Διηλεκτροφορητικής (ΔΗΦ) δύναμης. Στο μοντέλο αυτό ενσωματώνονται και άλλες δυνάμεις όπως η οπισθέλκουσα, η άνωση και η βαρύτητα. Ακολούθως, χρησιμοποιείται η μέθοδος των πεπερασμένων στοιχείων για την επίλυση των σχετικών εξισώσεων.

Στο επόμενο στάδιο, διερευνώνται τα Ηλεκτροϋδροδυναμικά (ΗΥΔ) φαινόμενα που συνυπάρχουν με την ΔΗΦ. Το πρώτο από αυτά είναι η Ηλεκτροοσμοτική Κίνηση Εναλλασσόμενου Ρεύματος (ΗΚΕΡ) του υγρού, η οποία προκαλείται από την αλληλεπίδραση των ιόντων του υγρού στο διπλό ηλεκτρικό στρώμα με το Ηλεκτρικό Πεδίο. Ένα γραμμικό φυσικό μοντέλο για το δυναμικό στο διπλό στρώμα χρησιμοποιείται για να προσομοιωθεί η ΗΚΕΡ. Οι προσομοιώσεις καθιστούν δυνατή την ανάλυση υπάρχουσων συσκευών ΗΚΕΡ και το σχεδιασμό νέων συστημάτων. Με τη χρήση των αριθμητικών προσομοιώσεων, ένα καινοτόμο σύστημα για αναπροσαρμοζόμενη άντληση υγρού με τη χρήση ΗΚΕΡ προτείνεται και αναλύεται η λειτουργία του.

Η δεύτερη ΗΥΔ κίνηση που διερευνάται είναι η Ηλεκτροθερμική Κίνηση Εναλλασσόμενου Ρεύματος (ΗΘΕΡ) του υγρού. Η ΗΘΕΡ προκαλείται από το γεγονός ότι το ανομοιογενές ηλεκτρικό πεδίο προκαλεί ανομοιογενή θέρμανση του υγρού. Το φυσικό μοντέλο που περιγράφει την ΗΘΕΡ χρησιμοποιείται για να παραχθούν αριθμητικές προσομοιώσεις για την περιγραφή της λειτουργίας συσκευών. Χρησιμοποιώντας τα φυσικά μοντέλα για την ΗΘΕΡ και την ΗΚΕΡ, αναλύονται συσκευές οι οποίες χρησιμοποιούν τα φαινόμενα αυτά για την ενίσχυση βιοαισθητήρων.

Το επόμενο μέρος διερευνά την δυναμική συστημάτων ΔΗΦ χρησιμοποιώντας ανάλυση των πεδίων ταχυτήτων, με απώτερο σκοπό μελέτη των σημείων παγίδευσης σε συνδυασμούς ΗΚΕΡ και ΔΗΦ. Αυτή η μελέτη επεκτείνεται με την εισαγωγή της εξίσωσης Smoluchowski για την περιγραφή της δυναμικής της συγκέντρωσης σωματιδίων. Εδώ διαφαίνεται ότι η επίδραση της ΗΚΕΡ σε συσκευές ΔΗΦ είναι δραματική, και συνεπώς η συμπερίληψη της σε μελλοντικές προσομοιώσεις συσκευών ΔΗΦ είναι αναγκαία.

Το μοντέλο που χρησιμοποιείται για την περιγραφή της συγκέντρωσης των σωματιδίων επεκτείνεται περαιτέρω στο επόμενο μέρος, με τη συμπερίληψη σε αυτό τροποποιήσεων οι οποίες λαμβάνουν υπ'όψιν τις πεπερασμένες διαστάσεις των σωματιδίων. Αυτές οι τροποποιήσεις είναι αναγκαίες για να καταστεί δυνατή η προσομοίωση συστημάτων στα οποία το μέγεθος των σωματιδίων συνεπάγεται μή ρεαλιστικές συγκεντρώσεις με το προηγούμενο μοντέλο, λόγω χαμηλής διάχυσης των σωματιδίων και μεγάλων δυνάμεων που αναπτύσσονται. Εδώ διαφαίνεται ότι οι τροποποιήσεις διαφοροποιούν ριζικά τη δυναμική του συστήματος και συνεπώς η χρήση τους σε μελλοντικές προσομοιώσεις βοηθά στη βελτίωση της ακρίβειας των αποτελεσμάτων.

Ανάλογες τροποποιήσεις εφαρμόζονται στο επόμενο βήμα και στις εξισώσεις Navier-Stokes, έτσι ώστε να καταστεί δυνατή η ταυτόχρονη προσομοίωση ΗΚΕΡ και ΔΗΦ σε μια συσκευή. Τα αποτελέσματα από την προσομοίωση μιας πραγματικής συσκευής για διαχείριση DNA συγκρίνονται επίσης με πειραματικά αποτελέσματα και επιδεικνύουν πιο ρεαλιστική συμπεριφορά από το προηγούμενο μοντέλο. Επίσης, η δυνατότητα επανάληψης της προσομοίωσης χωρίς ΗΚΕΡ επιτρέπει την επεξήγηση παρατηρήσεων οι οποίες δεν μπορούσαν να εξηγηθούν προηγουμένως, όπως η μή γραμμική σχέση του

αρχικού ρυθμού αύξησης της συγκέντρωσης σωματιδίων σε σχέση με την διπολική ροπή τους. Επίσης, ακόμα πιο ενδιαφέρον είναι το γεγονός ότι από τις προσομοιώσεις μπορεί να εξαχθεί ότι η μή γραμμική σχέση οφείλεται σε ενίσχυση της διαδικασίας.

Το τροποποιημένο μοντέλο επιτρέπει επίσης τη διερεύνηση πολλών μεταβλητών σχεδιασμού, όπως το μέγεθος των σωματιδίων και το ύψος των ηλεκτροδίων. Έτσι, η συμπεριφορά των συσκευών σε σχέση με διάφορες παραμέτρους σχεδιασμού μπορεί να διερευνηθεί με πολύ χαμηλό κόστος και σε πολύ λίγο χρόνο σε σύγκριση με αυτόν που απαιτείται με πειραματικές μεθόδους.

Nomenclature

Greek Symbols

ϵ	Electrical permittivity
ϵ_r	Relative permittivity
ϵ_0	Permittivity of free space
ϵ_{mr}	Medium relative permittivity
ϵ_m	Medium electrical permittivity
ϵ_{pr}	Particle relative permittivity
ϵ_p	Particle electrical permittivity
η_c	Suspension viscosity
η_f	Fluid viscosity
γ	Phase shift
Λ	Ratio of the diffuse double layer potential drop over the total double layer potential drop
λ_{Debye}	Debye length
Ω	Non-dimensional frequency
ω	Angular frequency
ϕ	Electric potential
π	3.14159265358...
ρ_f	Fluid density
ρ_p	Particle density
ρ_s	Suspension density

σ Electrical conductivity

σ_m Medium conductivity

σ_p Particle conductivity

Roman Symbols

$\vec{f}_{DEP}$ Suspension volume dielectric body force

$\vec{E}$ Electric field

$\vec{F}_{DEP}$ Dielectrophoretic force

$\vec{n}$ Unit vector normal to the boundary

$\vec{u_f}$ Fluid velocity

$\vec{u}_p$ Particle velocity

$\vec{v}_s$ Suspension velocity

a_m Real part of the particle polarisability

bp Base pairs

C Particle concentration

c Particle volume fraction

c_m Particle maximum volume fraction

$C_{diffuse}$ Diffuse layer capacitance

C_{DL} Double layer capacitance

C_{Stern} Stern layer capacitance

D Diffusion constant

D_a Damkohler number

F Frequency

f Friction factor

F_e Electrothermal body force

g Gravitational acceleration

$K(\omega)$ Clausius-Mossotti factor

k_T Thermal conductivity

k_B Boltzmann constant

kbp Thousands of base pairs

p Fluid pressure

p_d Dipole moment

Pe Péclet ratio

T Absolute temperature

U_p Pumping velocity

u_{slip} Fluid slip velocity

V_p Particle volume

$V_{applied}$ Electrode excitation potential

x x-coordinate

y y-coordinate

Z_{DL} Double layer impedance

Acronyms

ACEK AC Electrokinetics

ACEO AC Electroosmosis

ACET AC Electrothermal

DEP Dielectrophoresis

EHD Electrohydrodynamics

IHP Inner Helmholtz Plane

OHP Outer Helmholtz Plane

Contents

List of Figures

List of Tables

Chapter 1

Introduction

In this chapter, the background and motivation for the work presented in the thesis is outlined. Furthermore, work previously conducted in the field of AC Electrokinetics and numerical modelling in particular is presented. Also, justification for the use of the particular numerical scheme employed is provided.

1.1 Motivation

For a very long time, mankind has been fascinated with objects of great scale. This has led to the construction of huge buildings, monuments and machines for the majority of known history. However, recently another fascination has began. The fascination with the small world, one which is invisible to the eye and extends to the molecular or even atomic level.

One of the first expressions of this fascination was the famous lecture by Richard Feynman at an American Physical Society meeting at Caltech on December 29, 1959, 'There's Plenty of Room at the Bottom'. This was one of the first expressions of a new quest for exploration of the limits which could be broken on the small scale, therefore allowing for a new scientific field to emerge, that of Nanotechnology. Since then, a lot of progress has been made and nowadays Nanotechnology is considered one of the most promising fields of science.

Nanotechnology is not a 'technology' by itself, but usually a set of enabling technologies that can serve in many other fields. Progress in a number of manufacturing techniques has enabled the advancement of knowledge on the subject. Therefore, the scale over which it is possible to control the manufacturing of devices, particularly those manufactured using photolithography methods, is constantly decreasing.

Devices are nowadays required to be smaller and consume less power. New materials such as Carbon Nanotubes (CNTs) are utilised in the construction of devices. Novel techniques are investigated that can assist in the production, purification and handling of CNT nanocomponents. These techniques are essential in order to enable the manufacturing of devices that can be accurately built from such components, with large scale production ability and in a cost-effective manner. Therefore, it is of great importance to be able to handle and manipulate components of very small scale in order to manufacture such devices.

Furthermore, recent progress in the fields of genomics and proteomics has accelerated the identification of genes that cause or influence numerous diseases. Inexpensive, miniaturised and automated devices for molecular screening are expected to revolutionise the diagnosis and prognosis of diseases and disease risks even at points of care, in the home and in environments lacking any infrastructure. With the increasing interest in molecular nanodevices and their fabrication, techniques are developed in order to handle, manipulate and attach molecules such as DNA to surfaces at specific locations.

Methods utilising non-uniform electric fields are emerging as most promising techniques for this kind of particle manipulation. They require no moving parts and hence can be inherently scalable for massively parallel micro- and nano-particle manipulation. Dielectrophoresis (DEP) in particular, is an electronic analogue to optical tweezers: an AC electric field induces a dipole moment on an object in solution, which then experiences a force that depends on the gradient of the electric field magnitude and frequency, as well as on the particle and medium properties. For both types of tweezers, this force must compete with thermal Brownian motion to be effective, which becomes increasingly difficult as the particle size approaches the nanometre scale. However, the scaling of dimensions also favours the DEP force strength, since DEP depends on the electric field gradient. Therefore, it is one of the few candidate forces for particle manipulation for which the scaling of dimensions does not prohibit the use. In fact, modern electrodes constructed using photolithography techniques can achieve much higher electric field gradients than electrodes originally used for DEP and are therefore capable of manipulating much smaller particles than was originally thought possible.

In addition to direct methods of interacting with the particles, methods of indirect manipulation are also employed in so called lab-on-chip systems. These consist of the Electrothermal (or AC Electrothermal) and AC Electroosmotic (ACEO) motions of the fluid in which the particles are suspended. The Electrothermal fluid motion is caused by thermal non-uniformities in the fluid which are caused by the non-uniform electric field, which in turn cause conductivity and permittivity gradients. The ACEO fluid motion is a consequence of the interaction of the tangential electric field over a charged electrode surface, acting on the ions in the electrical double layer. The ions are mobilised by the electric

field resulting in the ACEO fluid motion. The fluid indirectly exerts a force on the particles through drag and may therefore be used to manipulate the suspended particles. The fluidics problems involved in micro- and nano-particle manipulation are inherently existent and have to be studied in accordance to the direct forces on the particles in order to produce systems that behave in the way they are designed to.

Since AC Electrokinetic (ACEK) phenomena are difficult to observe experimentally, other methods are sought in order to better understand the underlying processes. Such insight can be provided by numerical simulations of the devices in question. Therefore, there is a great need to provide numerical simulations in order to aid in the analysis and design of devices for ACEK particle manipulation. An essential step towards this direction is the formulation of a physical model able to describe the dynamics of such devices. The physical model must then be solved in order to obtain the device dynamics. This will enable fast and cheap analysis and design of devices utilising non-uniform electric field methods. The alternative would be costly and time-consuming trial and error methods.

The work presented in this thesis sets out to provide a solution to this problem by developing a numerical simulation for the system dynamics of ACEK particle manipulation devices. The simulations presented evolve in complexity as the thesis progresses and reach a state where they can be used to provide useful insights into the operation of real devices. In the course of this work, devices are analysed and new insights are provided in their operation, enabling the interpretation of experimental results which previously disagreed with theoretical predictions. Furthermore, new device designs are proposed that exhibit improved operation over existing devices.

1.2 Literature Survey

1.2.1 Theoretical and experimental work on AC Electrokinetics

The DEP force is a force exerted on a dielectric particle due to the presence of a non-uniform electric field. DEP was first studied in detail by Pohl (5) in one of the first publications on the subject. Furthermore, the same author investigated many experimental aspects of DEP in (6).

Biological applications of DEP are studied in (7), while a theoretical investigation of DEP is made by (8). Although methods which involve integration of the Maxwell stress tensor on the particle surface (9) and using the energy variation principle (10) can be used to calculate the DEP force, the effective dipole method is the most commonly used method due to the ease of implementation and its reasonable accuracy (11). The use of AC fields avoids the problem of electrolysis that is caused when using DC electrophoresis for

similar tasks (12). The effect of illumination of the microfluidic channel is an important parameter which has also been a subject of study (13).

DEP devices in the early stages used very large components such as steel conduits and wires and required very high potentials to operate. A major step in applying DEP in microscale and nanoscale problems was the development in the manufacturing of silicon chips using nanopatterning by photolithography, as well as the introduction of novel materials. This enabled the interaction with much smaller particles due to the very high electric field gradients and also required much lower operating potentials of the order of $1\ V$. DEP using new manufacturing techniques for devices was investigated by (14) and enabled the first fluidic integrated circuits to be manufactured (15). Such technology was used to investigate the dielectric properties of body tissues (16) and in order to enable the separation of yeast cells (17). The aforementioned advances also led to the construction of devices to separate leukaemia cells from blood (18). Important work was also conducted in order to link the dielectric properties of a suspension of colloidal particles to both the DEP and Electrorotational behaviour (19) (20).

Nowadays DEP can handle single cells, viruses and other nanometre scale particles and interact with them (since the DEP force depends on electric field gradients, smaller device features increase its magnitude significantly) (21) and even destroy their exterior to extract the contents (22). It has been demonstrated that DEP methods can be used to manipulate the position, orientation and velocity of micro- and nano-metre scale particles (23) (14), including CNTs (24) and biological particles such as viruses, DNA, bacteria, cells of various kinds and subcellular components (25). ACEK methods are widely accepted as the most likely methods of nanoscale particle manipulation (26) and find numerous applications for nanotechnology in general (27).

The application of DEP methods promises to improve the performance of devices such as sensors by orders of magnitude (12), (28), (29). ACEK methods may address issues such as separation (30), movement through capillaries and trapping or focusing particles on a surface so that they can be detected more easily (31). DEP can even be used to selectively destroy cells in a mixture (32). Important work has also been conducted in the use of DEP for cell fusion (33) (34) (35). It has also been demonstrated that DEP can be used to separate particles solely based on their dielectric properties (36) (37) (38). Combined with fluidic gradients DEP can also be used to separate solutions of particles (39).

The use of fabrication techniques based on the manipulation of components using electric fields is a very important step in devices for which nanoscale component assembly is required. These methods of fabrication can be massively parallelised and are ideal even in the case of biological nanocomponents, since they do not contaminate or destroy biological particles (40). It is even proposed that using electrodes of suitable size makes it possible

to trap 1 nm particles or single molecules (41). These can be used for pick-and-place devices instead of current AFM based methods.

DEP-based separation methods frequently employ fluid flow as a force competing with DEP in order to achieve the separation of two populations of particles. DEP can be used as the discriminating force in field flow fractionation (42) (43) (44) (45). DEP field flow fractionation is based on the fact that particles experiencing different DEP force will levitate to different heights in a capillary and therefore will travel at a different speed due to the parabolic profile of capillary flow. Further applications for total analysing systems are proposed in (46).

Another important method for particle manipulation is travelling wave DEP, in which the electrodes are excited using a time-varying magnitude of the voltage, therefore creating a propagating profile. This was investigated by (47) for pumping liquids. Further work on yeast cells was also performed (48). A unified theory for DEP and travelling wave DEP has been proposed in (49). Important work has also been conducted in a multipolar theory for DEP and Electrorotation, which takes into account higher than dipole order polarisation (50). Furthermore, using DEP it is possible to extract the dielectric properties of nanoparticles by employing non-uniform, AC electric fields (51).

For DNA in particular, DEP may be used for purification, rapid DNA separation and direct manipulation (52). This might be used in conjunction with microdevice electrophoresis (53). The use of the DEP method and possible developments in the field of electrical detection could enable DNA analysis on a single chip. DEP can also be used in the final stages of DNA analysis to concentrate DNA ensembles in order to increase the localisation of the fluorescence, instead of pure hydrodynamic focusing (52). Such DNA trapping can be achieved by using DEP potential wells formed by castellated electrode structures (54) (55). Using DEP it may even be possible to manipulate DNA so that it can be used as a storage device. DEP together with electrophoresis may provide the required accuracy in the positioning of DNA so that information can be obtained optically (31). Apart from increased concentration, electronic and optical methods of detection of DNA require methods of immobilising and possibly stretching of DNA so that small samples can be detected, preferably in a device that can be reusable.

Up to now it has not been very important for manipulation methods to be realisable on chip devices, since optical methods cannot be integrated on a chip. However, the development of electrical detection methods means that in order to benefit from these methods (of electrical detection) one needs to be able to integrate the manipulation stages on-chip (56) (57), together with the detection stage. The possibility of using DEP assisted nanoelectrodes has been suggested as a very good candidate method for DNA manipulation and preconcentration (58).

Another significant application of DEP is for sorting CNTs (1), a step essential in the fabrication of CNT based sensors (40), relying on the fact that different nanotube types have different dielectric properties and dimensions. DEP is also used for assembling CNT networks on electrodes (59) (60). The use of DEP manipulation may enable the construction of novel sensors based on CNT response properties. CNT electrodes utilising DEP suitable for DNA direct manipulation and preconcentration might also be designed based on past work (61) (62) (63) (64).

Already sensors have been tested for ammonia detection, using DEP to assemble the CNTs to desired locations on electrodes (40). Sensors for temperature and fluid flow have also been manufactured using DEP to deposit CNTs to desired locations (24). These sensors would otherwise be made by moving individual nanotubes in place using AFMs, which would require manual intervention and monitoring and would not be possible to move large numbers simultaneously. AFM-based methods would therefore render batch fabrication unrealistic, whilst DEP and other electrokinetic methods are very promising in this sense.

DEP has been used in manipulation and separation of biological organisms. It has been shown that it can also be used in the manipulation of Actin-Myosin systems (65). Additionally, it has been demonstrated that it is possible for DEP to separate human breast cancer cells from blood, again based on the fact that the dielectric properties of these differ significantly (66). The advancement of these methods will enable levels of control of biological systems that have not been achieved up to now by any other method.

In addition to DEP, it has been demonstrated that EHD phenomena can be used to enhance transport or placement of nanoparticles and therefore by careful design EHD effects can be used constructively (67). This is a very important concept that is now being proposed for transport enhancement and concentration in sensor devices (12) (68). DEP methods assisted by EHD can also be used in conjunction with CNT electrodes in order to achieve DNA preconcentration and manipulation (69) (70) (71) (72). Trapping of particles can be further enhanced by the use of EHD appearing in DEP devices (73) and can be utilised in lab-on-chip devices, such as for prospective devices for DNA analysis, where pressure-driven flow is almost impossible (74) (75).

An important EHD phenomenon associated with DEP is ACEO, the fluid motion due to the fluid ions being mobilised on the electrode surface. It was first reported by (76). ACEO has since been proposed for the pumping of liquids (77) and has been found to be very important in DEP particle manipulation through experimental observations (78). ACEO can also be used to enhance the performance of trapping (79) (80) (80). The pumping of fluids using asymmetric electrodes is investigated in (3) (81). Tunable asymmetries are investigated by (82) and then by (83) and demonstrated using ACEO pumps (84). The pumping of water using ACEO is achieved by (85). Electrical methods can also be

utilised in the form of ACEO in order to move fluids in microfluidic chips, where surface forces are too high to use pressure pumping (52).

The ACET fluid motion is an EHD phenomenon caused by the thermal gradients introduced in conductive fluids by a non-uniform electric field (86). Promising applications of these exist for biofluidic applications, where high conductivity electrolytes are required (87). ACET fluid motion requires a minimum hydraulic diameter to operate (88). The heating source can also be provided by means other than an electric field (89) (13).

Finally, a review of forces in microelectrode arrays is given in (90) and an investigation of the scaling laws regarding these in (88). Another review on lab-on-chip methods is given in (91).

1.2.2 Literature survey for numerical simulations

One of the first computational investigations of the DEP force acting on a single particle was performed in (92). Also, the simulation of the DEP of CNTs has been studied in (1), where the DEP force is calculated using finite elements and the particle trajectories are simulated using the drag force balance with DEP. Each particle is simulated individually taking into account Brownian motion and it was found that DEP can be used to separate Single Walled from Multi Walled CNTs.

Direct simulations for DEP are performed in (93) and (94), where the physics of the particle-fluid problem for a small number of particles is solved and the appearance of particle chains is demonstrated. The influence of experimental conditions on the measurement of dielectric properties of particles from Electrorotation measurements is investigated numerically in (95). Furthermore, a comprehensive velocity field analysis for ACEK is performed in (96) and simulations of a quadrupolar dielectrophoretic trap using a mesh free approach are presented in (97). In addition to these, DEP ratchet structure devices are simulated in (98). Finally, molecular dynamics investigation of DEP of nanocolloids is performed in (99).

The phenomena of AC Electrothermal (ACET) and ACEO fluid motion are very important in DEP manipulation devices and can also be used for pure pumping purposes. ACET pumping numerical simulations are performed by (87) and (100) and are compared to experimental results. Fluid motion caused by ACET is simulated in (101) in order to predict the operation of a stirring system while motion caused by travelling wave excitation was investigated numerically in (102). Two-dimensional simulations are performed for ACET fluid motion in novel biosensor devices in (103). Trapping of viruses using DEP and ACET fluid motion has been demonstrated and investigated using a numerical calculation of the induced velocity fields by (104).

ACEO is investigated in (105) and further work is performed in (106), where a linear model using the Helmholtz-Smoluchowski formula is proposed. ACEO fluid motion was simulated using finite elements in (2) and compared to experimental results. ACEO stagnation points are investigated in (107) and ACEO microfluidic particle transport using electrode asymmetric polarisation is simulated in (108). Furthermore, the linear ACEO and travelling wave ACET fluid motions are simulated in (109). Variations of this pumping method have been proposed, such as the use of AC Faradaic polarisation (110) and the use of non-planar electrodes (111) (112).

In addition to the above, several issues regarding ACEO pumps are examined in (113), such as the effect of geometrical confinement, Faradaic current injection and non-linear surface capacitance. A non-linear electrical double layer analysis taking into account surface conduction is simulated for ACEO in (114). The pumping of fluids using travelling wave electroosmosis is investigated in (115) and (47). Modified Nernst-Planck equations have been investigated in order to take into account the non-linearity of the double layer potential in (116) and (117). Numerical simulations are performed in (118) in order to study the effect of ionic concentration gradients generated by Faradaic currents.

The electric field and therefore the subsequent DEP and ACEO velocities in a particle manipulation system are investigated numerically in (119). Particle movement using a numerical calculation of the DEP and ACET velocity fields was performed in (120) and an investigation of DEP with travelling wave force by using velocity fields is conducted in (121). Guidelines on the simulation of DEP are also given in (122).

Simulations of the dynamics of particles under DEP are performed using a Langevin formulation in (123). Furthermore, the behaviour of DNA subject to DEP was simulated numerically using a Fokker-Planck approach in (4). The phase separation and formation of distinct fronts in negative DEP, taking into account the particle steric effect, has been analysed using a numerical simulation in (124), by utilising a single-particle model. The simulations and experiments in (124) are performed using insulating corn oil as the medium, therefore avoiding issues that have to do with the double layer. The steric effect of particle concentration on the electric field and hence on the DEP force, has been investigated using an Effective Medium Approximation (125), where it is found that this is important. An overview of recent advances in numerical simulation of a wide range of MEMs devices is provided in (126).

It is evident from the literature that previous numerical investigations usually deal with the aforementioned physical phenomena partially, because of the increased complexity in integrating many of these in a single simulation and the increased computational needs. This thesis attempts to integrate these phenomena simultaneously in one of the most complete numerical simulations up to date and use the numerical model to provide new insights into the operation of DEP and EHD devices.

1.3 Method Selection

In order to investigate the operation and design of particle manipulation devices several methods were initially considered. The analytical method was rejected as the only method for device analysis since it is limited to a very small range of geometries and system complexity. Therefore, the ultimate task of understanding the operation of such devices and designing novel systems could not be achieved solely by analytical means. The experimental method was also rejected as the only method for device design, because the trial and error method would prove too costly and time consuming to be of any practical use.

The best method considered for the analysis and design of ACEK manipulation devices is the numerical method. This consists of a family of techniques that can be used to produce the solution for an equation, which might otherwise be impossible to obtain. Numerical methods can be classified as either direct or iterative methods, depending on whether they are expected to produce an exact solution (given that infinite precision arithmetic is used) or an approximate solution.

The method of finite elements is particularly suitable for problems involving complex geometries. This method assumes a known function that is used to approximate the solution inside the discrete intervals and the matrix equations formed are solved using a numerical method. This technique has been particularly popular following the advent of powerful computers that can perform the necessary calculations in a very short time.

Therefore, the finite element method is selected as a method to solve the PDEs governing the physical model. It is a well-established method which can be used to solve a wide range of PDE types for arbitrary geometries. These features are essential for a model which will be of increasing complexity as this thesis evolves.

Chapter 2

Dielectrophoresis

In this section a theoretical model for the Dielectrophoretic (DEP) force on a particle is introduced. This is subsequently implemented using a numerical scheme and the method of solution is verified by comparing the observed results with an analytical solution for a specific geometry. Then, the particle dynamics in a DEP manipulation device are simulated using both the finite element solution of the Smoluchowski equation and the Monte-Carlo simulation of the corresponding Langevin equation, in order to assess the advantages and disadvantages of each method for the problem of interest.

2.1 Theory

2.1.1 Dielectrophoresis

Dielectric particles suspended in a dielectric medium are polarised under the action of electric fields. If the field is spatially inhomogeneous, it exerts a net force on the polarised particle known as the Dielectrophoretic (DEP) force. This force widely depends upon the temporal frequency (for AC Dielectrophoresis) and spatial configuration of the field, as well as on the dielectric properties of both the particles and the medium in which they are usually suspended. The choice of AC excitation of the electrodes offers many advantages over DC, such as the ability to use the different frequency response of different particles, the avoidance of electrolysis and the reduced power consumption. DEP can be positive or negative depending on whether the particle is more or less polarisable than the surrounding medium respectively (5). This is illustrated in figure 2.1. The grey particle experiences a force to the left and therefore positive DEP (towards the high electric field gradient region) whilst the white particle experiences negative DEP and therefore a force

to the right (towards the low electric field gradient region). The arrow inside the particles indicates the net dipole moment.

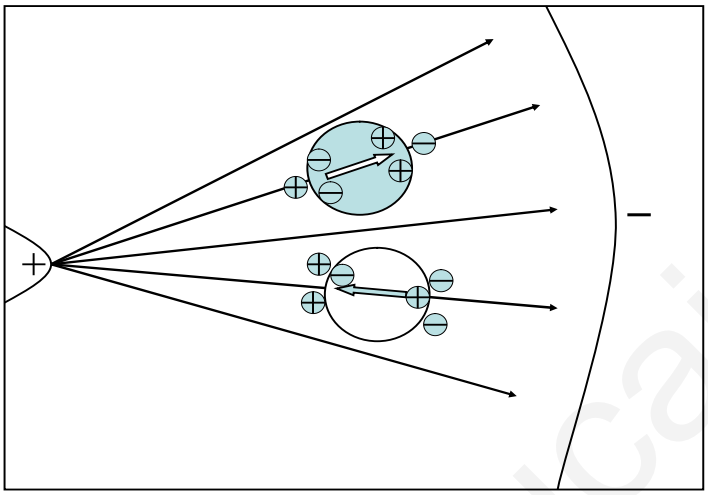

Figure 2.1: DEP force on two spherical particles, the arrows indicating the net dipole direction.

Although in absolute terms the strength of the DEP force is rather small, at the micro- and nano-scale it is very effective in manipulating and positioning particles by applying relatively small voltages on a proper configuration of electrodes. For this part of the model formulation, the fluid is assumed not to be mobilised due to any effects from the electric field. The DEP force for a spherical particle is given by [1] (122):

$$\vec{F}_{DEP} = 2\pi r^3 \epsilon_m (\mathtt{Re(K}(\omega)\mathtt{)}\nabla\vec{E}^2 + \mathtt{Im(K}(\omega)\mathtt{)}(\vec{E}_x^2\nabla\gamma_x + \vec{E}_y^2\nabla\gamma_y + \vec{E}_z^2\nabla\gamma_z)) \tag{2.1}$$

where r is the particle radius, ϵ_m the medium permittivity, $\vec{E}$ the rms electric field, γ the phase shift and $\mathtt{K}(\omega)$ is the Clausius-Mossotti factor. A proof of this can be found in (122). This proof only takes into account first order dipole formation on the particle.

The DEP force in the case of no phase gradients or gradients equal to 180^o is given by:

$$\vec{F}_{DEP} = 2\pi r^3 \epsilon_m \mathtt{Re(K}(\omega)\mathtt{)}\nabla\vec{E}^2 \tag{2.2}$$

The second part of equation 2.1 describes the force due to the phase gradients and is used in the case of travelling wave DEP and electrorotation. Travelling wave DEP is the motion of a particle caused by the lag of the dipole formed on a particle in relation to a

[1] For particles of other shapes there exist appropriate amendments to this and also an electro-orientation phenomenon.

propagating electric field. Electrorotation is the continuous rotation of the particle in a rotating electric field.

2.1.2 The Clausius-Mossotti factor

The Clausius-Mossotti factor mentioned in equation 2.1 is given by:

$$\mathrm{K}(\omega) = \frac{\epsilon_p * - \epsilon_m *}{\epsilon_p * + 2\epsilon_m *} \tag{2.3}$$

where ϵ_m is the medium permittivity, ϵ_p the particle permittivity and the complex permittivities are given by $\epsilon_p * = \epsilon_p - i\frac{\sigma_p}{\omega}$ and $\epsilon_m * = \epsilon_m - i\frac{\sigma_m}{\omega}$.

However, equation 2.3 for an elongated object such as a CNT becomes (1):

$$\mathrm{K}(\omega) = \frac{\epsilon_p * - \epsilon_m *}{\epsilon_m *} \tag{2.4}$$

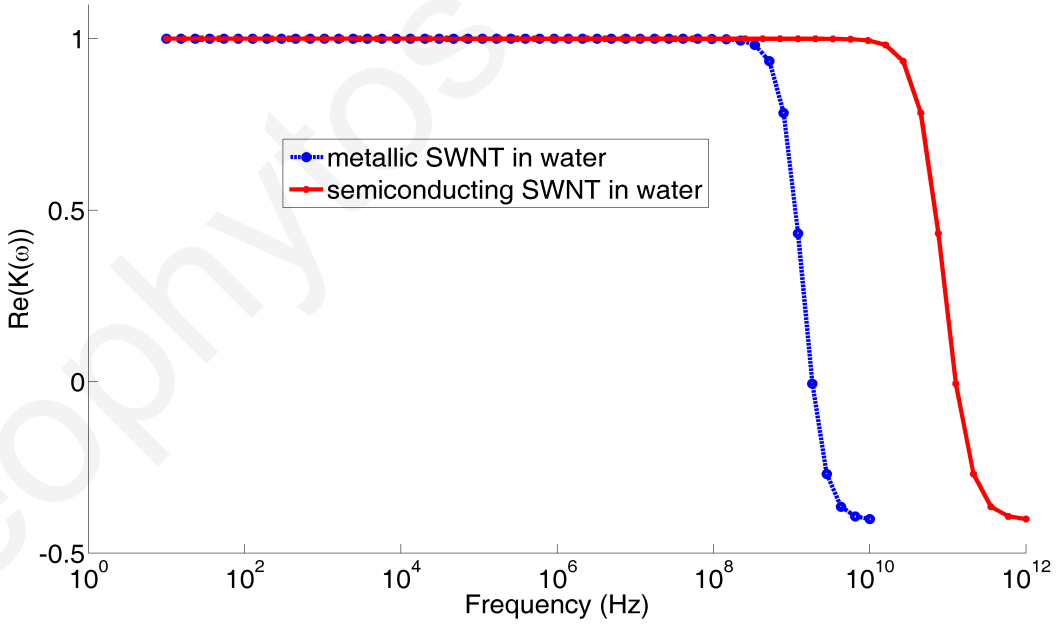

Figure 2.2: Real part of the Clausius-Mossotti factor for CNTs in water, plotted against frequency (1).

This force also depends on the shape of the particle and is modified accordingly for non-spherical particles. The structure of biological organisms is usually very complex and most commonly used models include spherical or elliptic multishell approximations (122).

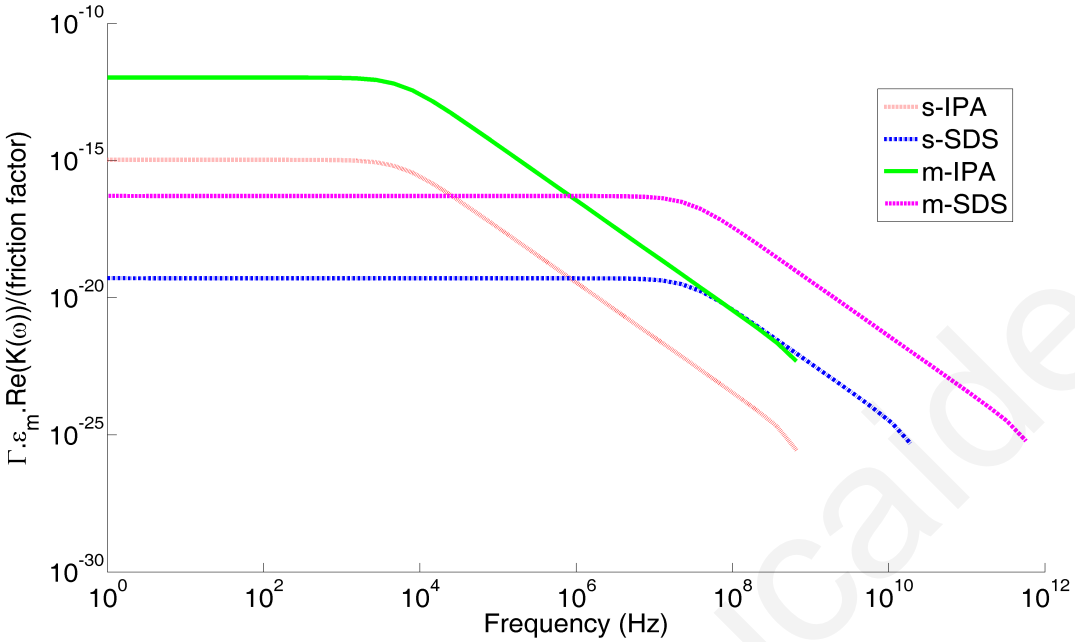

Figure 2.3: Factor proportional to the Real part of the Clausius-Mossotti factor (Γ is the volume factor) for carbon nanotubes in electrolytes, plotted against frequency (1).

Differences in dielectric properties provide a means of discrimination for otherwise similar particles. Figure 2.2 shows the real part of the Clausius-Mossotti factor for several frequencies of the AC electric field of metallic and semiconducting Single Walled CNTs in water.

It is evident that the Clausius-Mossotti factor and therefore the DEP force, is significantly different in magnitude for the two types of nanotubes and also the direction is different for a range of frequencies. This signifies that potentially separation of metallic and semiconducting CNTs can be achieved by utilising DEP at certain operating conditions. Furthermore, figure 2.3 shows the variation of the Clausius-Mossotti factor in different electrolytes for the same type of CNT.

2.1.3 Electrostatic force

Many particles under consideration might possess charge, either natural or induced. Hence they experience an electrophoretic motion under a DC electric field and this motion is used in a large number of applications. However, electrophoretic motion is not an issue and is not examined here, even in the case of charged particles, since the electric fields used are solely high frequency AC. The use of AC fields means that any electrostatic force has zero average and a time period too small for any noticeable oscillation of the particles to occur. Therefore, it is not considered as a force affecting the dynamics of the systems of interest.

2.1.4 Drag, buoyancy and gravity

For the vast majority of the systems of interest, the particles under manipulation are suspended in a fluid. What this means is that as they move through the fluid, they experience a drag force, which in its simplest form is given by the Stoke's drag:

$$\vec{F}_{drag} = -6\pi\eta_f r\vec{u}_p \tag{2.5}$$

where $\vec{u}_p$ is the particle relative velocity, η_f the fluid dynamic viscosity and r is the Stokes radius.

Another force on the particle is buoyancy given by:

$$F_{buoyancy} = \rho_f g V_p \tag{2.6}$$

where ρ_f is the fluid density, g the gravitational acceleration and V_p is the particle volume.

Also, the gravitational force is given by:

$$F_{gravity} = -\rho_p g V_p \tag{2.7}$$

where ρ_p is the particle density, g the gravitational acceleration and V_p is the particle volume.

The last two forces might be negligible for very small particles or when the particle and fluid densities are very similar, where these cancel each other out. The particle velocity $\vec{u_p}$ is subsequently found by equating:

$$\vec{F}_{drag} + \vec{F}_{total} = 0 \Rightarrow \vec{u}_p = \frac{\vec{F}_{total}}{|6\pi\eta_f r|} \tag{2.8}$$

Equation 2.8 assumes that the particles reach terminal velocity in a characteristic time that is negligible compared to the period of the applied electric field.

2.2 Model Verification

The first physical model used and verified here is the one described by (122) for the DEP force on a particle suspended in solution under a non-homogeneous electric field. The calculation of the DEP force for arbitrary geometries requires ∇E^2 to be calculated using finite elements, since E is not available analytically for most device geometries under

investigation. Choosing a 2D axisymmetric model for a spherical conductor, the surface charge is set as 1 $C/m2$ on a 10 μm radius sphere. The solution is then found for the electric field numerically. $\nabla\vec{E}^2$ is also calculated analytically using:

$$\nabla E^2 = -\frac{4}{d^5}\frac{r^4}{(\epsilon_0)^2} \tag{2.9}$$

where r is the sphere radius and d is the distance from the centre of the sphere.

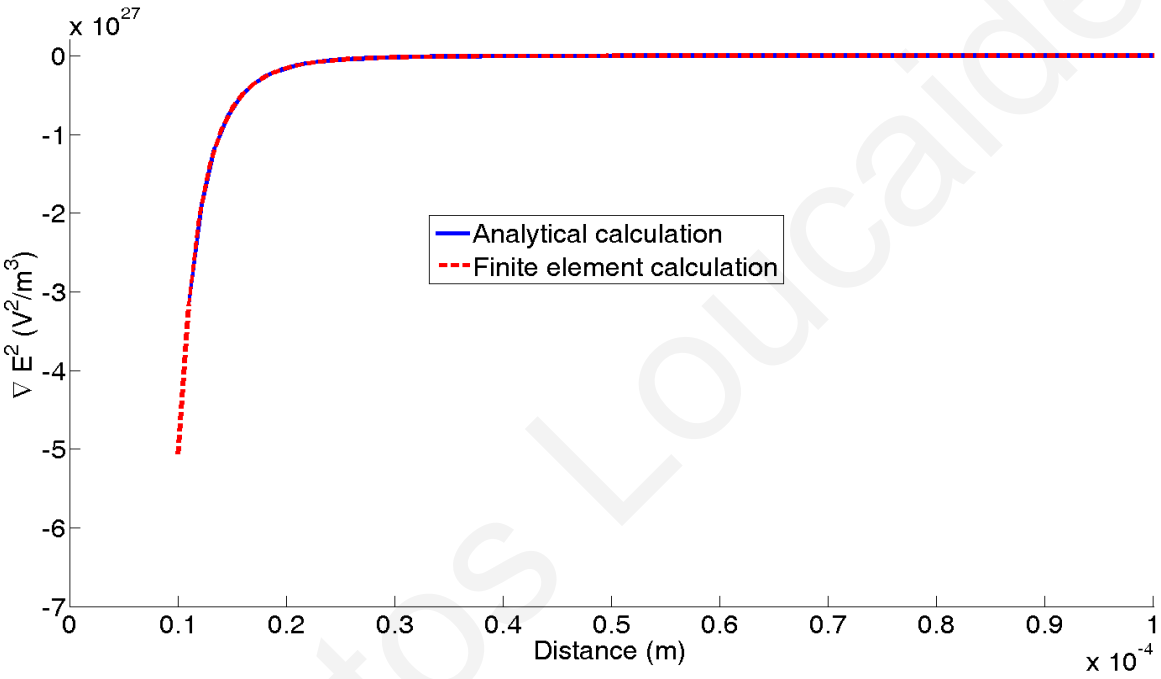

Figure 2.4: ∇E^2 vs Distance plotted for both the analytical and numerical solution.

Plotting the calculated ∇E^2 using the finite element solution of the electric field and the analytic result on the same plot figure 2.4 is obtained. The two solutions are identical and this indicates that the numerical method used to calculate ∇E^2 is correct.

2.3 Results

2.3.1 Monte-Carlo and Smoluchowski simulations

The simulation of the particle dynamics can either be investigated using a finite element solution of the Smoluchowski equation, or by performing the simulation of the corresponding Langevin equation for a large number of particles. Both are investigated below, in order to determine the method most suitable to this problem. In this section, the polynomial electrode system in figure 2.5 is simulated in terms of its DEP operation using

a numerical solution for the Smoluchowski version of the Fokker-Planck equation and a Monte-Carlo simulation of the corresponding Langevin equation.

The reason for doing this is to determine which method of the two is more suitable for the problem set here-that of simulating the particle dynamics of DEP devices, to verify the correct application of both methods and to estimate the computational resources and the solution time required for each of these methods. The parameters used are listed in table 2.1.

The Smoluchowski equation is solved here, as described in (127) (128):

$$\frac{\partial C}{\partial t} = \frac{1}{f}[-\frac{\partial}{\partial x}(F_{DEP}(x,y,t)) + k_B T\frac{\partial^2}{\partial x^2} - \frac{\partial}{\partial y}(F_{DEP}(x,y,t)) + k_B T\frac{\partial^2}{\partial y^2}]C(x,y,t) \quad (2.10)$$

where k_B is the Boltzmann constant, T the absolute temperature, f the friction factor and the other variables have the meaning stated before. Here the diffusion constant $D = \frac{k_B T}{f}$ is used. Equation 6.2 assumes that the motion of the particles is independent, that is, there are no collisions between suspended particles. This gives a distribution of concentration of the form shown in 2.6.

Figure 2.5: Geometry of polynomial electrodes (not to scale).

Table 2.1: Simulation parameters.

Property	**Value**
Diffusion constant	$2.55 \times 10^{-13}\ m^2.s^{-1}$
Relative permittivity of medium	18.6
Electrode peak potential	$5\ V$
Permittivity of free space	$8.8542 \times 10^{-12}\ F.m^{-1}$
Friction factor	$1.62 \times 10^{-8}\ N.s.m^{-1}$
Particle volume factor Γ	$3.77 \times 10^{-23}\ m^3$

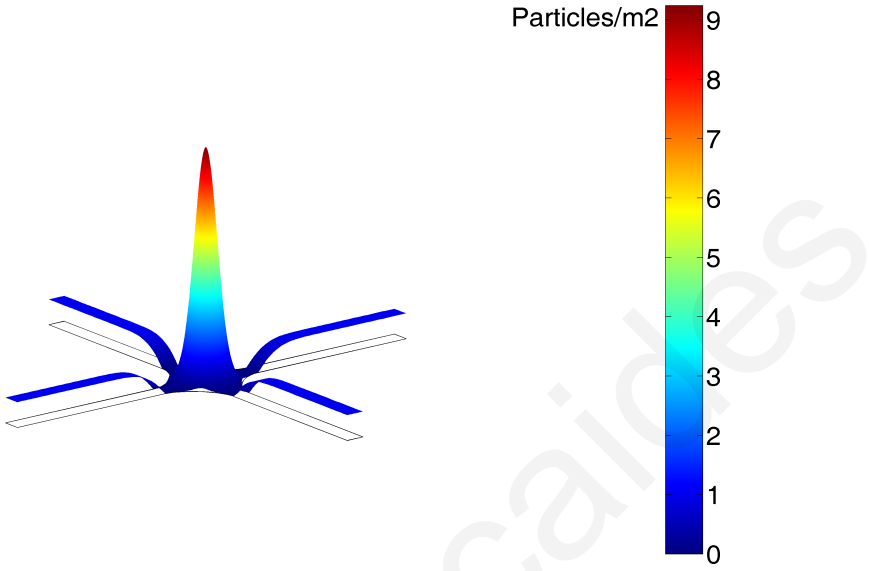

Figure 2.6: Concentration profile for particles under negative DEP 10 s after electrode excitation.

The update algorithm used for the Monte-Carlo simulation is:

$$\begin{aligned} x_{i+1} &= x_i + u_{DEP}(x,y) \times \Delta t + \sqrt{2 \times D \times \Delta t} \times W_i \\ y_{i+1} &= y_i + v_{DEP}(x,y) \times \Delta t + \sqrt{2 \times D \times \Delta t} \times V_i \end{aligned} \tag{2.11}$$

where (x, y) the particle coordinates, (u_{DEP}, v_{DEP}) the particle velocity components, D the diffusion constant and W_i, V_i are independent random variables drawn from a Normal distribution at each time step. This update algorithm creates paths of the type shown in figure 2.7.

In order to extract useful statistics for the particle behaviour and compare the Finite element/Smoluchowski solution and Monte-Carlo/Langevin method, the following problem is solved. An initially uniform particle distribution exists. In the Finite element/Smoluchowski this is set as an initial condition.

In the Monte-Carlo/Langevin this is set by taking the initial particle positions at equally spaced intervals in the problem domain. Then, the Finite element/Smoluchowski is solved up to a specific time point. The update algorithm from the Monte-Carlo/Langevin method is used to simulate the paths of a large number of particles, which are uniformly distributed in terms of initial coordinates in the domain. The results are then compared by counting the number of particles in a circular area of which the radius extends $r = 10^{-6}$ m from the electrode centre. In the Finite element/Smoluchowski the fraction of particles in that area is given by $\frac{\int_0^r C.dA}{\oint C.dA}$ where A is the area of the domain.

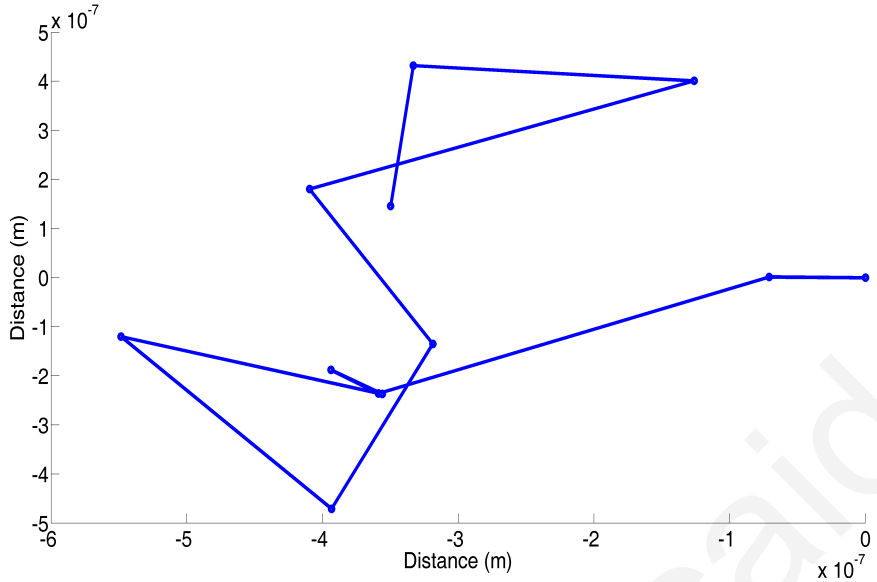

Figure 2.7: Path of a particle in the interelectrode space with 0.1 s time step for duration of 1 s.

Table 2.2: Fraction of particles within an area.

Circle radius and duration	**Langevin**	**Fokker-Planck**	**Difference**
10^{-6} m after 9 s	539/5996 = 0.089893 (0.5 s step)	0.105819	−15%
10^{-6} m after 9 s	209/2054 = 0.101752 (0.1 s step)	0.105819	−3.8%
10^{-6} m after 5 s	160/2261 = 0.070765 (0.2 s step)	0.0749495	−5.6%
10^{-6} m after 1 s	44/2261 = 0.0194604 (0.5 s step)	0.0212406	−8.3%
10^{-6} m after 1 s	48/2261 = 0.0212295 (0.2 s step)	0.0212406	+0.05%
10^{-6} m after 1 s	49/2261 = 0.021672 (0.1 s step)	0.0212406	+2%

For the Monte-Carlo/Langevin that is the number of paths which are located in that area at time t s over the total number of particle paths simulated. The results are summarised in table 2.2. It is evident that as the time step size is reduced and the number of simulated particles increased, the two methods converge and in the limit will give the same result. The results are also compared for the whole of the domain for the two forms of solution. This is done by plotting the fraction of particles within annuli from the centre. The results for the 1 s, 0.1 s time step case are presented in figure 2.8.

2.4 Conclusions

In this chapter, a model was introduced for the Dielectrophoretic force on a dielectric particle suspended in a medium. The DEP force was solved for a specific case using the method of finite elements and verified using an analytical formula. Furthermore, both the Finite element/Smoluchowski and Monte-Carlo/Langevin methods were used to investigate particle dynamics in a DEP system.

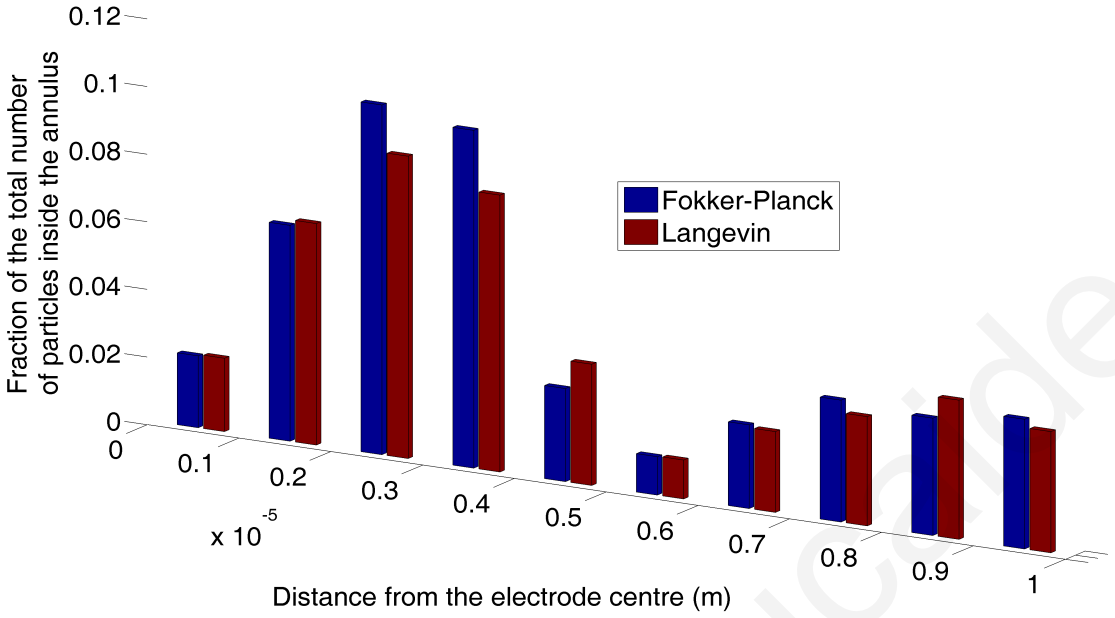

Figure 2.8: Comparison of the concentration of particles within specific annuli from the electrode centre (the number on the right of the bars is the external radius whilst the number on the left is the internal radius of each annulus).

Although both methods can be used to produce the solution for the problem, the Finite element/Smoluchowski solution was selected as the means of future investigation of the device operation and for the design of novel devices. While the Monte-Carlo/Langevin method can provide more information on particle trajectories, the most important data of interest here, which is the average particle concentration, can also be given using the Finite element/Smoluchowski. The latter is much faster and requires less computational resources, an issue which will prove very important as the complexity of the problem increases.

However, the physical model developed in this chapter only takes into account the DEP force on the particle. In most DEP manipulation devices, the fluid in which the particles are suspended is also mobilised due to the presence of the electric field. The fluid motion due to the electric field presence is a very important factor that has to be taken into account in the simulation of DEP devices and is therefore examined in the chapters to follow.

Chapter 3

AC Electroosmotic fluid motion

As mentioned earlier, the fluid-electrolyte in which particles are suspended in DEP manipulation devices is also mobilised due to the presence of the electric field. The most common phenomena that cause the fluid motion are AC Electroosmosis (ACEO) and the Electrothermal effect.

In this chapter a model for the ACEO motion of the fluid in an AC electric field is introduced and the ACEO motion is simulated using the method of finite elements. Furthermore, a novel system is proposed for fluid pumping and its operation is investigated.

3.1 Theory

3.1.1 The electrical double layer

An important concept throughout this thesis is that of the electrical double layer (referred to as the double layer hereafter). The double layer is a concept that describes the distribution of the electric charge near a surface and particularly that of a charged surface in contact with a fluid. Free charges in the solution will experience a Coulombic force (129), giving rise to a charge formation as displayed in figure 3.1.

The Inner Helmholtz Plane (IHP) is defined as the center of water molecules and ions in contact with the solid. The Stern layer extends from the solid surface to the Outer Helmholtz Plane (OHP). The OHP is the center of the solvated ions in closest approach to the surface. The zeta potential is the potential difference from the plane of no-slip to the bulk of electrolyte solution. The plane of no-slip is thought to be close to the OHP, towards the side of the bulk. In this model, the plane of no-slip is considered to be at the OHP for simplicity.

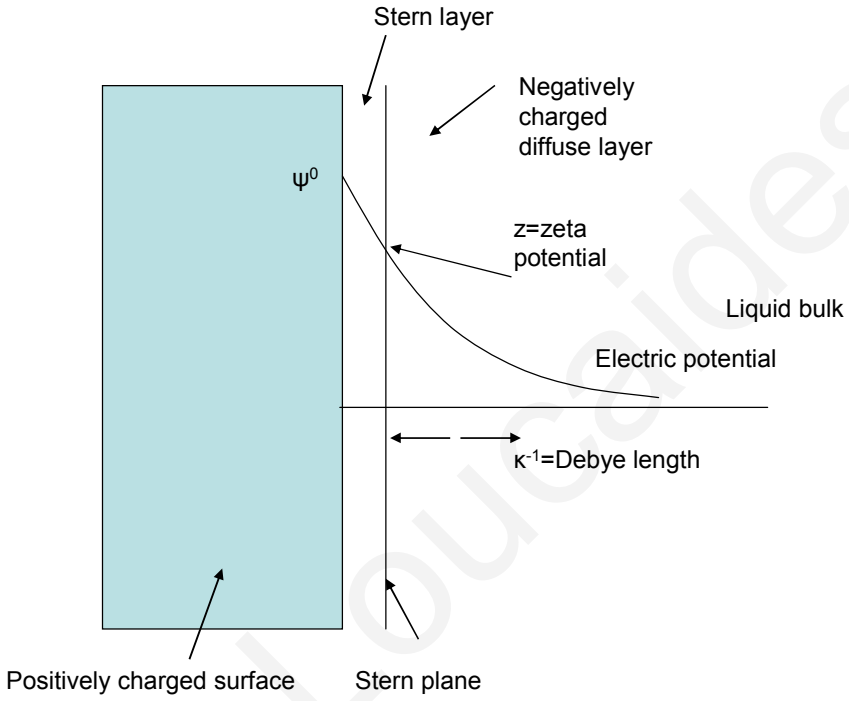

Figure 3.1: The electrical double layer.

The Debye length is defined as the typical thickness of the diffuse layer, which consists of exponentially decaying free charge (129). The double layer is very important when considering the behaviour of colloidal particles in suspensions and can be the decisive factor in the behaviour of the particle. It is also very important in the following theory of ACEO because it is the formation of this double layer over the electrode surface by the fluid ions that is responsible for the fluid motion.

3.1.2 AC Electroosmosis

ACEO is the fluid motion which is caused by the presence of a non-uniform electric field over a surface, most likely that of an electrode for the systems of interest. It was first reported by (76), where a linear double layer theory is also proposed in order to model the behaviour of the fluid.

The electric field over the electrode surface has a tangential component which causes ions in the electrolyte to move and carry the bulk fluid together with them. It is more significant at low frequency AC fields (≈1 kHz) and decreases significantly at higher frequencies (≈1 MHz). AC electroosmotic flow over electrodes (such as travelling wave DEP electrodes) is not the same as DC Electroosmosis in capillaries. The former causes an oscillating ion motion whilst the latter causes a constant flow of ions and therefore fluid motion (2). The model proposed by (76) makes the following assumptions:

1. The electrodes are ideally polarisable, that is, no charge is flowing from the electrode to the electrolyte.
2. The potential drop across the diffuse double layer is small (smaller than ≈25 mV) so that a linear approximation can be made.
3. The convection current is much smaller than the conduction current and therefore the electrical problem is independent of the velocity field.

Assumptions 1 and 3 are true for most real systems that are examined here. However, it is almost certain that for most cases assumption 2 is not valid. Therefore, the physical model provides a good insight into the behaviour of the fluid under ACEO, but the quantitative predictions are increasingly erroneous for potentials higher than ≈25 mV.

For the purpose of the numerical simulation of ACEO the following equations are used (2). The first is the Laplace equation that is solved in order to find the electric field distribution in the domain:

$$\nabla^2 \phi = 0 \tag{3.1}$$

where ϕ is the electric potential. This is solved with the following boundary condition on the electrode due to charge conservation (2):

$$\sigma \vec{n}.\nabla \phi_{ep} = \frac{\phi_{ep} - V_{applied}}{Z_{DL}} \tag{3.2}$$

where $\vec{n}$ is the normal unit vector to the electrode surface, ϕ_{ep} the potential at the outer edge of the electrical double layer, σ the fluid electrical conductivity, $V_{applied}$ the value of the voltage applied at the electrodes, $Z_{DL} = \frac{1}{i\omega C_{DL}}$ the impedance of the double layer, $C_{DL} = \frac{\epsilon_m}{\lambda_{Debye}}$ the capacitance of the double layer (if the size of the compact layer is negligible), ω the angular frequency of the electric field and λ_{Debye} is the Debye length on the electrode surface. The boundary condition used for all the electrodes is therefore given by equation 3.2. The Navier-Stokes equations are also solved, neglecting the inertial

terms (since the Reynolds number is small), to find the resulting incompressible fluid flow (under no external forces on the fluid):

$$\eta_f \nabla^2 \vec{u}_f - \nabla p = 0 \tag{3.3}$$

$$\nabla \cdot \vec{u}_f = 0 \tag{3.4}$$

where η_f is the fluid viscosity, $\vec{u}_f$ the fluid velocity and p is the fluid pressure.

This has the following boundary condition for the fluid velocity on the surface of the double layer (which coincides with the electrode surface in the model geometry):

$$u_{slip} = -\frac{\epsilon_m}{4\eta_f}\Lambda \frac{\partial \left|\phi_{ep} - V_{applied}\right|^2}{\partial x} \tag{3.5}$$

where Λ is the ratio of the diffuse double layer potential drop over the total double layer potential drop. The parameter

$$\Lambda = \frac{C_{Stern}}{C_{Stern} + C_{diffuse}} \tag{3.6}$$

is given by the ratio between the total capacitance and the diffuse double layer capacitance and is set here to be equal to 1 for verification purposes (2). It should be noted that a potential $2V_0 = 0.5\ V$ is used here to allow direct comparisons to be made with (3) and (2).

3.2 Model Verification

Data is used here from (3) and (2) to verify the model above. The geometry modelled is shown in figure 3.2 and the properties used in the simulations are shown in table 3.1.

This is modelled by the boundary conditions (by exploiting anti-symmetry) shown in figure 3.3, where $\phi_E = \phi_{ep}$ as defined in equation 3.2 and $U_{slip} = u_{slip}$ as defined in equation 3.5, $V_{applied}$ is the absolute value of the voltage applied at the electrodes and the rest of the variables have their usual meaning.

3.2.1 Electric potential

The electric potential given by the solution of the Laplace equation for the domain above the electrodes is shown in figures 3.4, 3.5, both real and imaginary parts.

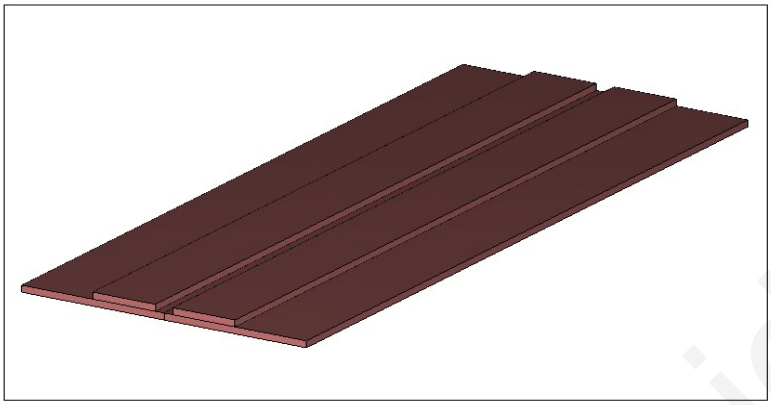

Figure 3.2: The geometry of the domain used for model verification (not to scale).

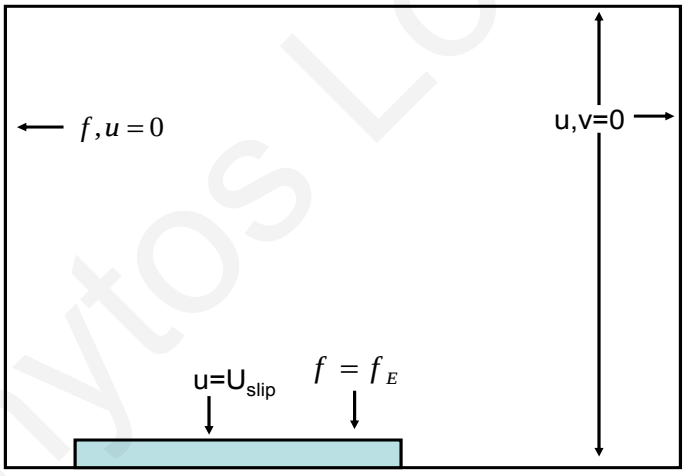

Figure 3.3: The boundary conditions used for model verification (not to scale).

A useful variable used here is the non-dimensional frequency $\Omega = \frac{\omega \epsilon_m L}{\sigma \lambda_{Debye}}$, where L is the device characteristic length (10^{-4} m) and ω is the angular frequency of the AC excitation used.

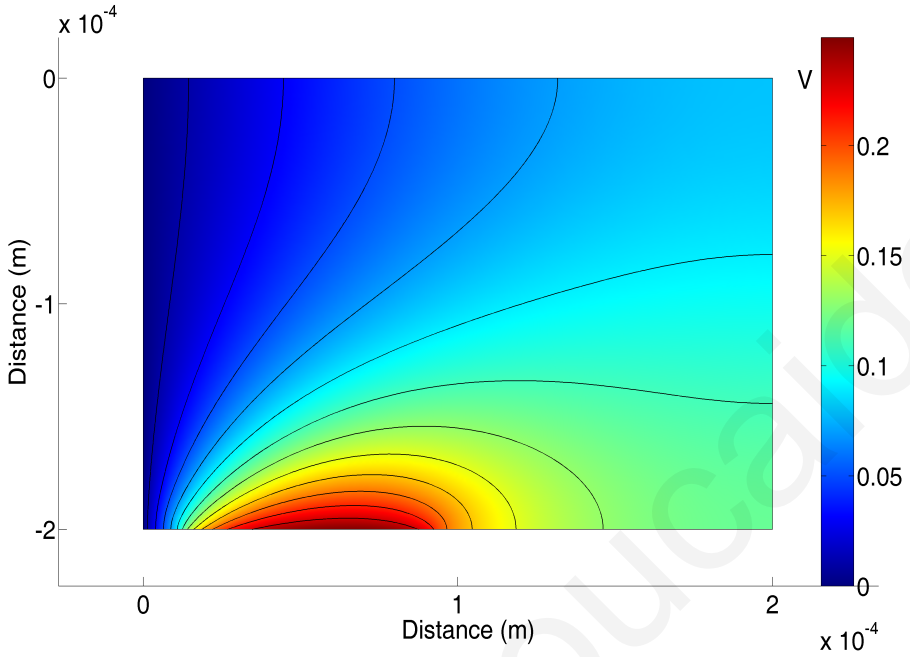

Figure 3.4: The simulated Real part of the potential.

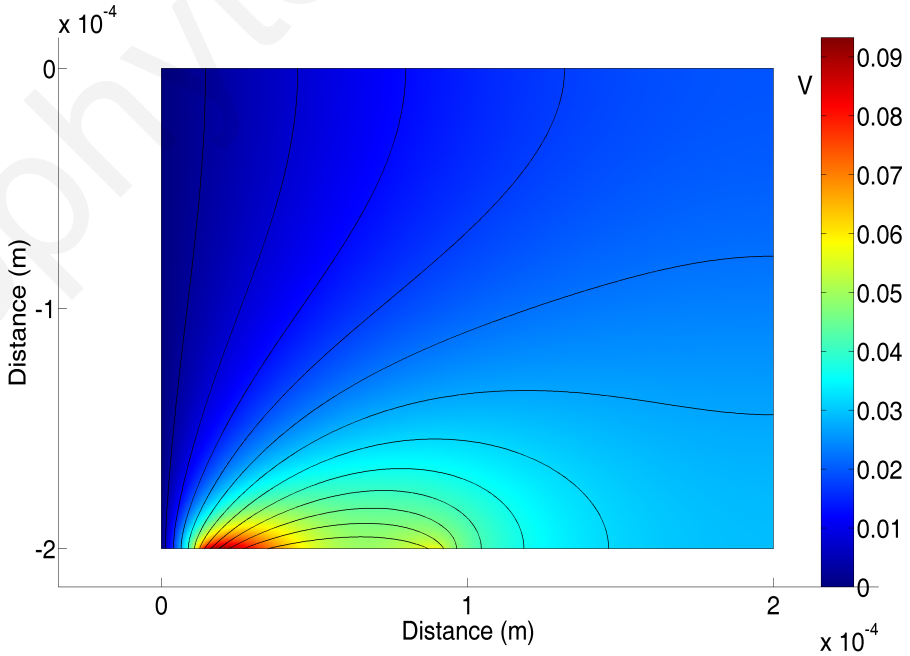

Figure 3.5: The simulated Imaginary part of the potential.

Table 3.1: Electrolyte properties.

Property	**Value**
Fluid Viscosity (η_f)	1×10^{-3} $Pa.s$
Relative permittivity of medium (ϵ_{mr})	80.2
Electrode peak potential difference ($2V_0$)	0.5 V
Λ	1
Permittivity of free space (ϵ_0)	8.8542×10^{-12} $F.m^{-1}$
Debye length (λ_{Debye})	1×10^{-7} m
Conductivity (σ)	8.6 $mS.m^{-1}$

3.2.2 Fluid motion

The potential is coupled with the Navier-Stokes equations by the boundary condition u_{slip} set at the electrode surface. The resulting fluid flow is calculated numerically and is demonstrated in figure 3.6. The characteristic circular patterns are clearly visible.

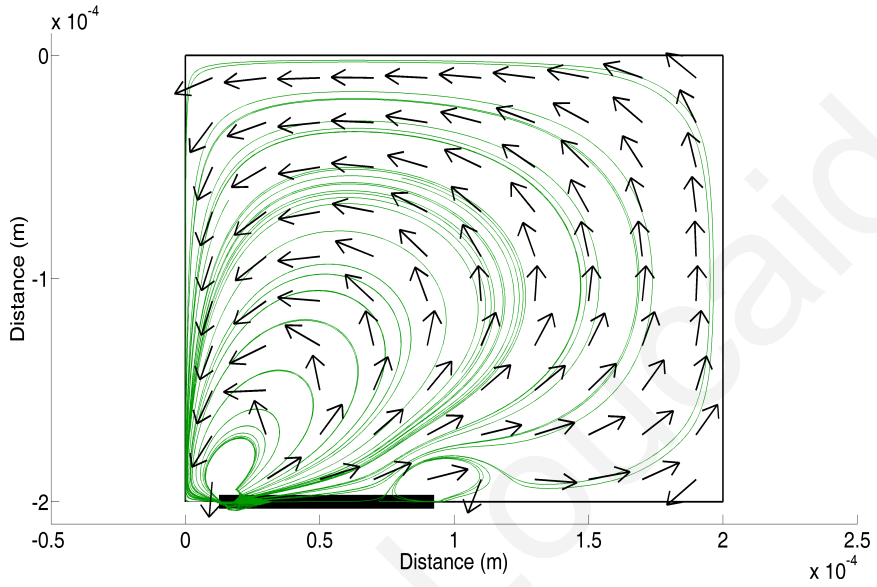

Figure 3.6: Fluid flow in the domain for $\Omega = 11$.

In figure 3.7 the fluid flow over the electrodes is plotted for different non-dimensional frequencies. The behaviour is again as expected, reaching a peak at an intermediate frequency, while reducing for higher and lower frequencies.

The surface velocity as a function of both the distance from the electrode gap centre and the non-dimensional frequency is plotted in figure 3.8. Furthermore, the surface fluid velocity is plotted in figure 3.9 for several fluid conductivities.

As a further validation, the reduced fluid velocity $U_n = \frac{4\times\eta_f\times(u_x)\times(W_e)}{\epsilon\times(2V_0)^2\times\lambda_{Debye}}$, where W_e is the electrode width, at several distances from the electrode inner edge is plotted versus the non-dimensional frequency (defined earlier) in figure 3.10. The plot is compared with figure 4 in (3) and it is evident that the results are very close to the ones presented both in this reference and in (2).

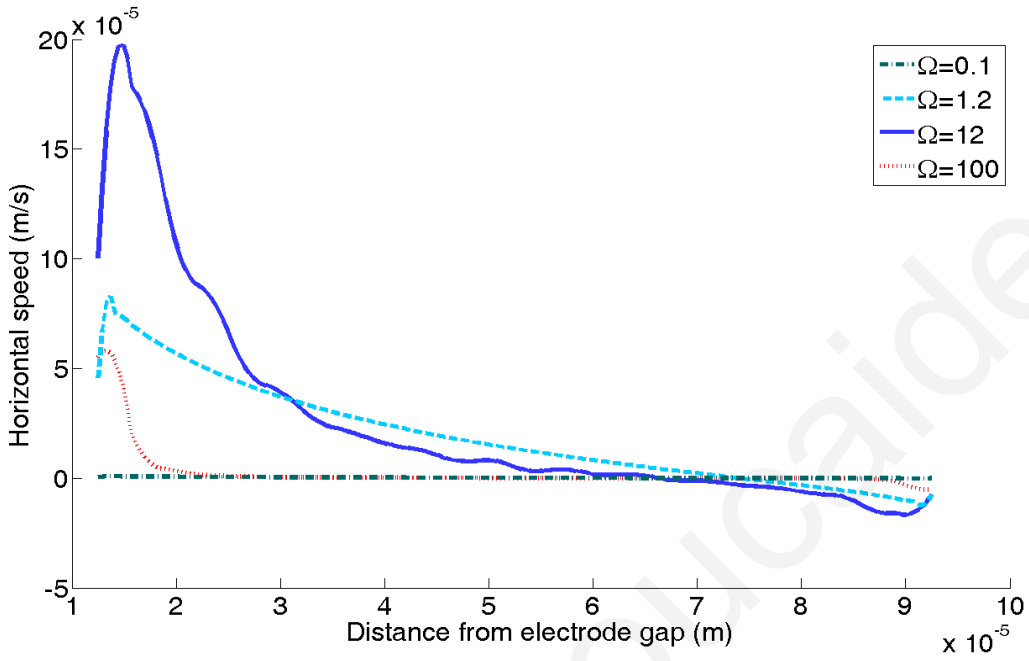

Figure 3.7: Fluid flow over the electrodes for different Ω.

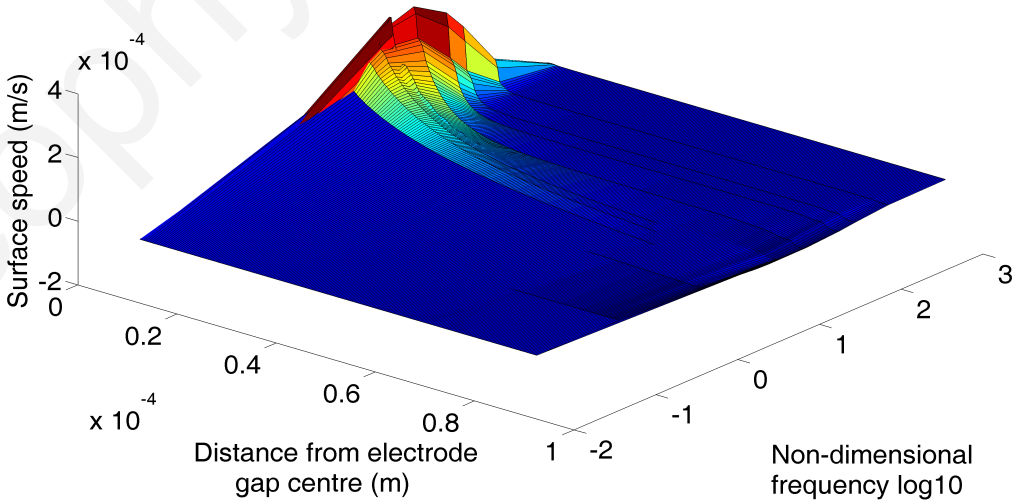

Figure 3.8: Fluid velocity on electrode surface vs Ω.

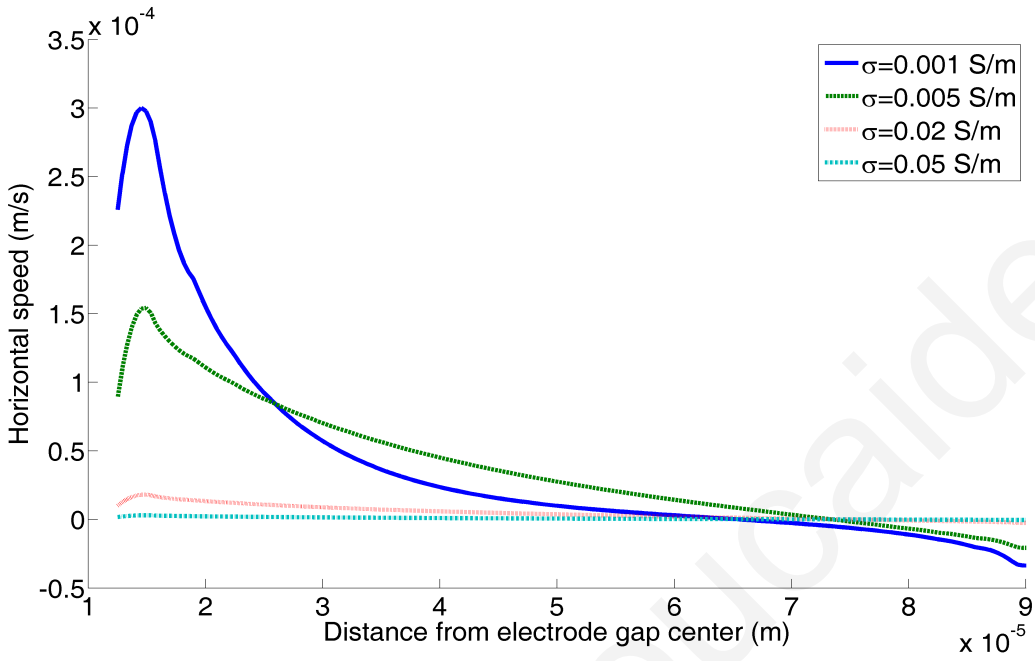

Figure 3.9: Fluid speed on electrode surface vs Conductivity of the electrolyte.

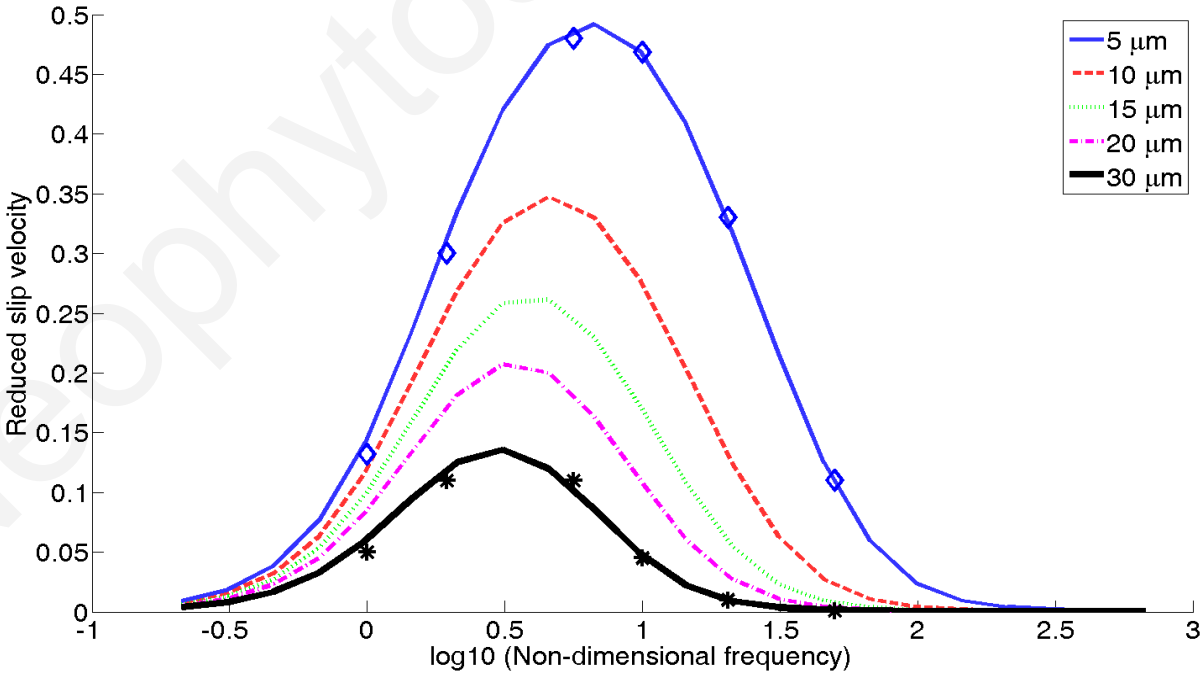

Figure 3.10: Reduced fluid velocity vs Non-dimensional frequency for several distances from the electrode edge closer to the gap. Results from (2) are presented as blue diamonds for the 5 μm case and black stars for the 30 μm case.

The results presented in this section provide a verification that the solution of the physical model for the ACEO fluid motion used here is correct. The verification of the solution is very important since the method of solution will be used throughout the thesis for the calculation of the ACEO fluid velocity.

The proposed model is used in the following section in order to analyse existing devices that utilise ACEO in asymmetric electrode systems for fluid pumping. Furthermore, novel systems are proposed that utilise configurable asymmetries in order to produce a configurable directional pumping effect.

3.3 Results

3.3.1 Novel systems for configurable ACEO pumping

Since the discovery of the ACEO fluid flow (90) (76), many methods have been proposed to utilise this in the pumping of fluids in capillaries, due to several advantages over DC Electroosmosis. The main advantage is that the use of low AC voltage can reduce or eliminate Faradaic currents, which reduces or eliminates the generation of bubbles and new species in the liquid.

An important set of pumping systems that have been proposed and demonstrated, are ones that utilise asymmetries in the electric field, created by planar electrode structures in capillaries to produce a directional ACEO net flow of fluid (77). In particular, a method utilising an asymmetry in the electrode geometric configuration has been demonstrated experimentally by (85) and analysed theoretically in (3), which describes the asymmetric array and predicts the right direction of the fluid flow. This electrode structure has also been utilised in the trapping of DNA using ACEO (130). Another important set of pumping methods has been described in the literature that utilise travelling wave electric fields generated by symmetric electrode arrays for the purpose of fluid pumping (131) (115). Asymmetries in this type of pumping systems can be introduced in many ways, such as asymmetries in the shape of the electrodes (85) or their properties (77) or even by adding DC bias in the electrode excitation (132) (80). Proposed methods also include three-dimensional asymmetric electrode structures (111) (112).

An interesting issue in ACEO pumping using asymmetric electrode arrays is the reversal of the pumping direction. For low voltages and frequencies, the expected flow occurs at the side of the smaller electrode towards the larger one. This flow has been shown to reverse at higher voltages and frequencies (84) (81). However, the mechanism that causes flow reversal is yet unclear (although Faradaic currents have been proposed as an explanation for this (77) (110)). Possible undesirable effects on the electrodes have also

been associated with high voltages, such as the formation of bubbles due to electrolysis and the degradation of the electrodes (81). Recently, there has been an investigation into the effect of Faradaic currents, as well as other important factors on ACEO flow (113), such as vertical confinement and non-linear surface capacitance.

In this section a method of creating configurable geometric asymmetries in a system of arrays of identical electrodes is proposed, as shown in figure 3.11 (system B) and figure 3.12. The system operates by applying the same AC voltage on two adjacent electrodes (say 1 and 2) while applying a voltage of equal magnitude in anti-phase to the other electrode (therefore the system consists of triplets of identical electrodes instead of pairs of non-similar electrodes, with another possibility being an arbitrarily wide middle electrode with identical electrodes at the two sides) (82).

This can also be implemented by applying a single AC signal to one electrode group while earthing the other. A geometric asymmetry similar to the one in a system of asymmetric electrodes is created, as described in (84) and shown in figure 3.11 (system A), with the significant advantage that in the proposed system this asymmetry is configurable, as shown in figure 3.11 (system B).

The proposed method may be used to create configurable asymmetry by employing a number of identical electrodes and therefore can be used to control the direction of the pumping velocity, without the need for high applied voltage. It is also demonstrated here that the amplitude of the pumping velocity can be controlled in a step-wise manner depending on the number of electrodes in a group.

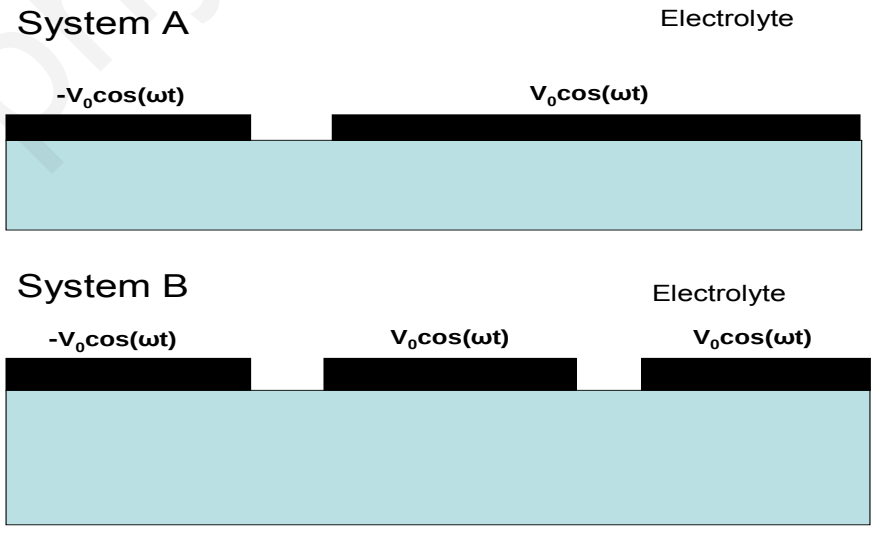

Figure 3.11: Geometry of the electrodes of the standard asymmetric system A and the proposed system B (basic form)(not to scale).

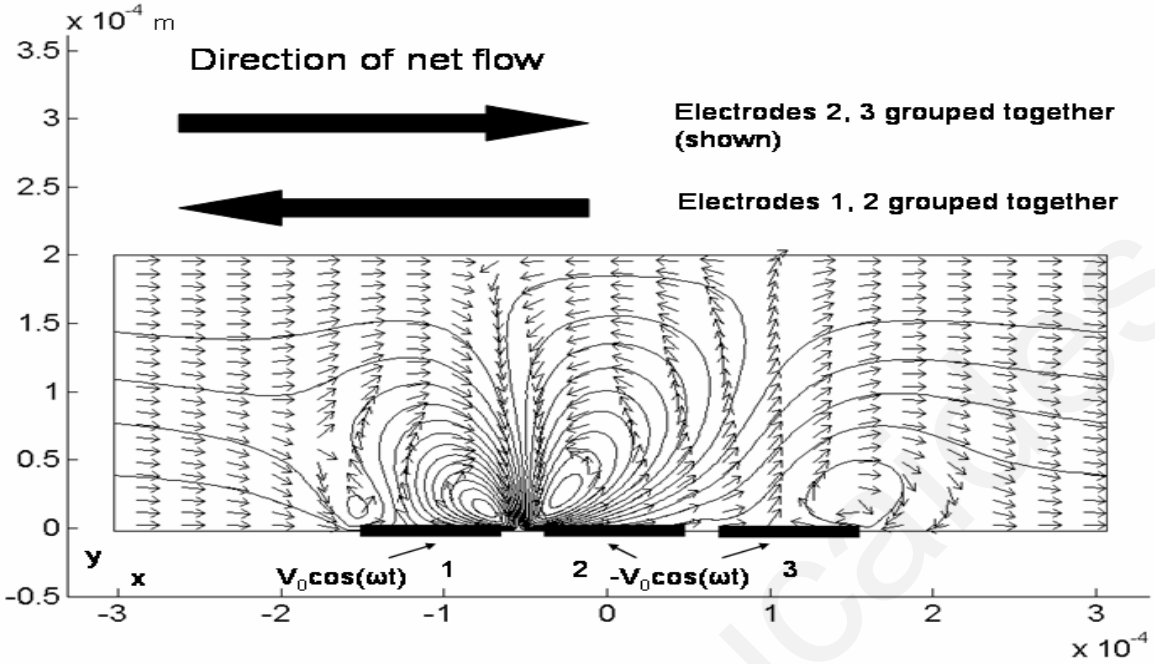

Figure 3.12: Schematic of the configuration and operation of the proposed system (not to scale). The arrows and streamlines indicate the fluid flow direction.

Finally, it is worth noting that the proposed system allows for flow reversal at any voltage (both low and high) without the need to change the magnitude of the applied voltage.

The theory used in the simulation of the device has been presented in section 3.1.2, while the properties used in the simulations are presented in table 3.2.

Table 3.2: Electrolyte properties.

Property	**Value**
Fluid Viscosity (η_f)	$1 \times 10^{-3}\ Pa.s$
Relative permittivity of medium (ϵ_{mr})	80
Electrode peak potential difference ($2V_0$)	$1\ V$
Λ	0.25
Permittivity of free space (ϵ_0)	$8.8542 \times 10^{-12}\ F.m^{-1}$
Debye length (λ_{Debye})	$3 \times 10^{-8}\ m$
Conductivity (σ)	$1.23\ mS.m^{-1}$

The two side boundaries of the domain have periodic boundary conditions (i.e. $\phi(-l/2, 0) = \phi(+l/2, 0)$ where $l = 600\ \mu m$ here) and the rest of the boundaries are set to a homogeneous Neumann boundary condition $\vec{n}.\nabla\phi = 0$, where $\vec{n}$ is the vector normal to the surface. The electrode width is 100 μm, the channel depth is 200 μm, the interelectrode gap is 10 μm and the distance between electrode groups is 280 μm.

The boundary condition at the surface of the electrodes is $u = u_{slip}$ (defined earlier), where $V_{applied}$ is different for each electrode, while the side boundaries are set to periodic boundary conditions and the boundaries at the interelectrode gaps are set to a no-slip condition.

Both the electrical and fluid flow problems are solved numerically using the method of finite elements. A parameter useful for the analysis of such a system (and used here) is the non-dimensional frequency $\Omega = \frac{\omega \epsilon L}{\sigma \lambda_{Debye}}$, where L is the device characteristic length (here the value used is twice the length of an electrode, 200 μm), λ_{Debye} the Debye length, σ the electrolyte conductivity and ω the angular frequency of the AC excitation. Another such parameter is the non-dimensional velocity given by $U_{non}=\frac{4\eta_f L u_{slip}}{\epsilon(\Delta V)^2 \Lambda}$ where η_f is the fluid viscosity, u_{slip} the dimensional velocity and ΔV the potential difference between electrode groups, which is equal to $2V_0$ in this case.

3.3.1.1 Proposed method and system

Here the system of interest is one of parallel electrodes in a narrow channel, where both the electrode width and the channel depth are much larger than the electrode height so that the electrodes can be considered flat and the length of the electrodes is much larger than their width, so that the problem can be treated as two-dimensional.

The proposed system is related to the one shown in figure 3.11 (system A) and demonstrated experimentally in (85) and theoretically in (3), with the significant difference that the asymmetry is configurable and not fixed into the system (system B).

In the simplest form, the proposed system consists of a repeating pattern of three identical electrodes as shown in figure 3.11 system B and in more detail in figure 3.12. The idea is that by applying a potential so that electrodes 2 and 3 are in anti-phase with electrode 1, an asymmetry of the electric field is created. This asymmetry is almost the same as if electrodes 2 and 3 were connected and the system was asymmetric in shape (system A in figure 3.11). This type of excitation will create circular flow patterns above the electrodes, which results in a net flow towards the larger group of electrodes, as shown in figure 3.12. The advantage of this system is that by applying the same potential on electrodes 1 and 2 this time, with electrode 3 in anti-phase, the asymmetry is reversed and therefore the flow is also reversed.

The fluid slip velocity over the electrodes at non-dimensional frequency $\Omega = 6.03$ is shown in figure 3.13. It can be seen that by using different grouping of the electrodes it is possible to reverse the asymmetry and therefore the flow.

The pumping velocity is defined here as:

$$U_p = \frac{1}{l} \int_{-l/2}^{l/2} u_{slip} dx \tag{3.7}$$

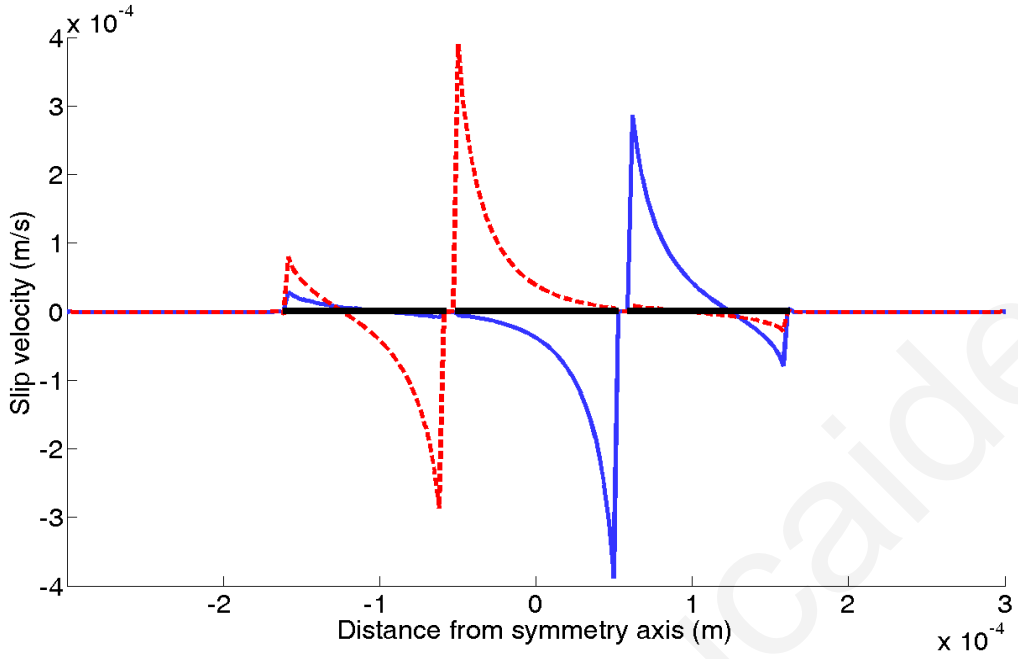

Figure 3.13: Flow over the electrodes for two cases. Dashed line is for electrodes 2 and 3 grouped together, solid line for electrodes 1 and 2 grouped together. The electrode position is also indicated on the figure.

where l is the length of the periodic segment of the device and u_{slip} is the slip velocity at the electrode surface, as found by equation 3.5, with $u = 0$ at the gaps between electrodes.

The non-dimensional pumping velocity for system A is plotted against the non-dimensional frequency in figure 3.14 and compared to the results obtained by (3) (figure 9) for a system with the form shown in figure 3.11 system A, with a non-dimensional interelectrode gap $G_1 = 0.1$. This has been done for verification purposes and the results were found to be in good agreement with the results obtained in (3).

On the same plot in figure 3.14 the solid line is for system B, the system proposed here, with the electrode dimensions adjusted to (width of first electrode) $W_1 = 0.3$, (gap after first electrode) $G_1 = 0.1$, $W_2 = 0.6$, $G_2 = 0.1$, $W_3 = 0.3$ and $G_3 = 1$ in order to be consistent with the dimensions used in (3) and the channel height set to 200 to approximate an infinite channel height such as in (3)(note that the above parameters are non-dimensional). It can be seen clearly in this plot that the effect of using the triple electrode system is a 10% reduction in velocity at the peak, while this is lower for other frequencies. This small drop in performance is more than compensated for by the added convenience of being able to alter the flow direction.

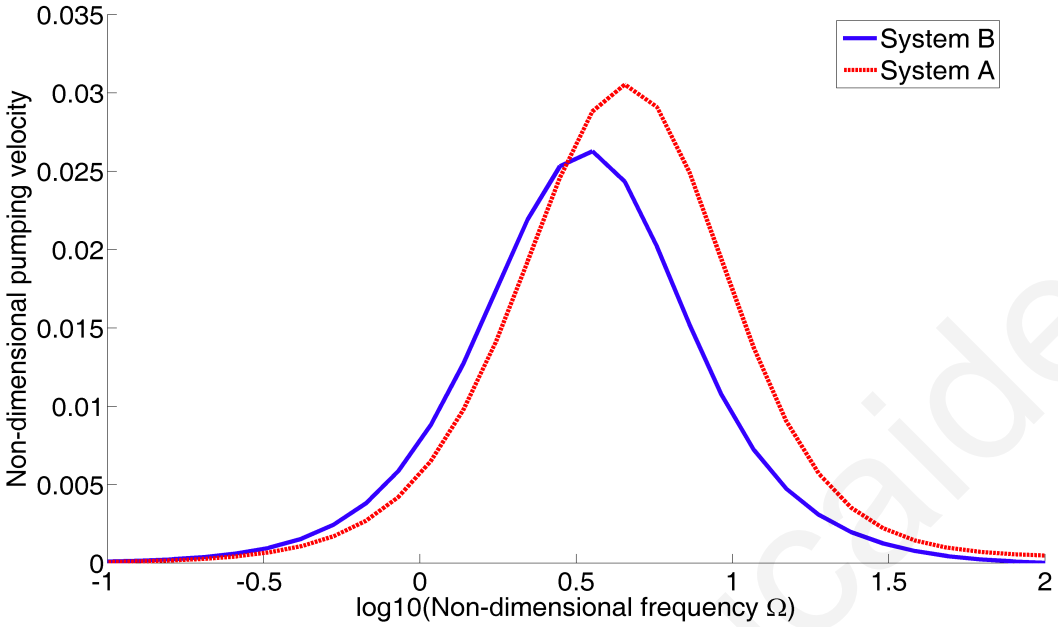

Figure 3.14: Non-dimensional pumping velocity against non-dimensional frequency. Black dashed line is for the case plotted in (3) (corresponds to figure 9 top curve for non-dimensional interelectrode gap $G_1 = 0.1$), solid red line is for the device proposed here.

3.3.1.2 Other electrode structures

It has been demonstrated here that it is possible to construct a system with controllable asymmetry by using at least three identical electrodes per periodic array set. It is also possible to construct more interesting systems by adding more electrodes in the periodic array. As an extension of the previous system, one could make this array out of four electrodes and group 1, 2 and 3 together in terms of excitation, or 2, 3 and 4 to reverse the flow. Larger numbers of electrodes give the possibility of controlling the pumping velocity in a step-wise manner solely by inverting the polarity of the applied voltage on the electrodes.

For example, in a five-electrode array, grouping the first four or first three electrodes together would give pumping velocity in the same direction but of different magnitude. Therefore control of the pumping velocity can be achieved by simple switching between $V_0 cos(\omega t)$ to $-V_0 cos(\omega t)$ on certain electrodes, which minimises the required power circuitry and hence constitutes a great advantage for such systems. The velocities in the two cases for such a system are demonstrated in figure 3.15. The electrodes are of length 80 μm each while the gap between them is 25 μm. The array periodic length is the same as in the three-electrode system described before, equal to 600 μm.

The pumping velocity when one electrode is a group on its own is 4.638×10^{-6} $m.s^{-1}$ while it becomes 2.102×10^{-6} $m.s^{-1}$ when the first two are grouped together.

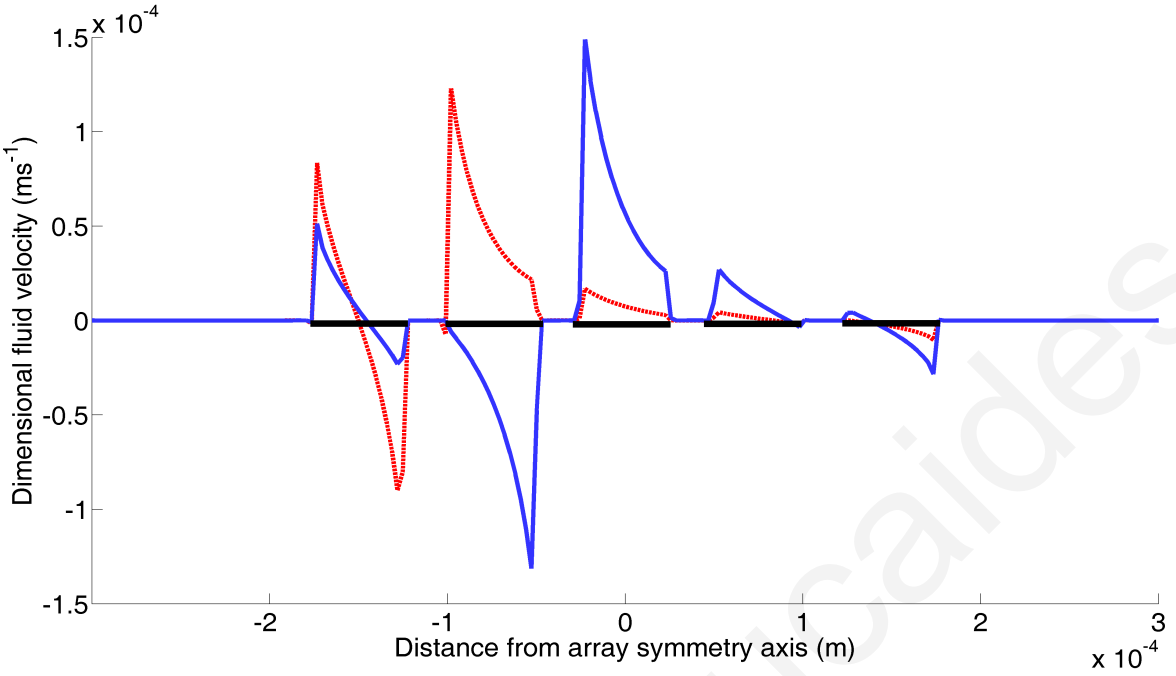

Figure 3.15: Dimensional slip velocity against distance from symmetry axis. Dashed line is for the case where electrodes 2 to 5 are grouped together (electrode 1 constitutes the other group), solid line for the case where electrodes 3 to 5 are grouped together (electrodes 1 and 2 form the other group). The electrode position is indicated on the plot.

This decrease in pumping velocity is due to the decrease in the asymmetry of the system (at $\Omega = 4.12$). This observation demonstrates the fact that the pumping velocity can be controlled by varying the system asymmetry. The flow rate F can be obtained by $F = \frac{u_{slip} \times (Area_{cross-section})}{2}$, given that the channel height is much smaller than the electrode length (the electrode length being the dimension perpendicular to figure 3.11 as viewed here).

It is clear that increasing the number of electrodes in the length of one period will give a higher level of control on the system, as well as the ability to introduce more complex phenomena into the system.

It must be stated here that in terms of system fabrication, the proposed design requires an extra layer for every two electrodes added per periodic array, in order to accommodate the electrode connections. This means that there is an extra manufacturing cost incurred compared to the planar asymmetric electrode arrays. What also has to be noted is the alternative method of using travelling wave devices for fluid pumping. This is superior in terms of efficiency and can be realised by a two layer design. The proposed design can be readily implemented on travelling wave arrays by electrode grouping as described here (where three electrodes out of four are used and one is left as a spacer) and is a possible mode of operation in the case when a multi-phase supply is not available for portable micro-devices. In order to realise the application of this method to existing devices, one could envisage the replacement of the two asymmetric concentric electrodes in (130) with

three concentric electrodes of equal width. That would enable the reversal of the flow at a given voltage and therefore would allow the device to operate with more flexibility.

Another possible use of the proposed system could be in the local control of the flow direction in microfluidics networks. One could think of such a system to be similar to the one proposed by (133), the difference being that the electrode arrays are replaced by the arrays proposed here. In this way the direction of the flow can be changed in a cross-shaped channel intersection by changing the direction of flow at each array and therefore at each channel. This also has applications in mixing, where the change in flow direction facilitates it.

3.4 Conclusions

In this chapter, a physical model for the ACEO fluid motion has been introduced. ACEO fluid flow has been simulated using a finite element method and verified using results from the literature.

Furthermore, using this model, a novel method has been demonstrated that enables the creation of configurable geometric asymmetries. This method has interesting applications in ACEO pumping at low voltages. Initial numerical simulations of a system designed using the described method, show that it is possible to produce inversion of the pumping velocity direction at low voltages, unlike systems where the asymmetry is fixed into the system. Such systems are particularly useful in microfluidics pumping applications where the use of low voltages is required, as in the local control of flow in microfluidic networks and the pumping of secondary flows that can enhance stirring and mixing.

The ACEO fluid motion is one of the two most important fluid phenomena associated with DEP manipulation systems. The other important phenomenon is the Electrothermal fluid motion. This is a direct subsequence of the heating of the fluid and that is why it is significant in fluids of high conductivity. This is examined in the following chapter.

Chapter 4

Electrothermal fluid motion

In this part, a theoretical model for the Electrothermal motion of a fluid is introduced. The phenomenon is then simulated using the finite element method and verified using data available from the literature. Furthermore, numerical simulations of Electrothermal and ACEO fluid motion are used to investigate their use in biosensor enhancement devices.

4.1 Theory

The Electrothermal force on a fluid is caused by the non-uniform heating of the fluid due to the interaction with the electric field. The electric field causes gradients in the temperature of the fluid and therefore introduces permittivity and conductivity gradients. These in turn lead to dielectric and Coulombic forces on the fluid and mobilise the fluid.

Heat is transferred to the fluid through the electric field and can be found by balancing Joule heating with thermal diffusion (90):

$$\nabla^2 T = -\frac{\sigma E^2}{k_T} \tag{4.1}$$

where T is the temperature, k_T the thermal conductivity, σ the electrical conductivity and E is the rms electric field.

This causes a body force on the fluid, due to gradients in permittivity and conductivity, which is given by (90):

$$\vec{F_e} = -\frac{1}{2}\left[\left(\frac{\nabla\sigma}{\sigma} - \frac{\nabla\epsilon}{\epsilon}\right)\vec{E}\frac{\epsilon\vec{E}}{1+(\omega\tau)^2} + \frac{1}{2}\left|\vec{E}\right|^2\nabla\epsilon\right] \tag{4.2}$$

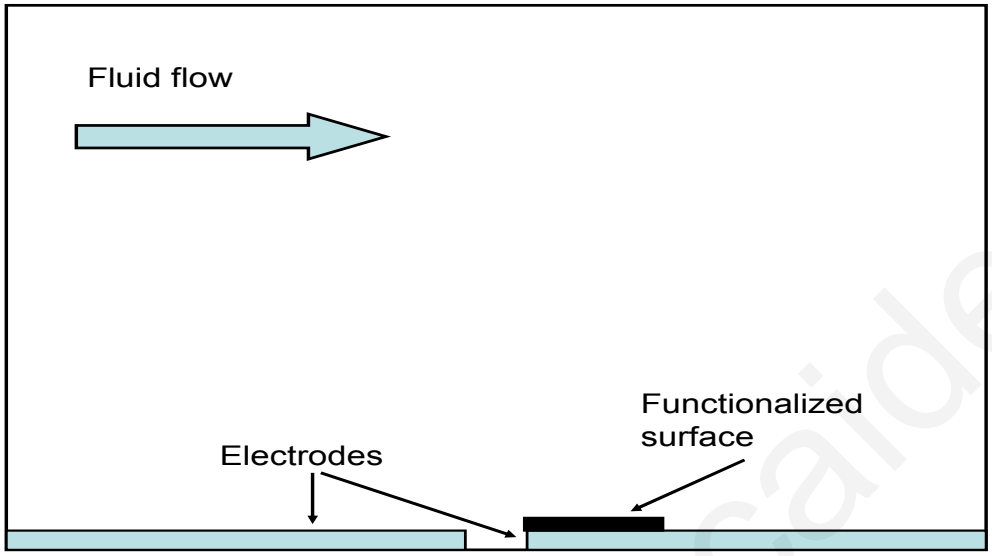

Figure 4.1: System geometry and electrode placement (not to scale).

where $\nabla\epsilon = \frac{\partial\epsilon}{\partial T}\nabla T$, $\nabla\sigma = \frac{\partial\sigma}{\partial T}\nabla T$ and $\tau = \frac{\epsilon}{\sigma}$ is the charge relaxation time. It is evident from this equation that the first term is the Coulomb force whilst the second is the dielectric force on the fluid. As a consequence of the scaling of the first term with frequency there exists a crossover frequency at which the dielectric force becomes dominant. After solving the heat equation, the Navier-Stokes equation is then used to calculate the Electrothermal fluid velocity.

4.2 Model verification

In order to verify the solution method for the Electrothermal motion of a fluid, a system for which there is available literature is analysed and the results are compared. The system chosen is described in (12) and is shown in figure 4.1. The boundaries are numbered in figure 4.2 for ease. The properties for the electrolyte used in the following simulations are shown in table 4.1.

Table 4.1: Electrolyte properties.

Property	**Value**
Thermal conductivity	$2.66\ W.m^{-1}.K^{-1}$
Fluid Viscosity	$1 \times 10^{-3}\ Pa.s$
Diffusion constant	$1 \times 10^{-11}\ m^2.s^{-1}$
$\alpha = \frac{\partial\epsilon}{\partial T}\frac{1}{\epsilon}$	$-0.004\ K^{-1}$
$\beta = \frac{\partial\sigma}{\partial T}\frac{1}{\sigma}$	$0.02\ K^{-1}$

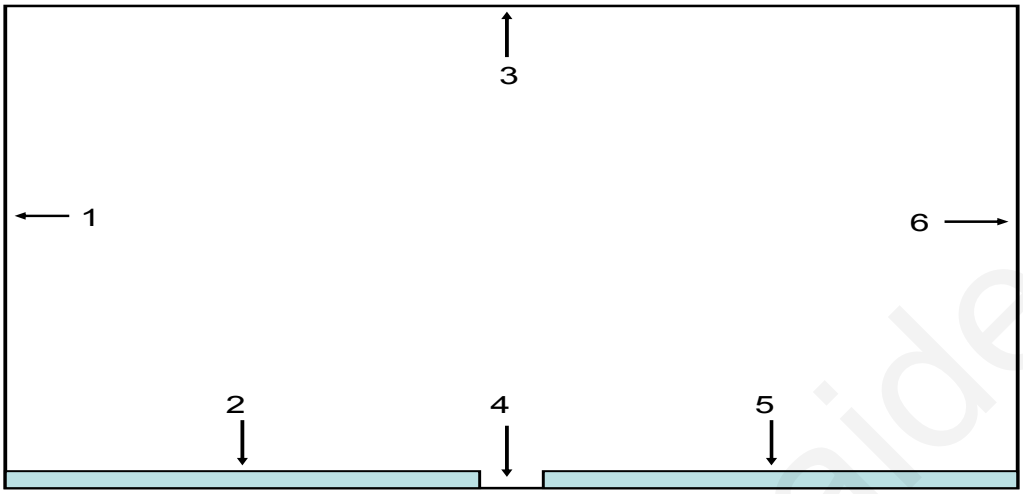

Figure 4.2: Geometry for the domain used in the Electrothermal motion verification, boundaries 2 and 5 are the electrode surfaces (not to scale).

4.2.1 Electric potential

In order to find the electric field distribution in the domain, Laplace's equation is solved with the boundary conditions used for the electrical problem shown in table 4.2. The electric potential formed with 6 V excitation is shown in figure 4.3.

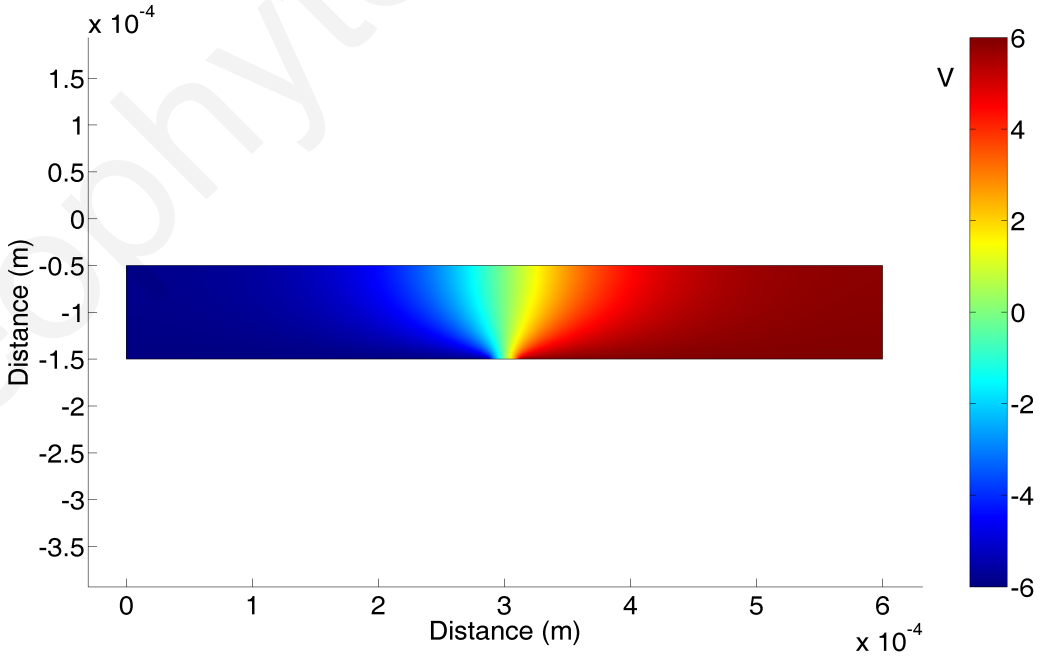

Figure 4.3: Electric Potential by $+6$ V and -6 V electrode excitation.

Table 4.2: Boundary conditions for electric problem.

Boundary Number	**Boundary Condition**
5	Dirichlet boundary condition, $V = 6\ V$
2	Dirichlet boundary condition, $V = -6\ V$
1, 3, 4, 6	Neumann boundary condition

4.2.2 Heating of the fluid

The heating of the fluid due to the presence of the electric field is given by the solution of equation 4.1 described earlier. The boundary conditions used for the heat problem are shown in table 4.3 and the resulting temperature distribution is shown in figure 4.4.

Table 4.3: Boundary conditions for heat problem.

Boundary Number	**Boundary Condition**
3, 4	Thermal insulation, $T = 300\ K$
1, 2, 5	Fixed Temperature, $T = 300\ K$

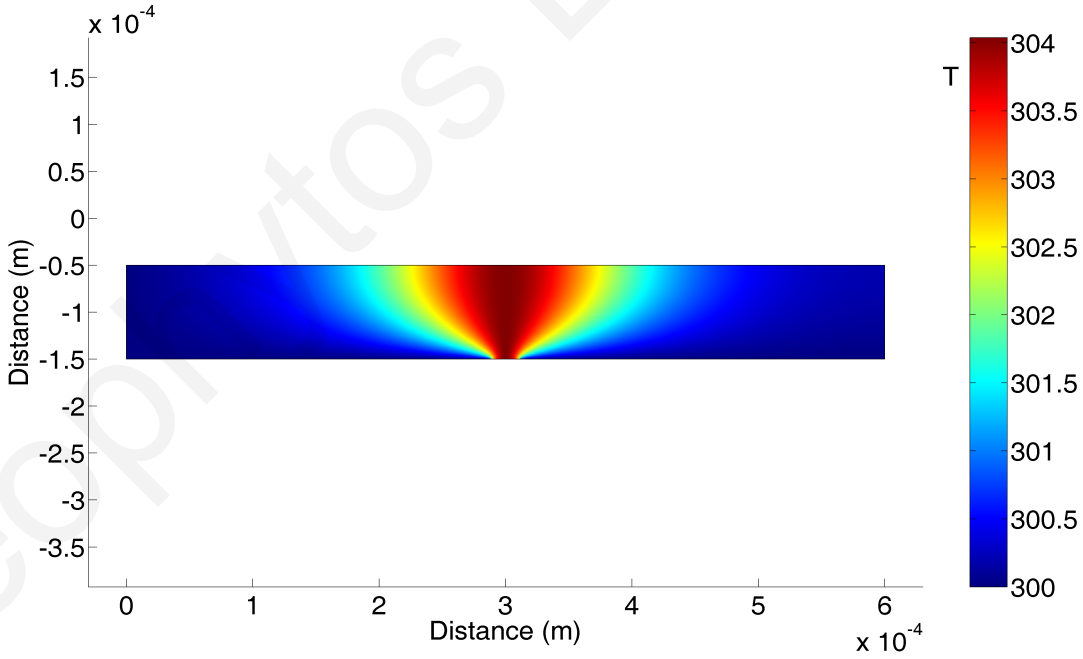

Figure 4.4: Temperature distribution in the domain after 5 s under electrode excitation.

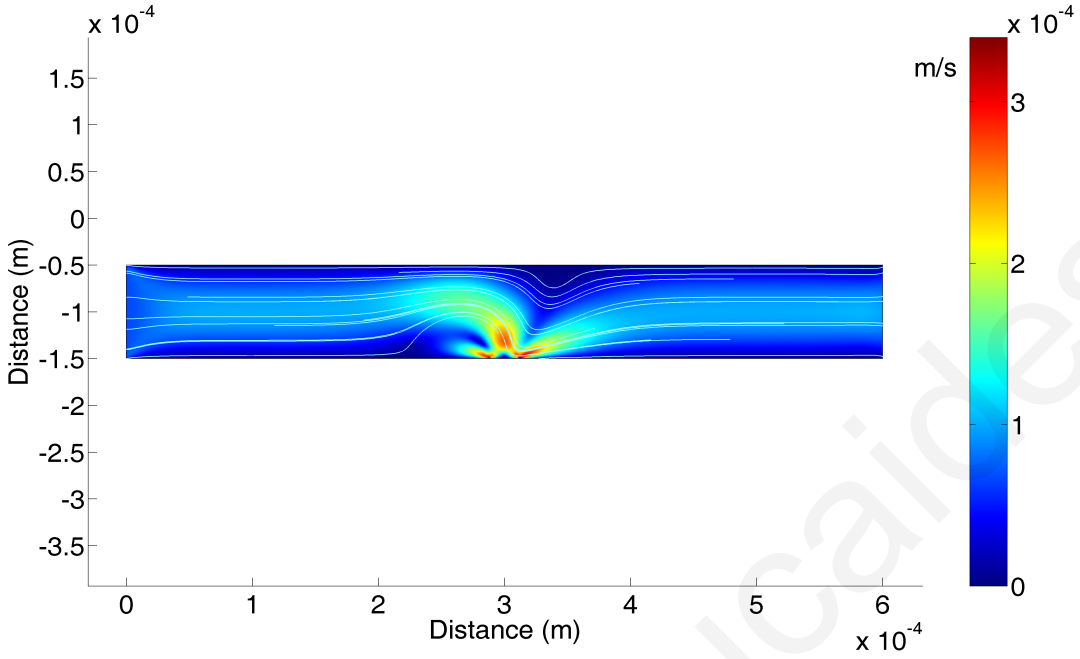

Figure 4.5: Velocity distribution in the domain after 5 s under electrode excitation.

4.2.3 Electrothermal motion of the fluid

The Navier-Stokes equation for the fluid under the Electrothermal force becomes (90):

$$\eta\nabla^2\vec{u}_f - \nabla p + \vec{F}_e = 0 \tag{4.3}$$

$$\nabla\cdot\vec{u}_f = 0 \tag{4.4}$$

where $\vec{F}_e$ is the Electrothermal body force, p the fluid pressure, $\vec{u}_f$ the velocity of the fluid and $\vec{F}_e$ is given by equation 4.2 described earlier. The boundary conditions for the fluid motion are given in table 4.4. The resulting fluid motion is shown in figure 4.5.

Table 4.4: Boundary conditions for fluid dynamics problem.

Boundary Number	**Boundary Condition**
2, 3, 4, 5	No slip
1	Inflow, Fixed velocity
6	Outflow, Pressure=0

4.2.4 Characteristics of the Electrothermal motion

By choosing a point in the domain and noting the maximum induced velocity and the temperature variation the results presented in table 4.5 are obtained.

The results in table 4.5 demonstrate a factor of four increase in temperature rise and the factor of sixteen increase in maximum velocity, a relation predicted theoretically in (90).

Table 4.5: Temperature and velocity variation with electrode voltage.

Property	**Value 1**	**Value 2**
Voltage on electrodes	6 V	12 V
Maximum velocity	0.39 $mm.s^{-1}$	6.3 $mm.s^{-1}$
ΔT	4.1 K	16.3 K

In this section the model used for the Electrothermal motion of the fluid has been verified using data available from the literature. In the following section, this model is used to investigate the operation of a device (and a number of variations) proposed by (101) for Electrothermal stirring, as well as the possibility of using ACEO in similar applications.

4.3 Results

4.3.1 ACEO and Electrothermal biosensor enhancement

An interesting subject is the possibility of using ACEO and/or Electrothermal fluid motions to produce an enhancement of the concentration of a species on the surface of a sensor in a microchannel. The enhancement can be achieved by utilising these methods at different stages of the manipulation or at the same time by using a fluid conductivity strong enough to give Electrothermal motion without making ACEO too small. Furthermore, the ACEO fluid motion can be used in devices where it is necessary for some reason for the fluid conductivity to be low, therefore rendering the use of Electrothermal stirring impossible.

In this section the effects of EHD phenomena on the enhancement of reactions in capillary sensors are analysed, as well as methods to combine these (ACEO and Electrothermal). It is shown here that ACEO can cause significant enhancement during the operation of the device, which is smaller in magnitude than the one caused by Electrothermal, but also consumes significantly less energy. It is also shown that the use of ACEO and Electrothermal enhancement simultaneously in a device produces an effect greater than the effect of each method separately, for certain ranges of solution conductivity.

The system of interest is one that consists of a functionalised surface in a capillary. Such systems are expected to appear frequently in lab-on-chip devices, since one of the most important applications of such devices is the detection of a substance in a fluid by reacting with a receptor substance.

The system geometry is shown in figure 4.1. The channel length is 600 μm, the channel depth is 100 μm, the interelectrode gap is 25 μm and the functionalised surface length is 50 μm. The dimensions have been chosen so that a direct comparison with previously published results (101) can be made.

In this particular system, the process under investigation is the detection of an antigen present in the fluid injected at the left side of the capillary. This antigen is detected by binding to a functionalised surface of immobilised antibodies, indicated in figure 4.1. Very often the reaction slows down if the diffusion of the antigen alone is not capable of feeding the reaction and the area above the functionalised surface is depleted of antigen (101), posing a significant shortcoming in its operation. In order to alleviate the problem above, it has been proposed that using Electrothermal fluid stirring the reaction can be enhanced at the functionalised surface (101) (134). The EHD stirring carries away the depleted antigen and therefore fresh antigen is exposed to the functionalised surface. As a result the reaction becomes faster, or alternatively the required sample for the same detection time becomes lower.

4.3.1.1 AC Electroosmotic fluid motion

The ACEO fluid flow is caused by the interaction of the ions in the double layer with the tangential electric field on the electrode surface. The theory used to simulate the phenomenon is analysed in section 3.1.2.

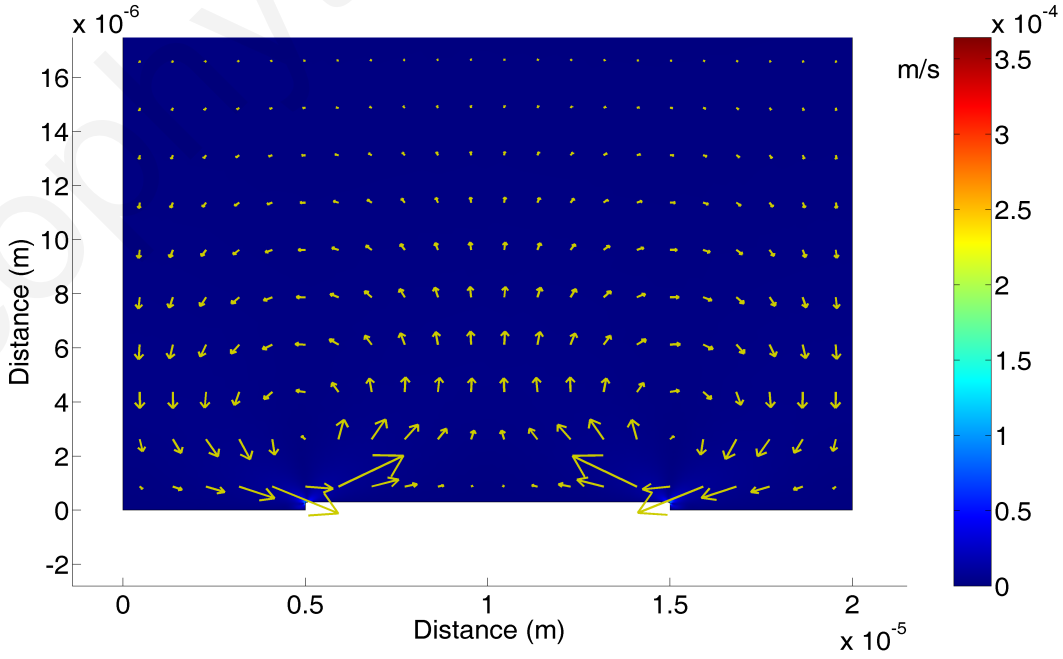

Figure 4.6: ACEO fluid velocity over an electrode in a parallel array.

The ACEO fluid flow over an electrode is shown in figure 4.6. One can observe here the characteristic circular patterns produced by ACEO above the electrode edges.

4.3.1.2 Electrothermal fluid motion

The Electrothermal fluid motion is found using the Navier-Stokes equations 4.4 described earlier, where the body force is found using equation 4.2. The Electrothermal fluid flow over two electrodes is shown in 4.7. Here the characteristic pattern of the flow can be seen, with the fluid moving down the symmetry line between the electrodes and towards the electrode centre.

4.3.1.3 Fluid flow problem

A fluid (water with KCl in this case) is injected into the capillary, containing the antigen to be detected. The Navier-Stokes equations are used to model the fluid motion under both EHD phenomena.

The entry boundary is set to constant speed u_f, the exit to a neutral boundary condition, the electrode surface to the ACEO induced slip velocity and the rest of the boundaries are set to a no-slip condition. Depending on whether the Electrothermal or ACEO effects are deactivated, $\vec{F_e}$ or u_{slip} are set to zero respectively.

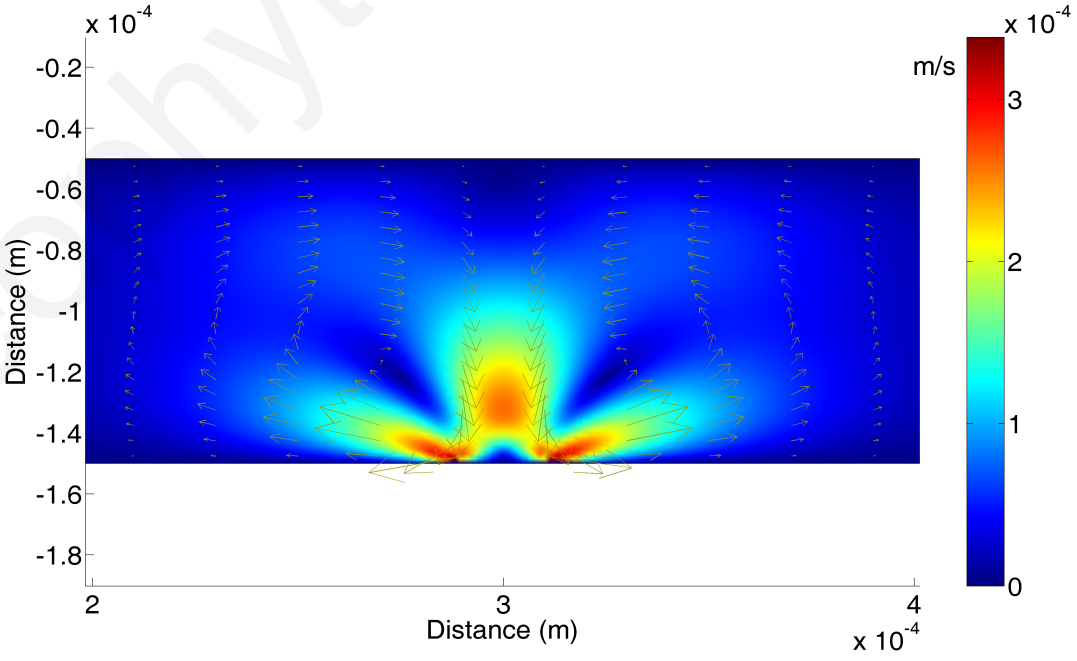

Figure 4.7: Electrothermal fluid velocity between two electrodes in a parallel array.

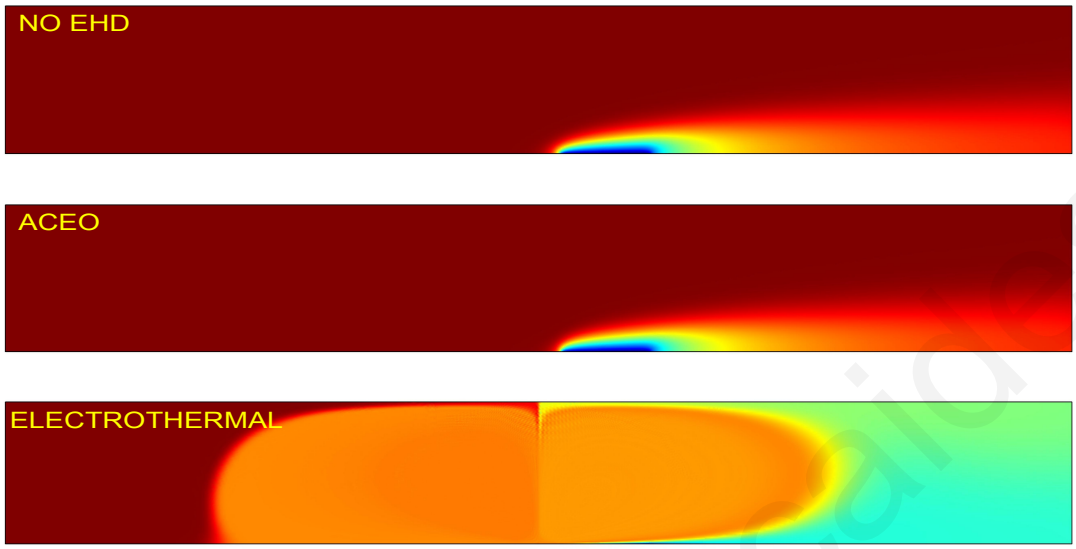

Figure 4.8: Antigen concentration for the three cases of (a) No EHD enhancement, (b) ACEO enhancement and (c) Electrothermal enhancement.

4.3.1.4 Antigen motion and reaction

The antigen motion is described by the convection-diffusion equation:

$$\frac{\partial C}{\partial t} = D\nabla^2 C - \vec{u}_f.\nabla C \tag{4.5}$$

where C is the concentration of the antigen and $\vec{u}_f$ is the velocity of the fluid, which is due to pressure pumping and any EHD induced motion.

The reaction of the antigen with the immobilised antibodies at the functionalised surface is given by (135):

$$\frac{\partial B}{\partial t} = k_{on}C(R_T - B) - k_{off}B \tag{4.6}$$

The definition of the parameters and their values are given in table 4.6. The rate of antigen binding must be equal to the diffusive flux at the functionalised surface (135):

$$\frac{\partial B}{\partial t} = \vec{n}.D\nabla C \tag{4.7}$$

where $\vec{n}$ is the vector normal to the surface. The antigen introduction is simulated by imposing a steady concentration at the entry of the capillary, at 0.1 nM, whilst the exit is set to convective flux and the rest of the boundaries to insulation.

Table 4.6: Properties of the system.

Property	Value
k_{on} (on rate constant)	$10^{-3}\ s^{-1}$
k_{off} (off rate constant)	$10^{6}\ (M.s)^{-1}$
D (antigen diffusion constant)	$10^{-11}\ m^2.s^{-1}$
R_T (receptor concentration)	$3.3 \times 10^{-11}\ M.m$
σ (fluid conductivity)	$0.66\ S.m^{-1}$
η_f (fluid viscosity)	$10^{-3}\ Pa.s$
Pe (Péclet ratio)	100
Da (Damkohler number)	330
u_{fp} (pressure induced fluid velocity)	$10\ \mu m.s^{-1}$
C_0 (concentration at entrance of channel)	$0.1\ nM$
F (frequency)	$200\ kHz$

4.3.1.5 Electrothermal enhancement

The enhancement of the bound antigen is studied here, which is defined as $B_e = \frac{B}{B_0}$, the ratio of the bound antigen after the EHD is introduced, over the value of the bound antigen concentration before the EHD is introduced. More specifically, the system is studied with the properties listed in table 4.6. A snapshot of the system antigen concentration after 100 s of introducing the antigen to the capillary is shown in figure 4.8, for various cases. One can see that both in the case of the fluid flow alone (no EHD enhancement) and in the case where ACEO is introduced, the depleted antigen remains largely over the functionalised surface, as can be seen by the darker colour of the antigen concentration over the electrode in figure 4.8 cases (a) No EHD and (b) ACEO only. The case with ACEO enhancement shows that the depleted region over the electrode moves slightly to the right due to the ACEO velocity. This means that significant enhancement is expected at the left side of the functionalised surface and much less at the right side. The Electrothermal enhancement is less localised and mobilises a larger amount of antigen, forming large circular loops.

The enhancement factor is dependent on the Damkohler number ($D_a = \frac{k_{on} R_T h}{D}$), the ratio of reaction speed to diffusion speed and the Péclet ratio ($Pe = \frac{uh}{D}$), the ratio of convective velocity to diffusive velocity. The analysis of this dependence has been carried out in (101).

Another issue of interest is the effect of the voltage applied on the electrodes (the voltage that causes the Electrothermal motion) on the enhancement factor. The enhancement factor is plotted against applied voltage in figure 4.9. It can be seen from this figure that for the inner side of the functionalised surface, there is a voltage where the enhancement obtained is maximum, before and after which the enhancement decreases.

For the case of lower voltage than the voltage at the peak enhancement, the reduction exists because the depleted antigen is not removed fast enough. For the case that the voltage is larger than the voltage at the peak, the reduction exists due to the fact that

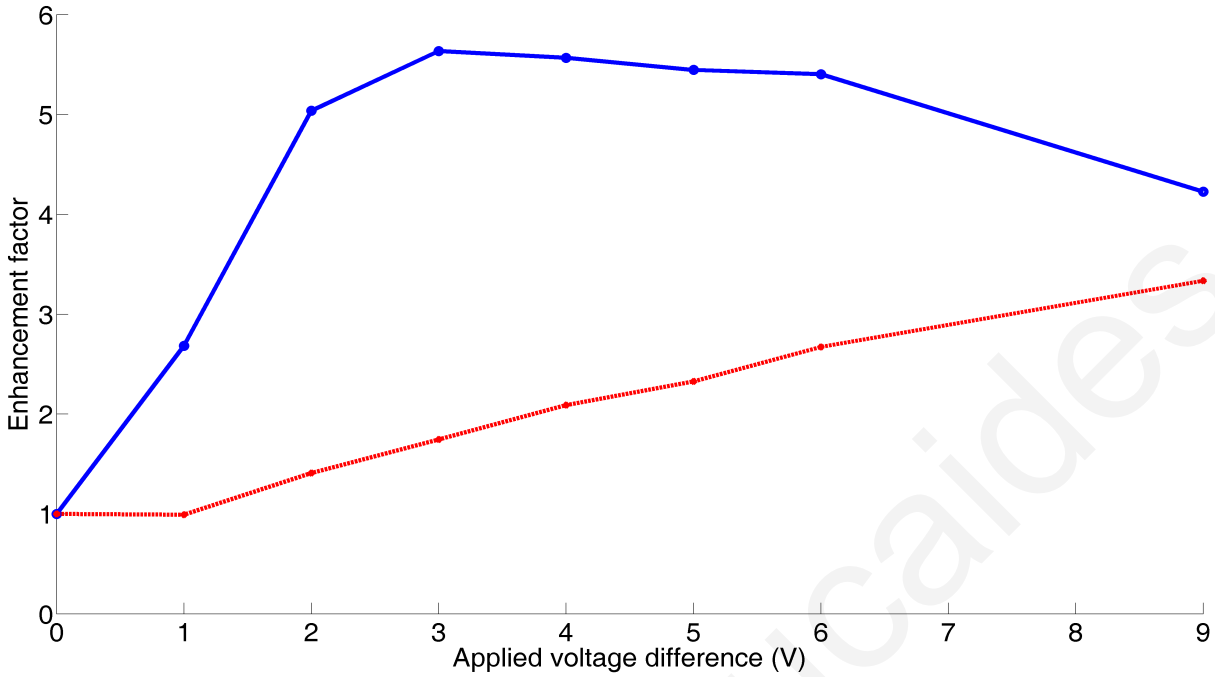

Figure 4.9: Enhancement of bound antigen vs applied Voltage for Electrothermal fluid motion after 100 s. Dashed line is for the outer side, solid line is for inner side of the functionalised surface.

the velocity of the fluid becomes such that it not only removes the depleted antigen, but also removes the non-depleted part. For the outer side of the surface the enhancement increases constantly with voltage. This happens because the form of the flow is such that the outer side is always exposed to the streamlines of the non-depleted antigen, in contrast to the inner side.

4.3.1.6 ACEO enhancement

A similar enhancement effect can also be produced by ACEO. To achieve ACEO fluid motion, lower conductivity is required, so that the induced double layer is deep enough. Therefore the fluid motion is examined at the inner side of the functionalised electrode surface for conductivity $\sigma = 1.23\ mS.m^{-1}$, for which the Debye length is approximately 30 nm. The frequency of peak ACEO velocity for this system is approximately at 10 kHz and therefore this value is used in the ACEO simulations. The enhancement versus applied voltage for ACEO at this frequency is shown in figure 4.10. It is evident that there is a significant enhancement using ACEO. This is lower by approximately a factor of two compared to the enhancement obtained by Electrothermal methods. However, it should be noted that the ACEO method theoretically consumes a very small amount of energy compared to Electrothermal and does not heat the fluid significantly, which could be a significant advantage in some devices.

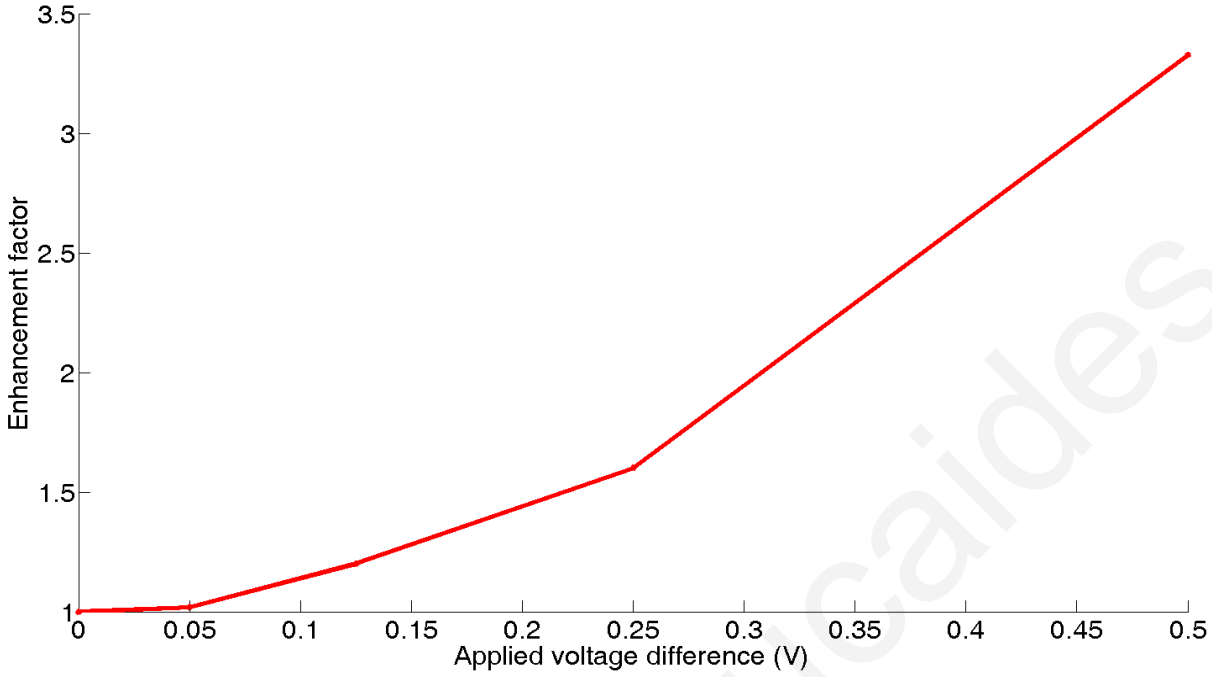

Figure 4.10: Enhancement of bound antigen vs Voltage difference for ACEO after 100 s. The results are for the inner side of the functionalised surface.

An important issue is discussed in (101) on the possible effect of ACEO, which has large surface velocity, on the lifetime of the bonds on the functionalised surface. Here the effect of ACEO on the shortening of the lifetime of the bonds is not taken into account. This characteristic of ACEO, with high surface velocity, might be beneficial (if one wants the bonds to break), destructive (if one does not want the bonds to break) or negligible (if the bonds do break but their lifetime is very high anyway) depending on the reaction on the surface and the general operation of the system. Therefore, this should be considered depending on the system, its use and type of bonds forming.

In the past, ACEO has been demonstrated to aid in focusing particles for detection in devices where low particle concentration was a problem (132). This was done by depositing the particles at the stagnation point on an electrode, where ACEO was zero. Therefore possible effects of the position of the functionalised surface and the electrode size and placement could be beneficial in using ACEO for enhancement and should be further investigated.

4.3.1.7 Joint enhancement

For the low conductivity case, the system is also examined under the influence of both the ACEO and Electrothermal effects. This is done by imposing the slip velocity condition caused by ACEO on the electrode surface and the Electrothermal body force simultaneously, using the same settings as in the previous two sections for both effects.

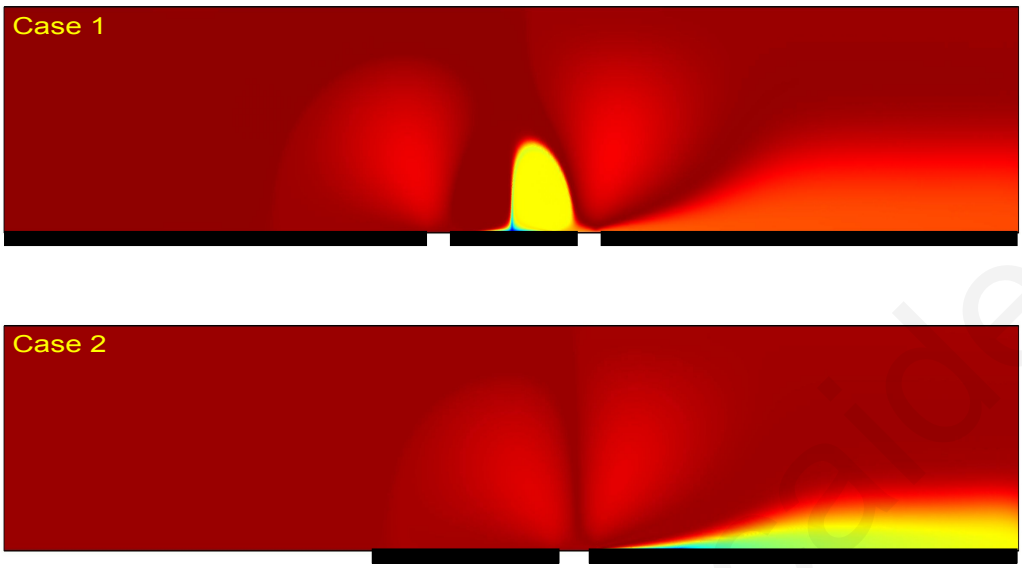

Figure 4.11: Antigen concentration for two alternative cases of electrode designs(a) Case 1: Three-electrode design and (b) Case 2: Two-electrode design.

It was found that the ACEO alone at 0.5 V potential difference between the electrodes produces an enhancement of 3.3, whereas at 6 V rms the Electrothermal enhancement at this conductivity (with the rest of the settings as before) is 3.0. The joint enhancement (when both are used simultaneously) is 4.2 for the inner side of the functionalised surface for these conditions. These results indicate that there is a possibility to combine the flows to produce increased enhancement, also exploiting the reduction in power consumed due to the lower heat dissipated. It might also be possible to combine the flows by using each one at different stages during the operation of the device. Electrothermal fluid motion is more powerful in the bulk and therefore will carry more antigen towards the functionalised surface, whilst ACEO is stronger on the surface and may help in carrying away the depleted particles.

4.3.1.8 Other electrode configurations

Other electrode configurations were also tested in order to investigate the possibility of improving the enhancement by changing the electrode geometry. The investigation (utilising Electrothermal fluid motion only) showed that the set-up proposed by (101) was actually better than the ones tested for this purpose. The two alternative configurations are shown in figure 4.11. Case 1 consists of two larger electrodes with a smaller one (where the functionalised surface is placed), while case 2 consists of an asymmetric configuration of electrodes where the functionalised surface is placed at the inner edge of the larger

electrode. The antigen concentration in case 1 indicates that the depleted material is actually trapped over the electrode. This might be useful where the intention is to keep the material over the functionalised surface long after the reaction has taken place.

4.4 Conclusions

In this chapter a physical model for the Electrothermal motion of the fluid was introduced. The operation of a number of devices utilising Electrothermal motion was simulated using the finite element method and compared with results available in the literature.

Furthermore, the enhancement of the binding of antigen on a functionalised surface in a capillary sensor by using EHD was analysed. The dependence of enhancement on voltage was investigated and the behaviour was explained for both Electrothermal and ACEO fluid motion. It was also demonstrated that ACEO and Electrothermal fluid motion can be combined by the use of different frequency signals applied on the same electrode at low conductivities, so that each can be controlled separately to produce a hybrid effect. The advantage of using ACEO for fluid stirring is the reduced power consumption and the avoidance of excessive heating of the sample, which can be significant for some cases when using Electrothermal stirring.

Up to this point, the fluid phenomena and DEP have been examined separately. However, these are usually co-existent in real systems and it is important that they are investigated simultaneously. In the following chapter, this is done for DEP and ACEO simultaneously, in a low conductivity electrolyte.

Chapter 5

Combined Dielectrophoresis and AC Electroosmosis using velocity field analysis

The phenomena of DEP and ACEO are usually coexistent in DEP manipulation devices, such as the parallel electrode device. Due to the increased complexity of both phenomena acting on the particles simultaneously, several trapping regions are formed, which are very important for DEP manipulation devices. The position and nature of these is investigated in this chapter.

5.1 Introduction

Investigations into the nature of particle traps formed in parallel electrode arrays by joint DEP and ACEO have shown that there is trapping both at positive and negative DEP which changes form as the particle size varies (136) (137). This is an important phenomenon with many applications, such as in sensor devices where one needs to selectively trap and manipulate nanoparticles for detection purposes. What is also important is that the method can operate at very small scales and can be used for mass processing of a sample, in contrast to mechanical methods. The trapping and manipulation of nanoparticles by joint ACEO and DEP is investigated in this chapter. The combination of DEP with ACEO and Electrothermal fluid motions is a very promising technique due to the properties of each phenomenon. DEP is very strong close to the electrodes and can trap the particles once there, while ACEO or Electrothermal phenomena have a longer reach due to the fact that they mobilise the surrounding fluid.

Table 5.1: Electrolyte properties.

Property	Value
Fluid Viscosity (η_f)	$1 \times 10^{-3}\ Pa.s$
Relative permittivity of medium (ϵ_{mr})	80
Relative permittivity of particle (ϵ_{pr})	2.5
Λ	0.25
Permittivity of free space (ϵ_0)	$8.8542 \times 10^{-12}\ F.m^{-1}$
Conductivity of medium (σ_m)	$1.23\ mS.m^{-1}$
Conductivity of particle (σ_p)	$9\ mS.m^{-1}$
Fluid density (ρ_f)	$1 \times 10^{3}\ kg.m^{-3}$
Particle density (ρ_p)	$1.1 \times 10^{3}\ kg.m^{-3}$

The current state of the art uses combined ACEO with DEP (28) (138) (78) or combined Electrothermal with DEP (139) (104).

In this chapter, nanoparticles are used in a solution over an array of parallel or configurable asymmetric electrodes (82) and a potential is applied on the electrodes, to cause the DEP force on the particles and induce the ACEO fluid motion. The concept of nanoparticle trapping by joint DEP and ACEO is extended in this work by using a configurable asymmetric electrode system to create stable trapping zones of which the location can be changed by altering the electrode excitation. These zones are observed at the location where an electrode of finite height meets the substrate, instead of the electrode edge as ACEO is also strong at the edge and hence carries the particles away.

5.2 Results

In this investigation a device is simulated that consists of an array of identical parallel electrodes 20 μm wide and placed 20 μm apart. The electrolyte and particle properties used are stated in table 5.1, unless otherwise stated. The Clausius-Mossotti factor for the fluid and particle is shown in figure 5.1. A potential is applied on the electrodes and as a result a DEP force is exerted on the particles in the fluid. The fluid is mobilised by ACEO and therefore through drag a force is also exerted on the particles. The important feature that is of interest here is the particle radius at which the stable DEP/ACEO traps form over the electrodes, which are defined as the points where the particle velocity is zero. The stable trapping points are those with restoring velocity near the point, whereas unstable are the points for which if the particle moves even by an infinitesimal degree away from the point, it will be carried away from the point (140).

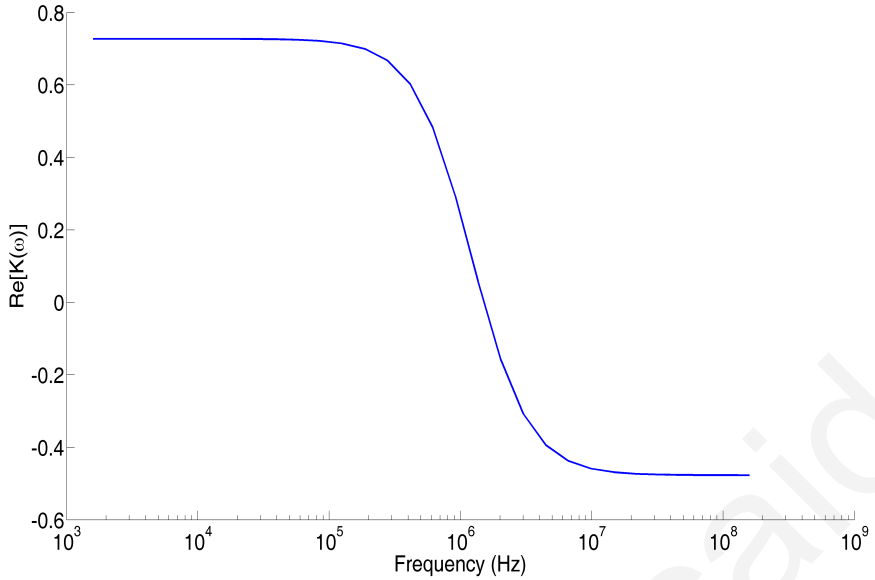

Figure 5.1: Real part of the Clausius-Mossotti factor for the system of particle and fluid with the properties given in table 5.1.

5.2.1 Positive DEP

In this part of the work, the voltage settings are 5 V, 10 kHz. The particle radius is varied and the flows shown in figures 5.2, 5.3, 5.4 and 5.5 are observed. The trapping points at the electrode edges are well known and are not discussed here, since they exist even without the presence of ACEO. In figure 5.2 it can be seen that for particle radius of $a = 0.1$ μm there are two unstable trapping points formed inside the ACEO whirls.

The points here are formed because ACEO is dominant at lower particle radii as it does not scale with particle radius while DEP scales with the particle volume. The points are unstable for positive DEP because when the particle is disturbed (say by Brownian motion) from the zero velocity point, it will move towards the electrodes. Therefore the instability is in the vertical direction. This is not the case for negative DEP, where the DEP and ACEO also balance in the vertical direction, therefore making these trapping points stable. As the particle radius increases, the trapping point moves towards the electrodes. The ACEO-induced velocity is constant, therefore as the particle gets larger the positive DEP has a longer reach and the trapping point will move further away from the electrode, as seen in figures 5.3 and 5.4. The meaning of this is that for all points vertically above the electrode centre and closer to the electrode than this point, the velocity field is pointing vertically downwards and therefore the particle will move towards the electrode.

In this investigation, it was also found that a situation arises in positive DEP where a stable trapping point forms on the electrode surface in the middle, as shown in figure 5.5. This situation arises when DEP is stronger than ACEO in the vertical direction and ACEO is stronger in the horizontal direction.

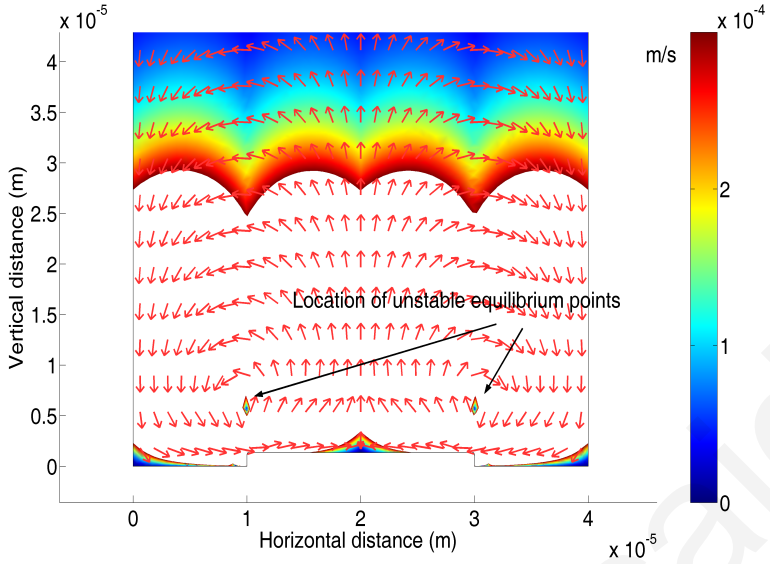

Figure 5.2: Plot of overall velocity of a particle at 10 kHz for particle radius $a = 0.1$ μm.

The same phenomenon has also been observed in (137).

5.2.2 Negative DEP

Here the effect of the particle radius in the formation of stable trapping points is investigated, using the same settings as before but the frequency is changed to 5 MHz. The frequency of 5 MHz means that the DEP is now in the negative DEP region, as seen in figure 5.1. The flows shown in figures 5.6, 5.7 and 5.8 are observed for the different particle radii. It can be seen that again, as in positive DEP, for small particle radius ACEO motion dominates in the fluid bulk as in figures 5.6 and 5.7.

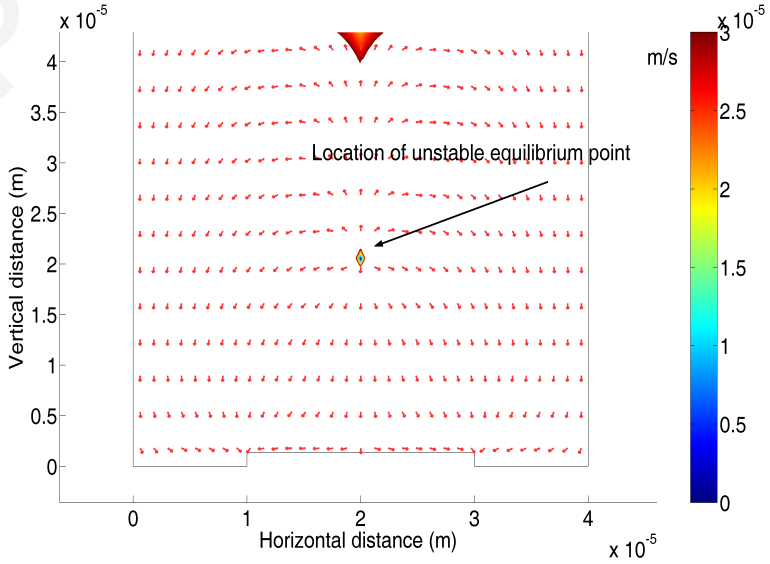

Figure 5.3: Plot of overall velocity of a particle at 10 kHz for particle radius $a = 2$ μm.

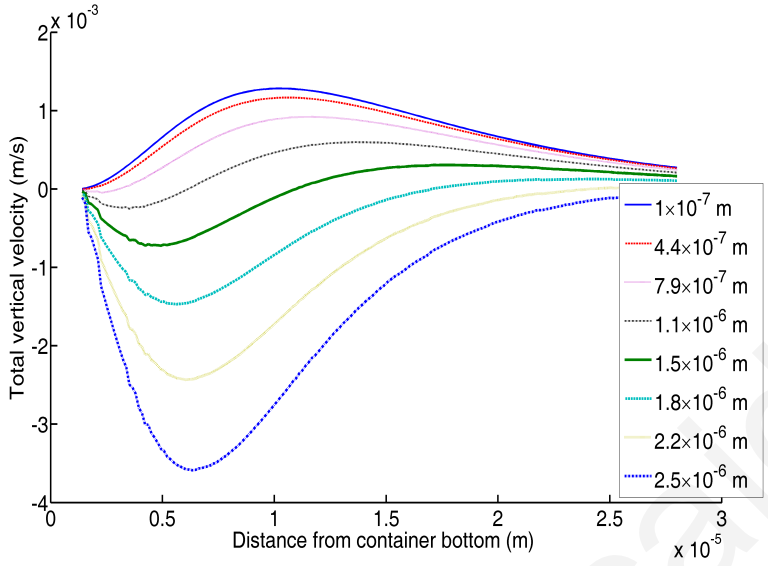

Figure 5.4: Plot of the unstable trapping point (point where the curves cross the x-axis) movement as the particle size changes from $0.1 - 2.5$ μm.

As the particle radius gets larger DEP begins to become comparable with ACEO and it can be observed in figure 5.8 that after 5 nm the ACEO characteristic whirls start to disappear. The trapping points in the middle of the interelectrode space and in the middle of the electrode surface are not discussed here because these exist in negative DEP even when ACEO is not present. It has to be noted here that while the particular settings for frequency and particle size might be of little use in practical systems, similar system dynamics might be obtained for real devices. Therefore, the trapping regions investigated here could appear in combined negative DEP/ACEO situations at different particle sizes and frequencies of excitation.

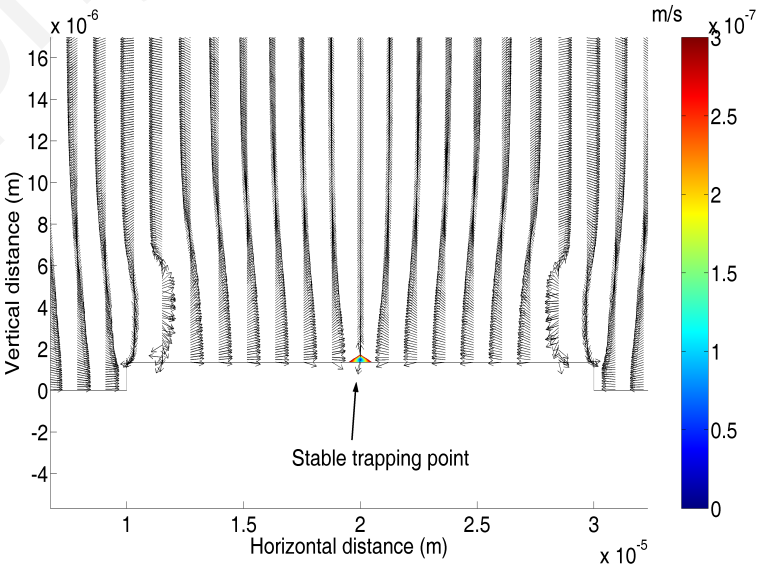

Figure 5.5: Plot of the stable trapping point over electrode at 10 kHz, for particle radius 900 nm and electrode excitation of 0.5 V.

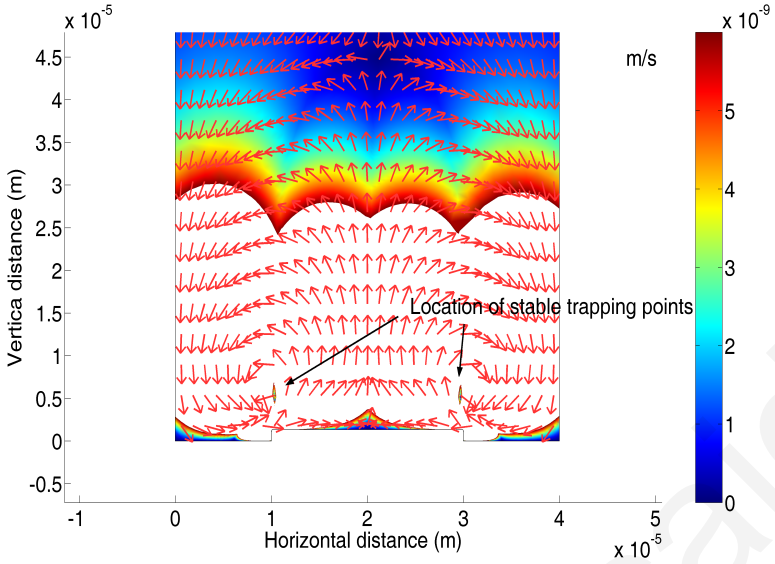

Figure 5.6: Plot of overall velocity of a particle at 5 MHz for particle radius $a = 0.1$ nm.

5.2.3 Asymmetric electrodes

Trapping is also investigated for the case of configurable asymmetric electrodes. The system is described in detail in (82) and consists of arrays of three identical electrodes. The simulations are performed with the same settings as in table 5.1, except that the particle radius is 1 nm and the excitation is 0.5 V. The grouping of electrodes in terms of excitation creates an asymmetry that is configurable. For example, if the two electrodes on the left are grouped together the asymmetry is reversed from the case where the two electrodes on the right are set at the same AC potential. This method of configurable asymmetry has already been demonstrated to be capable of creating a reversible pumping effect.

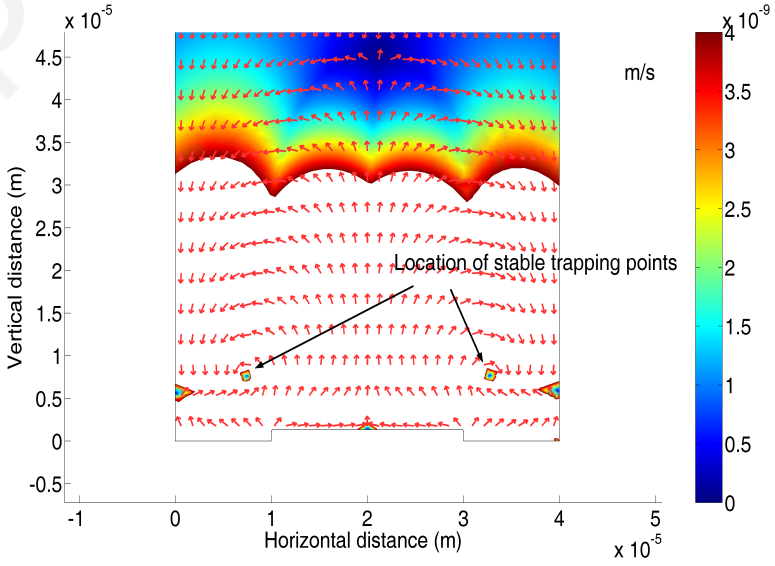

Figure 5.7: Plot of overall velocity of a particle at 5 MHz for particle radius $a = 5$ nm.

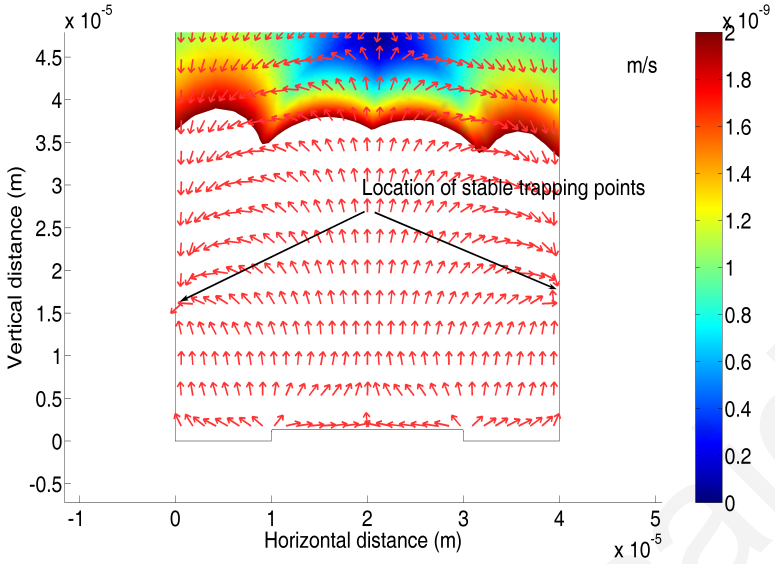

Figure 5.8: Plot of overall velocity of a particle at 5 MHz for particle radius $a = 10$ nm.

Here it is demonstrated that it can be used to create stable trapping points whose position can be changed by altering the electrode grouping.

5.2.3.1 Asymmetric electrode simulation

It is of great interest to describe not only the velocity field for a particle, but also the concentration distribution of an ensemble of particles of finite size, taking into account that some diffusion is present. To describe the particle concentration one may use the Smoluchowski equation, as described in (127). The particles described in the previous section are large enough for diffusion to be very small compared to the velocities induced here.

This causes two major problems in the simulation of the concentration for such a system. The first one is that the very high spatial concentrations require the use of a very high number of mesh points. The second problem is that in the Smoluchowski equation, the finite size of the particles and therefore the maximum possible volume fraction of particles at close packing is not taken into account.

In order to avoid the issues aforementioned, some modifications have been implemented. Firstly, a function is applied that multiplies the DEP velocity so that it takes into account the fact that as particles come close to maximum close packing, their velocity decreases. Secondly, the diffusion constant is modified to include a step function which introduces large diffusion in the system so that the concentration does not exceed the value of $C = 0.64$ for maximum close packing of spheres (124). The subject of steric effects is dealt with in more detail in chapter 7.

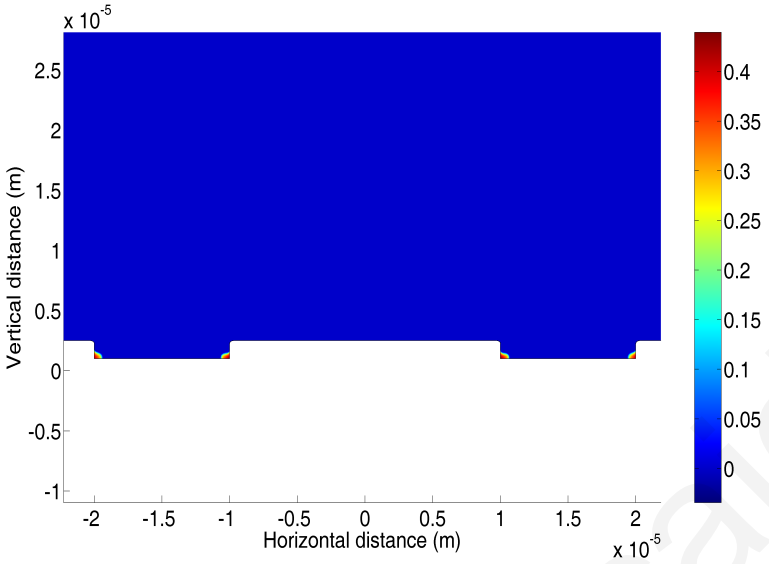

Figure 5.9: Volume fraction of particles of 600 nm particle radius at 10 kHz, 0.5 V under both DEP and ACEO at steady state symmetric excitation.

The modifications used here effectively limit the maximum concentration and achieve convergence without compromising the physical insight. The results obtained for an initial volume fraction of 1×10^{-4} of 600 nm radius particles under the same parameters as in the previous section are displayed in figures 5.9 and 5.10 for the symmetric and figures 5.11 and 5.12 for the asymmetric excitation of the electrodes, after they have reached steady state. The main distinguishing features are that the particles are not trapped at the electrode centre in the symmetric excitation, as shown in figure 5.9 and that in both cases the particles are trapped at the interface between the electrode and the substrate and not at the electrode edges.

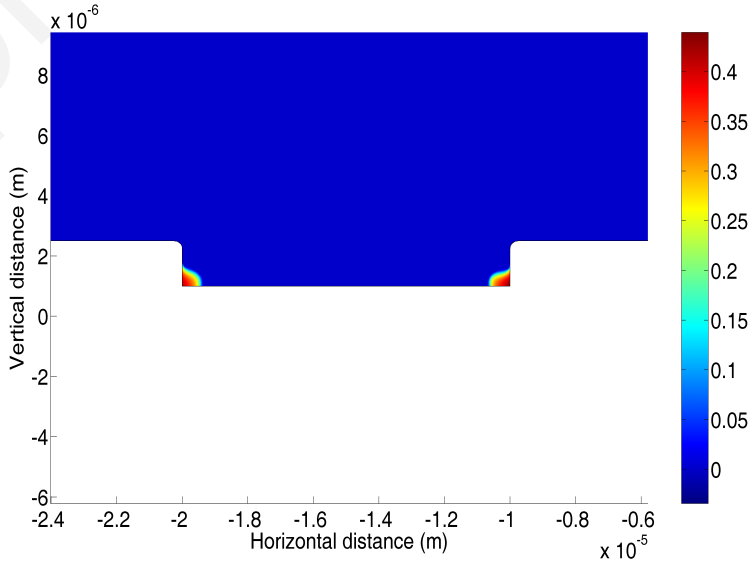

Figure 5.10: Volume fraction of particles of 600 nm particle radius at 10 kHz, 0.5 V under both DEP and ACEO at steady state symmetric excitation, zoomed.

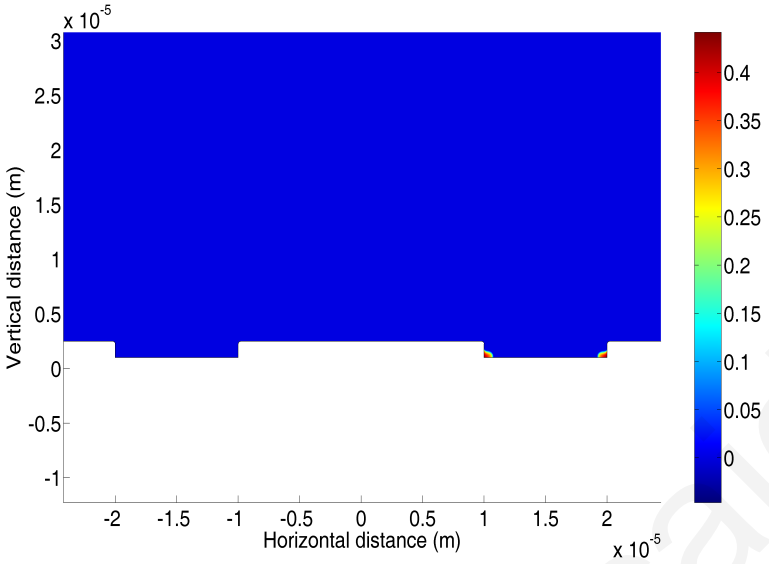

Figure 5.11: Volume fraction of particles of 600 nm particle radius at 10 kHz, 0.5 V under both DEP and ACEO at steady state asymmetric excitation, where electrodes 1 and 2 are in-phase.

This can be attributed to the fact that while DEP is strongest at the electrode edge, so is ACEO, therefore carrying the particles away (an issue that is pointed out in (101) as a possible disadvantage when using ACEO to collect particles to sensor surfaces located at the electrode edges). In relation to the trapping at the electrode centre, taking diffusion into account makes trapping at the electrode centres disappear for this system. It must be noted that these observations are valid for the system examined subject to these particular parameters.

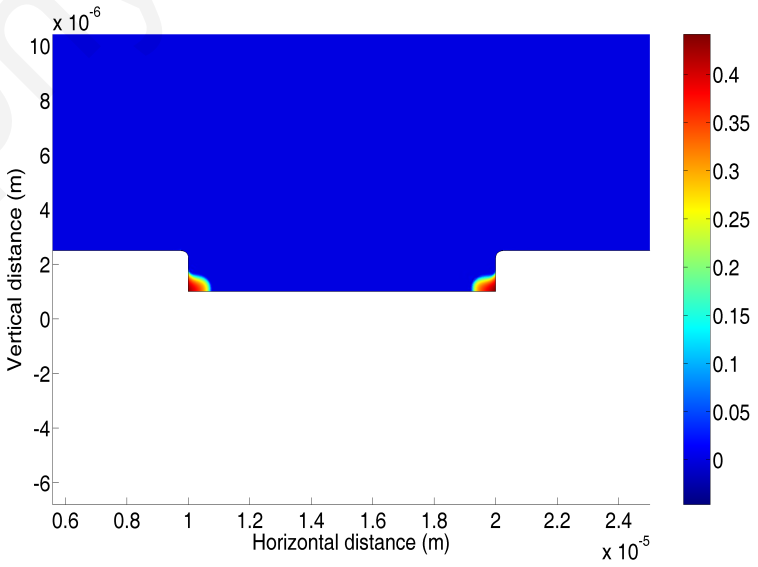

Figure 5.12: Volume fraction of particles of 600 nm particle radius at 10 kHz, 0.5 V under both DEP and ACEO at steady state asymmetric excitation, where electrodes 1 and 2 are in-phase, zoomed.

The observation that particles gather preferentially to one side due to higher DEP in that region, can be useful for many applications, such as moving a particle to different sensor surfaces in sequence or assembling different particles to different positions on a surface.

5.3 Conclusions

Numerical simulations were used here to investigate the existence and behaviour of trapping points in parallel electrode and configurable asymmetric electrode systems, under the combined influence of positive DEP and ACEO.

It was found that using a configurable asymmetric system it might be possible to trap particles either in a symmetric or an asymmetric manner, with the degree of precision and flexibility being related to the device characteristic scale and number of electrodes in an array. Therefore, such a system might be useful in devices where small scale precision manipulation of particles is required, such as in sensor devices.

Furthermore, the DEP and ACEO velocity fields were investigated simultaneously, revealing the joint effect on the particles. However, in order to examine the system dynamics, it is necessary to model the evolution of the particle concentration taking into account diffusion of the particles. This is done in the next chapter, where the system dynamics of a device for DNA trapping are analysed using a Smoluchowski equation to describe the evolution of the particle concentration.

Chapter 6

Combined Dielectrophoresis and AC Electroosmosis using a Concentration analysis

The dynamics of the particle concentration are investigated in this chapter using a Smoluchowski equation. This is very important in examining the system operation because the particle concentration is the desired information that must be extracted from the simulations of DEP manipulation systems. The previous analysis has examined the velocity fields due to the two phenomena, ACEO and DEP, but did not take into account diffusion and nor did it provide direct information on the particle concentration.

6.1 Introduction

The manipulation of DNA particles is a subject of increasing interest, due to applications in lab-on-chip systems (56). A very useful method for DNA manipulation utilises the DEP force. Experimental investigations of DEP particle concentration suggest a difference between experimental and numerical results, which is attributed to other factors, such as the ACEO flow (4). The manipulation problem therefore becomes more complicated by the fact that ACEO fluid flow is induced in the system, which disturbs the DEP concentration of particles. As a result, the inclusion of the ACEO effect is required to more accurately simulate the behaviour of the system.

In this section, the Smoluchowski form of the Fokker-Planck equation (141) (142) (127) is used in order to study the steady state concentration of dsA5 DNA in a sample under both DEP and ACEO. The ACEO and DEP induced velocities are used as the convective

terms in the equation, whilst the diffusion of DNA is also taken into account (143). It is assumed that the particles do not affect the electric field or the fluid flow and that the particles do not interact with each other. The results from this investigation clearly indicate the significant effect of ACEO. The fluid flow caused by ACEO effectively carries the particles from the electrode edges towards the electrode centre, therefore reducing the DEP concentration at the edges. This observation is consistent with experimental observations.

6.2 Theory

6.2.1 Dielectrophoresis of DNA using experimental polarisability data

The system in figures 6.1 and 6.2 is used as an example of a possible electrode configuration in a lab-on-chip system to manipulate DNA, which is suspended in water with KCl. The combined force from gravity and buoyancy is neglected in this domain since, at this distance from the electrodes, the DEP force is orders of magnitude higher. The DEP force was given earlier in equation 2.2. However, since the dielectric properties for the DNA particles under investigation are available in relation to the particle polarisability at specific frequencies, the DEP force is given by the following alternative expression (141) (144):

$$F_{DEP} = \frac{a_m \times \nabla \vec{E}^2}{4} \tag{6.1}$$

where $a_m = \frac{p_d}{E}$ $(F.m^2)$ is the polarisability of the DNA particle, p_d the dipole moment and $\vec{E}$ $(V.m^{-1})$ the peak electric field applied.

Investigations of the diffusion of dsA5 DNA estimate its diffusion coefficient to be 1.07×10^{-10} $m^2.s^{-1}$ (143). Furthermore, studies on the dielectric relaxation of 12 *kbp* (thousands of base pairs) plasmid DNA (51) give approximate values for the polarisability of the DNA at several frequencies. A reasonable assumption for the dsA5 polarisability, which has 20 *bp* (base pairs) length, would be to consider the ratio of the a_m of the dsA5 to the a_m of the 12 *kbp* plasmid DNA to be equal to the ratio of their volumes. This estimate of a_m is accurate enough to give an order of magnitude value of the DEP force on DNA particles of this scale. The friction factor is found by $f = \frac{6\pi\eta l}{ln(\frac{2l}{r})} = 4.387 \times 10^{-11}$ $N.m.s^{-1}$ (1) and the diffusion constant gives $D_1 = \frac{k_B T}{f} = 9.22 \times 10^{-11}$ $m^2.s^{-1}$ which is very close to the one used and which was observed experimentally (143). The Debye length for the system here is approximately $\lambda_{Debye} = 10$ nm.

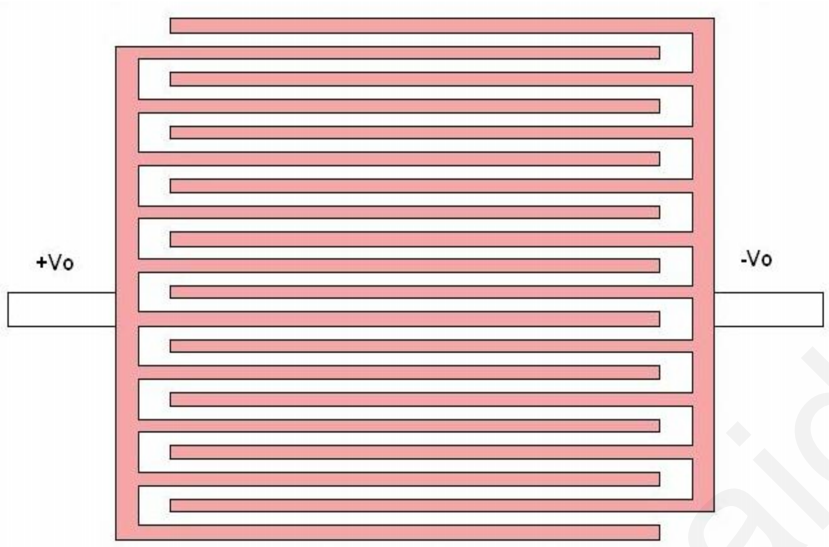

Figure 6.1: Geometry of parallel electrodes (not to scale)

6.2.2 Stochastic motion

The concentration or probability density function for the particles in two dimensions C(x,y,t) is given by the Smoluchowski equation, as described in (127), (128)

$$\frac{\partial C}{\partial t} = [-\frac{\partial}{\partial x}(v_{DEP}(x) + v_{fluid}(x)) + D\frac{\partial^2}{\partial x^2} - \frac{\partial}{\partial y}(v_{DEP}(y) + v_{fluid}(y)) + D\frac{\partial^2}{\partial y^2}]C \quad (6.2)$$

where D is the diffusion constant and the other variables have the meaning stated before. Here the diffusion constant $D = 1.07 \times 10^{-10}\ m^2.s^{-1}$ found experimentally (143) is used. For the solution of the Smoluchowski equation, all boundaries are set to be reflective. The properties employed for the simulations are summarised in table 6.1.

Table 6.1: Electrolyte and particle properties.

Property	**Value**
Fluid Viscosity (η_f)	$1 \times 10^{-3}\ Pa.s$
Diffusion coefficient for dsA5 DNA (D)	$1.07 \times 10^{-10}\ m^2.s^{-1}$
Relative permittivity of medium (ϵ_{mr})	80
Electrode peak potential (V_0)	$4.5\ V$
Λ	0.25
Permittivity of free space (ϵ_0)	$8.8542 \times 10^{-12}\ F.m^{-1}$
Debye length (λ_{Debye})	$1 \times 10^{-8}\ m$
Conductivity (σ)	$8.6\ mS.m^{-1}$
Friction factor (f)	$4.387 \times 10^{-11}\ N.s.m^{-1}$
Particle polarisability a_m	varied from 0.1667 to $5.333 \times 10^{-33}\ m^2$

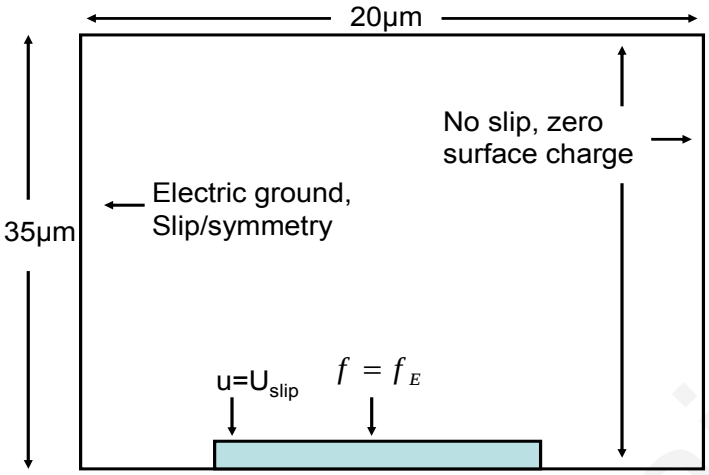

Figure 6.2: Computational domain for the periodic problem of parallel electrodes

6.3 Results

6.3.1 Steady state simulations

The interest here lies in the relationship between the particle polarisability (or equivalently frequency) and the steady state DNA concentration under DEP. The steady state concentration at a point is the concentration after this no longer changes with time. This will allow the investigation of how ACEO flow affects the final distribution of particles in the device when ACEO is also considered. It is predicted by theory that the relationship is exponential (141), however the relationship indicated by experimental results is a linear one (4). It is also found experimentally that the concentration is much lower than the one predicted by DEP theory alone. The main issue of interest is the relation between the particle polarisability and steady state concentration, which is why the concentration is plotted as the non-dimensional ratio $\frac{C}{C_0}$, the ratio of the steady state concentration C to the initially uniform concentration C_0. The point tested is $(1.499 \times 10^{-5}\ m,\ 3 \times 10^{-7}\ m)$, which is close to the electrode edge.

By using the properties in table 6.1 and the boundary conditions in figure 6.2, the system shown in figure 6.1 is simulated. A 4.5 V peak voltage is applied and equation 6.1 is used for the DEP force. It can be seen in figure 6.3 that the steady state concentration with DEP alone is of exponential form, as predicted by theory (the logarithmic plot is linear) (141). The concentration due to ACEO and DEP is simulated using the Smoluchowski equation, by using the DEP and ACEO induced velocities as the convective terms.

The effect of ACEO flow (which is the induced fluid velocity) is superimposed to the DEP-induced particle velocity and then it is incorporated into the Smoluchowski equation.

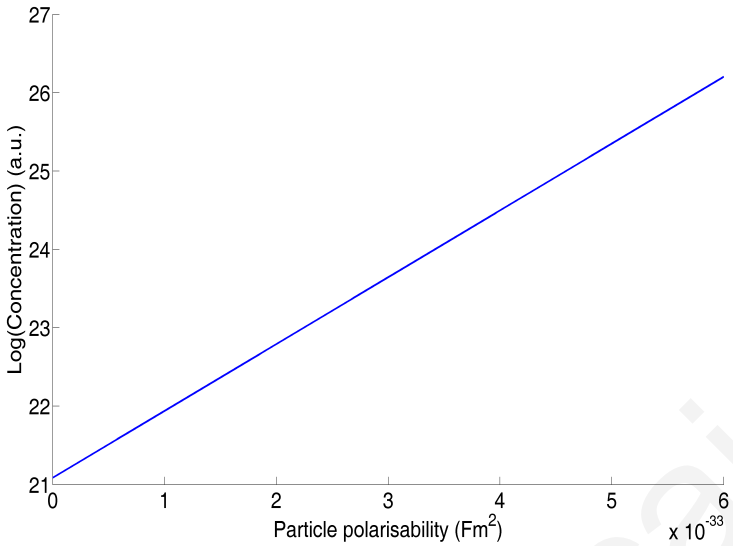

Figure 6.3: Natural logarithm of the steady state concentration due to DEP alone vs particle polarisability ($F.m^2$)

The steady state concentration is clearly disturbed by the ACEO flow, as seen by the circular patterns of the concentration isocontours formed by the DNA in figure 6.4. Figure 6.4 is a side view of one of the electrodes shown in figure 6.1, of length equal to one periodic length of the array.

When ACEO flow is introduced, it can be seen in figure 6.5 that the local steady state concentration at a point dramatically decreases, which agrees with experimental observations (4), where very modest collections of DNA on the array were observed in comparison to the concentrations predicted experimentally by DEP.

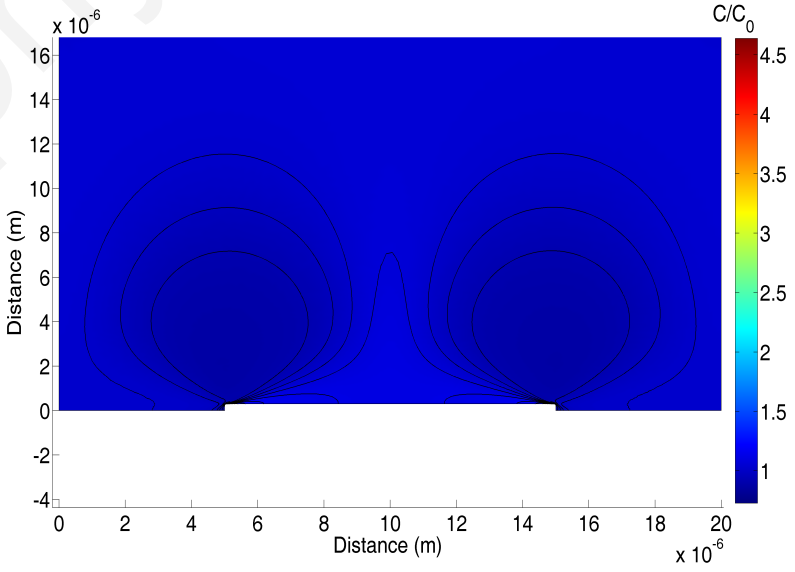

Figure 6.4: Concentration of DNA ($\frac{C}{C_0}$) in steady state over the electrodes, taking both DEP and ACEO into account

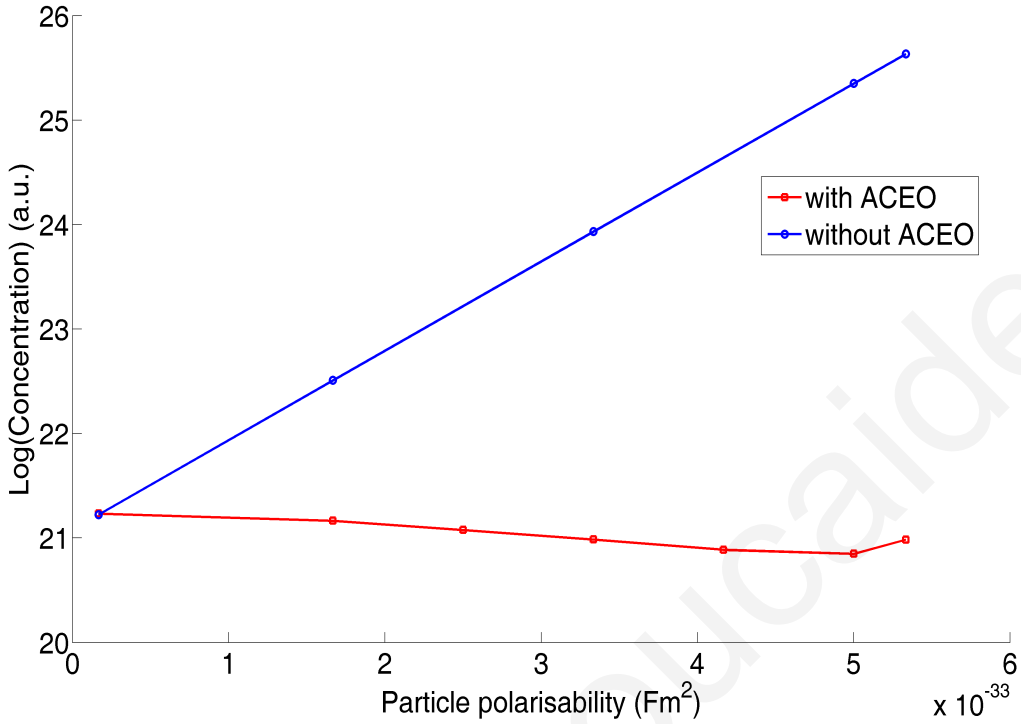

Figure 6.5: Natural logarithm of the steady state concentration due to DEP alone and joint DEP and ACEO vs particle polarisability ($F.m^2$)

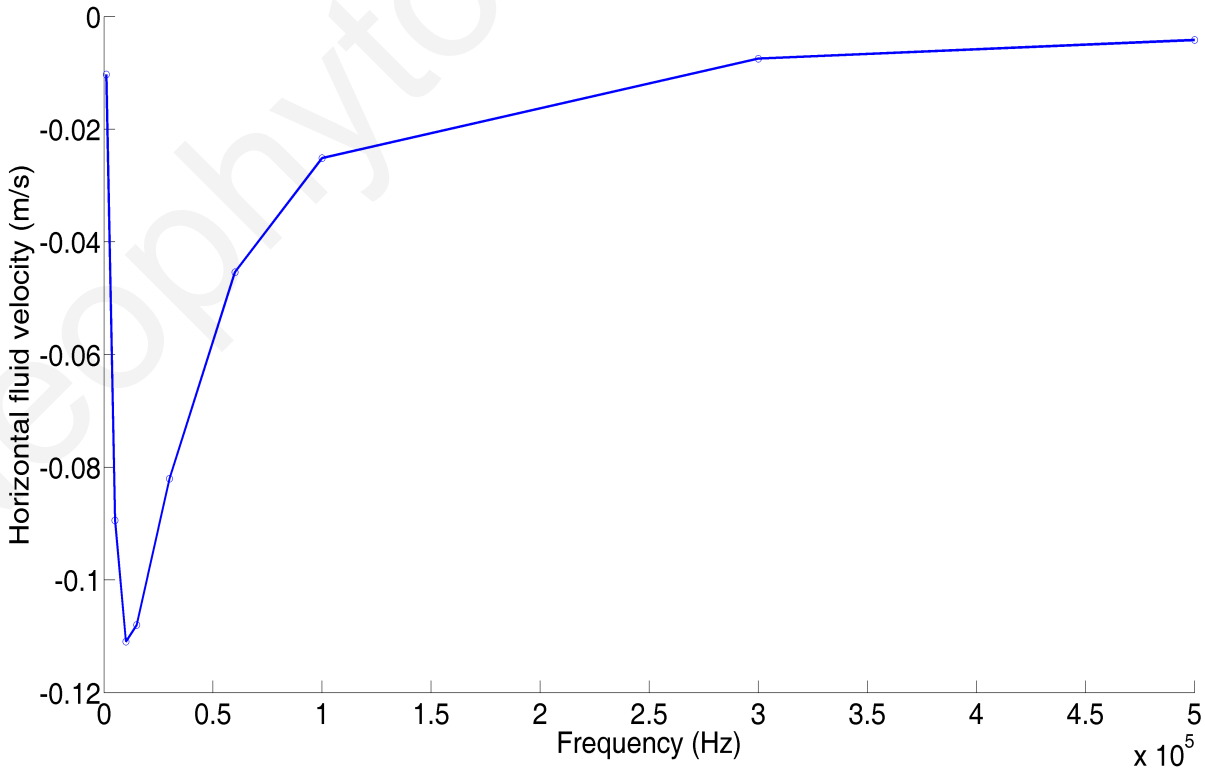

Figure 6.6: Fluid speed at the point (1.499×10^{-5} m, 3×10^{-7} m) over the electrode surface as a function of frequency (Hz)

It can be seen that the induced velocity due to ACEO is of the same order of magnitude or larger than the particle velocity induced by DEP.

ACEO is therefore strong enough to distort the exponential relationship predicted by theory and is found to be significantly modified and very dependent on ACEO flow. More specifically, ACEO flow is maximum at the electrode edges, where DEP is also maximum. The ACEO flow effectively removes the particles from the edges and carries them towards the electrode centre. Furthermore it can be observed that the effect of ACEO is at its highest at a particle polarisability of 5.3×10^{-33} $F.m^2$ or equivalently at a frequency of about 10 kHz, as shown in figures 6.5 (the minimum concentration is at particle polarisability 5.3×10^{-33} $F.m^2$ for the combined ACEO and DEP case) and 6.6 (the maximum ACEO velocity magnitude is at 10 kHz). This frequency corresponds to a non-dimensional frequency of 8, which agrees with the literature (2).

6.4 Conclusions

The DEP manipulation of dsA5 DNA particles in a suspension was investigated numerically. ACEO fluid motion was also simulated and the results with and without ACEO were compared. These indicate a strong decrease in the concentration at the edges and subsequent movement of particles towards the centre of the electrode, a fact verified by experimental observations (4). Finally, the ability of the Smoluchowski equation to simulate combined diffusion, ACEO and DEP to describe the evolution of particle concentrations in such a system has been verified.

While this chapter has revealed the ability of the numerical model to simulate the dynamics of the system, it is limited by the fact that the particle size simulated can not be large enough for the particle concentration to become significant, since it does not take into account the finite particle dimensions and would therefore predict unrealistically high volume fractions, which would require the particles to overlap in space. Therefore, it is of great importance to include the particle steric effect in order to be able to simulate the dynamics of larger particles than the ones simulated here.

Chapter 7

Particle steric effects: Dielectrophoresis

In order to improve the physical model presented in chapter 6, it is necessary to introduce a modification to the Smoluchowski equation to account for the limitations imposed on the particle concentration by the finite particle dimensions. This is done here and the simulation results are compared with the previous model in order to understand the effect of the modifications.

7.1 Introduction

The physical model used in chapter 6 does not take into account the finite size of the particles. The particle finite size means that two particles cannot overlap with each other and therefore a maximum volume fraction limit exists for the particles, depending on their shape. Furthermore, as the particle concentration becomes higher, the motion of a particle is affected by the presence of nearby particles.

If the particle size is large enough for the diffusion to be negligible, the device operation can be analysed by studying the velocity fields as in chapter 5. However, in a region where both the concentrations can be large but diffusion is still significant, such as in the case of the 12 *kbp* pTA250 DNA, the steric effects of the particle concentration have to be taken into account in a model that also incorporates the effects of diffusion, such as the Smoluchowski equation. This is one of the tasks pursued here, so that numerical results can subsequently be comparable with experimental data.

The first direct effect of this modification is that the maximum possible concentration is limited. The maximum possible concentration can be assumed to be equal to approxi-

mately 0.64 volume fraction (0.64 random close packing or 0.74 maximum close packing-when the spheres are orderly placed in adjacency to each other (125)). The maximum volume fraction is not 'strictly' imposed (i.e. instead of the steric parameters becoming infinite or zero at the set limit, these are set to become very high or very low respectively), as such a strategy would cause numerical problems, but practically the volume fraction is kept very close to the limiting value. Further analysis and discussion on this issue is provided in section 8.2.2.

7.2 Theory

The system in figure 6.1 of the previous chapter is investigated. This consists of parallel electrodes of 10 μm width and interelectrode spacing of the same size. It is assumed here that the length and width of the array are infinitely long so that end effects are not taken into account. A water solution with DNA particles is placed on top of the electrodes.

7.2.1 Particle dynamics

The concentration of the particles in two dimensions C(x,y,t) is given by the Smoluchowski equation, as described in (128), (127)

$$\frac{\partial C}{\partial t} = [-\frac{\partial}{\partial x}(v_{DEP}(x) + v_{fluid}(x)) + D\frac{\partial^2}{\partial x^2} - \frac{\partial}{\partial y}(v_{DEP}(y) + v_{fluid}(y)) + D\frac{\partial^2}{\partial y^2}]C \quad (7.1)$$

where D is the diffusion coefficient and the other variables have the meaning stated before. Here the diffusion constant $D = \frac{k_B T}{6\pi\eta_f l/\ln\frac{2l}{r}}$ (where $6\pi\eta_f l/\ln\frac{2l}{r}$ the friction factor) is used (1). Also, the DEP velocity is calculated as $\vec{v}_{DEP} = \frac{\vec{F}_{DEP}}{6\pi\eta_f l/\ln\frac{2l}{r}}$. For the solution of the Smoluchowski equation, all boundaries are set to be reflective. The properties employed for the simulations are summarised in table 7.1. The motion of the fluid due to ACEO must also be taken into account for the analysis of such a device, but is not presented in this section in order to study the steric effect before introducing further complexity to the problem. More details on this can be found in (82) (144) (105) (106).

7.2.2 Steric effect modification

Based on theory presented in (124) (not including concentration effects on the electric field or DEP) the equation for the conservation of particles is given by equation 7.2 (145)

(146)

$$\frac{\partial c}{\partial t} + \nabla.(c\vec{v_s} + \vec{j_p}) = 0 \tag{7.2}$$

where $\vec{v_s}$ is the suspension velocity, $c = nV_p$ the particle volume fraction (n is the number density, V_p is the particle volume) and $\vec{j_p}$ is given by

$$\vec{j_p} = \frac{cV_p(1-c)^2}{6\pi a\eta_c}[-\nabla\mu_p + (\rho_p - \rho_f)g] \tag{7.3}$$

where $V_p\mu_p$ is the chemical potential (increment of the system energy by adding a particle), a the particle radius and ρ_p , ρ_f are the particle and fluid densities respectively. Therefore

$$\nabla\mu_p = \frac{\partial\mu_p}{\partial c}\nabla c = \frac{k_BT}{V_p}(\frac{Z(c)}{c} + \frac{\partial Z}{\partial c})\nabla c \tag{7.4}$$

and

$$\vec{j_p} = -\frac{(1-c)^2}{6\pi a\eta_c}k_BT\frac{\partial cZ(c)}{\partial c}\nabla c + \frac{(1-c)^2}{6\pi a\eta_c}(\rho_p - \rho_f)cV_pg \tag{7.5}$$

Z is the suspension compressibility factor and $\eta_c = \eta_f[1 + \frac{1.5c}{1-\frac{c}{c_m}}]^2$ is the effective viscosity of the suspension (η_f is the fluid viscosity and c_m the maximum packing volume fraction, here set to $c_m = 0.64$). One can write

$$\vec{j_p} = -\frac{K(c)}{6\pi a\eta_f}k_BT\frac{\partial cZ(c)}{\partial c}\nabla c + \frac{K(c)}{6\pi a\eta_f}(\rho_p - \rho_f)cV_pg \tag{7.6}$$

The Carnahan-Starling equation (147) gives

$$Z(c) = \frac{(1 + c + c^2 - c^3)}{(1-c)^3} \tag{7.7}$$

and

$$K(c) = \frac{(1-c)^2}{(1 + \frac{1.5c}{1-\frac{c}{c_m}})^2} \tag{7.8}$$

Including DEP the equation for the volume fraction becomes

$$\frac{\partial c}{\partial t} + \nabla.(c\vec{v}_s + cK(c)\vec{u}_F - D_0K(c)\frac{\partial cZ(c)}{\partial c}\nabla c) = 0 \tag{7.9}$$

where $\vec{v}_s$ is the suspension velocity, $\vec{u}_F$ the particle velocity induced by external forces (DEP, buoyancy and gravity) and D_0 is the diffusion constant for a particle without any interactions between the particles.

7.3 Results

Simulations of concentration dynamics are produced here using the method of finite elements for DNA particles for lengths of 1 *kbp*, 2 *kbp* and 4 *kbp*. The dynamics of an initial concentration of particles are simulated for 10 s under the conditions described earlier and the results are presented here.

7.3.1 Time evolution

After the sudden application of an AC potential difference of 9 V peak-to-peak, the particle concentration starts to evolve. A point is selected close to the electrode edges and the evolution of concentration as a volume fraction is presented for all the three particle size cases so that the behaviour of the suspension is investigated. The results are plotted in figure 7.1. The point under investigation is given by coordinates ($x = 1.499 \times 10^{-5}$ m, $y = 3 \times 10^{-7}$ m) and can be seen in figure 7.3. It can be seen that the general form of the plots indicates that all the cases tend towards a steady state that is reached faster for larger particles. It is also evident that the rise in concentration is faster as the particles get larger. At 4 *kbp* the rise time becomes very short, an issue that might cause numerical problems with simulations of larger particles.

Table 7.1: Electrolyte and particle properties.

Property	**Value**
Fluid Viscosity η_f	1×10^{-3} $Pa.s$
Relative permittivity of medium ϵ_{mr}	80.2
Electrode potential V_0	4.5 V
Permittivity of free space ϵ_0	8.8542×10^{-12} $F.m^{-1}$
Conductivity σ	5 mSm^{-1}
Friction factor f	$(6\pi\eta l)/log(2l/r)$
Real part of particle polarisability a_m	$variable$
DNA base length	0.23×10^{-9} m
DNA width	1.275×10^{-9} m
Initial concentration	0.5×10^{-3}

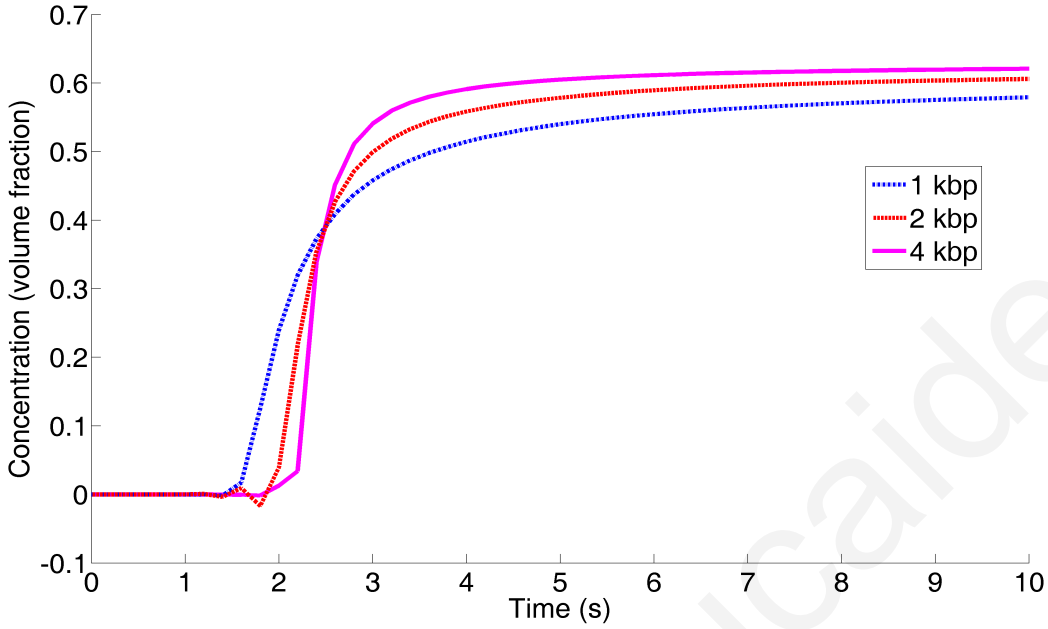

Figure 7.1: Plot of the concentration at one point ($x = 1.499 \times 10^{-5}\ m$, $y = 3 \times 10^{-7}\ m$) for the three cases simulated.

Comparing these with experimental results from (4) it can be seen that the time scale from initial concentration to steady state agrees qualitatively. Quantitative comparison requires the transformation of concentration to normalised fluorescense.

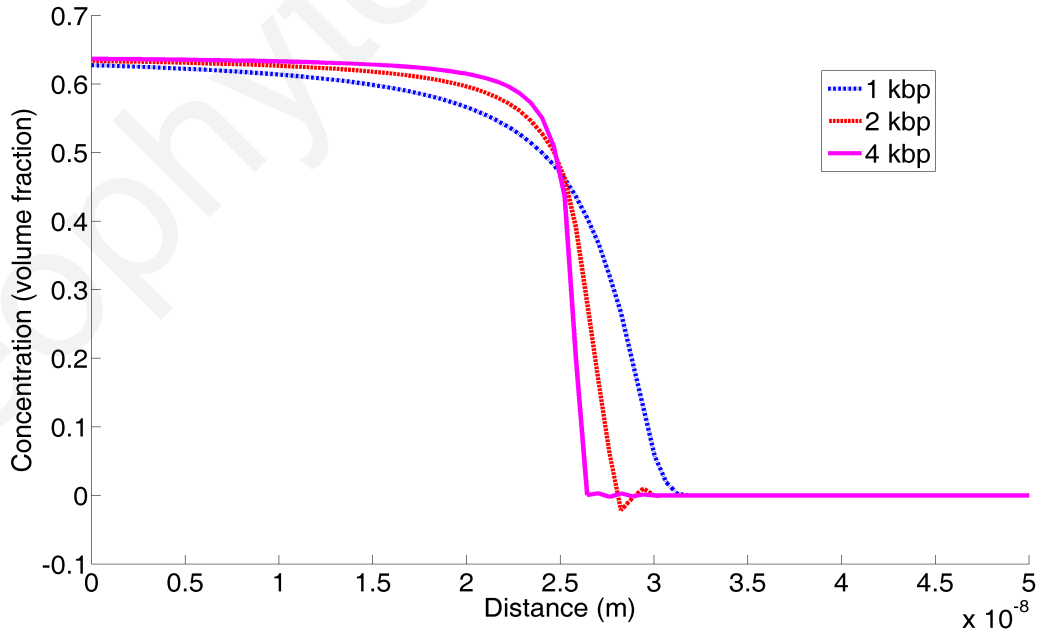

Figure 7.2: Plot of the concentration profile at a radial distance from the electrode edge for the three cases simulated. The profiles are taken at $t = 10\ s$.

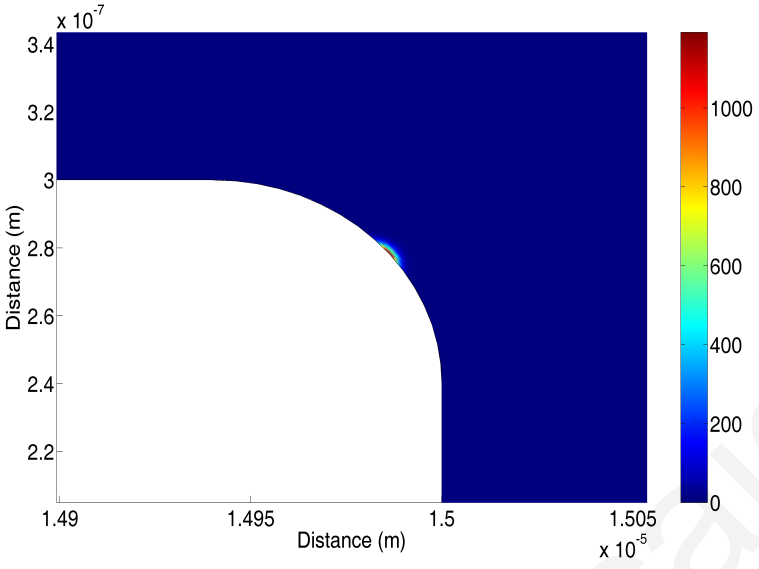

Figure 7.3: Steady state without the steric modification.

7.3.2 Concentration profile

A cross section of the concentration profile is presented here in order to investigate its evolution. The results are plotted in figure 7.2. It can be seen that the rise time for the larger particles is faster, as observed in figure 7.1. Furthermore, it can be seen that the dynamics of the system as the particle size increases move asymptotically towards a well defined step. It may therefore be possible to use these to extrapolate to larger particle sizes.

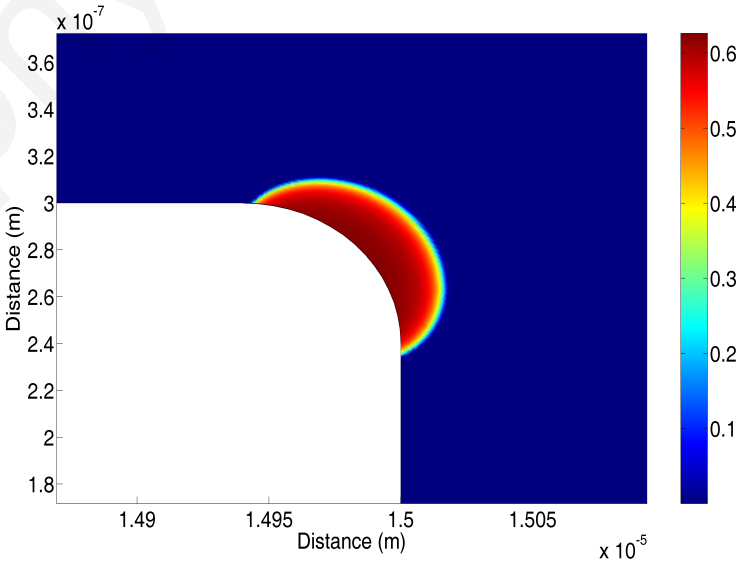

Figure 7.4: Steady state with the steric modification.

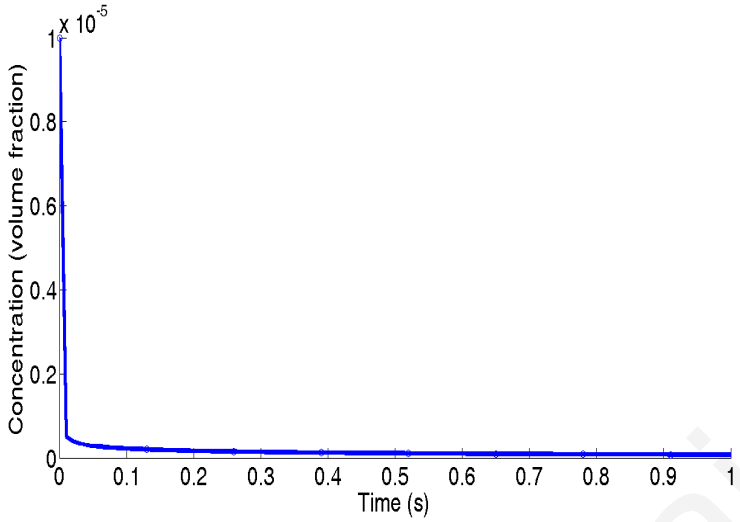

Figure 7.5: Plot of the concentration evolution versus time for 1 *kbp* particles at the same point as figure 7.1 without the steric modification.

7.3.3 Comparison with non-steric case

The evolution of the concentration is also simulated using equation 7.1 without the modifications. A comparison of the non-steric and steric cases at the same time instant under the same conditions is presented in figures 7.3 and 7.4. It is evident in the non-steric case, that the particles, as can be seen in figure 7.3, have reached an unrealistically high concentration at the electrode edge (in a region which is theoretically a point), while the region near the electrodes has negligible concentration.

This is further supported by figure 7.5 which shows that the initial concentration decreases rapidly and remains very low for the rest of the time in the non-steric case. This essentially means that for the non-steric case all particles within range collect at an infinitesimal region near the electrode surface, which is not realistic. However, the finite particle dimensions limit the particle concentration in real devices, therefore producing a profile shown in figure 7.4, which has been produced after 10 *s* by the modified model.

7.4 Conclusions

A physical model for the collection of DNA on parallel electrode arrays by DEP has been introduced that incorporates steric effects in the particle concentration. This is important in the simulation of real devices where the particle concentration under DEP is of interest. The model has been compared with simulations without the modification introduced and there has been significant impact on the results, making the results more realistic. Also, it has been possible to extract the dynamics of a system of particles suspended in a device

as the particle size increases.

As a next step the physical model will be further expanded by including the ACEO fluid motion in the simulation. This requires the introduction of particle steric effect modifications in the Navier-Stokes equations for the suspension. The simulations can then be comparable with experimental data, since the most important phenomena for this problem will have been taken into account.

Chapter 8

Particle steric effects: Joint Dielectrophoresis and AC Electroosmosis

In the previous chapter the Smoluchowski equation was modified in order to take into account the particle steric effects. In this chapter the effects on the suspension motion are also modelled by modifying the Navier-Stokes equations and the ACEO fluid motion is included in the simulations. The simulation results are then compared with experimental data and are also used to investigate a number of variables affecting the device operation.

8.1 Introduction

High local concentrations mean that the suspension effective viscosity and density are modified. The complications of this are taken into account by introducing modified Navier-Stokes equations. The effect of these modifications is that as the local concentration becomes higher, the density, viscosity and therefore local suspension velocity are modified to reflect this. Therefore, the density increases, the viscosity also increases and the particle DEP velocity is reduced as the concentration increases. The modifications are also helpful in the numerical convergence of the model, since a number of variables are confined to a more limited range of values whereas by using the simpler model these could become very large in regions of high concentration.

8.2 Theory

8.2.1 Particle steric effect modifications on the suspension motion

The modified Navier-Stokes equations for the suspension flow are given in equations 8.1, 8.2 (124) (23):

$$\rho_s(\frac{\partial \vec{v}_s}{\partial t} + \vec{v}_s.\nabla\vec{v}_s) = -\nabla p + \nabla.(\eta_s\nabla\vec{v}_s) - c\nabla\mu_p + \vec{f}_{DEP} + c(\rho_p - \rho_f)g \tag{8.1}$$

$$\nabla \cdot \vec{v}_s = 0 \tag{8.2}$$

where $\vec{v}_s$ is the velocity of the suspension, c the volume fraction, $\rho_s = (1-c)\rho_f + c\rho_p$ the suspension density using an effective medium approximation, $\nabla\mu_p$ defined in equation 7.4 and the fluid viscosity is given by equation 8.3 (124).

$$\eta_c = \eta_f[1 + \frac{1.5c}{1 - \frac{c}{c_m}}]^2 \tag{8.3}$$

The force $\vec{f}_{DEP}$ is the volume dielectric body force on the suspension and is given by equation 8.4, assuming low concentration or polarisability of the particles.

$$\vec{f}_{DEP} = \frac{ca_m\nabla\vec{E}^2}{4V_p} \tag{8.4}$$

where a_m is the real part of the particle polarisability and V_p the particle volume.

The boundary condition on the electrode surfaces is given by equation 3.5 defined earlier (in the slip velocity definition the viscosity is set as constant $\eta_f = 1 \times 10^{-3}\ Pa.s$ because the particles are assumed not to stick to the surface). Furthermore, the Navier-Stokes equations are solved simultaneously with equation 7.9 for the volume fraction in order to simulate the particle concentration evolution.

The model used is modified as above and simulations are performed to investigate the impact of these modifications.

The modified steric model can simulate larger particle sizes in the form of the modified Smoluchowski equation. Also, the steric model can be used to perform simulations of systems already analysed and the results can be compared in order to examine its impact on smaller as well as larger particle suspensions.

The model described above is implemented and solved using a finite element formulation.

Table 8.1: Properties used in the simulations.

Property	Value
Fluid Viscosity (η_f)	1×10^{-3} $Pa.s$
Relative permittivity of fluid (ϵ_{mr})	80.2
Electrode peak Voltage (V_0)	4.5 V
Λ	*variable*
Permittivity of free space (ϵ_0)	8.8542×10^{-12} $F.m^{-1}$
Debye length (λ_{Debye})	1.31×10^{-8} m
Conductivity of fluid (σ_m)	5 $mS.m^{-1}$
Frequency	variable
Initial concentration/volume fraction	0.0005 $a.u.$

Table 8.2: Relation of particle polarisability with Frequency (4).

Particle polarisability	Frequency
2.4×10^{-30} Fm^2	100×10^3 Hz
1.5×10^{-30} Fm^2	200×10^3 Hz
0.84×10^{-30} Fm^2	500×10^3 Hz
0.61×10^{-30} Fm^2	1×10^6 Hz
0.39×10^{-30} Fm^2	2×10^6 Hz
0.14×10^{-30} Fm^2	5×10^6 Hz

The settings used for the simulation here are presented in table 8.1. The particles considered are plasmid pTA250 DNA 12 *kbp* long. The DNA properties of interest are its size, density and particle polarisability. The size is taken as a cylinder of radius= 1.275 nm, length = 0.23 nm $\times 12 \times 10^3$ bp and with density of 1.1×10^3 Kg/m^3. The particle polarisability is shown in table 8.2 for all frequencies used in the following work.

8.2.2 Exponential models for the polynomial expressions

After a number of initial simulations, it was found that the parameters η_c, $Z(c)$, $K(c)$ caused problems and instability to the numerical simulations, due to the singularities inherently existent in the expressions. Therefore, they were approximated by exponential expressions that are listed here for $Z(c)$, $K(c)$, η_c in equations 8.5, 8.6 and 8.7 respectively. These were selected due to the fact that the exponential functions have smooth derivatives and no discontinuities over the regions of interest. Furthermore, the exponential models can be tuned easily to approximate the required polynomials, as can be seen in figures 8.1, 8.2 and 8.3 . The impact of using such approximations is investigated in section 8.4.

$$\eta_c = 1 \times 10^{-3} \times e^{|(c)/0.35|)^4} \tag{8.5}$$

$$Z(c) = 0.5 \times (e^{c/0.15} + e^{-c/0.15}) \tag{8.6}$$

$$K(c) = e^{-|(c)/0.15|} \tag{8.7}$$

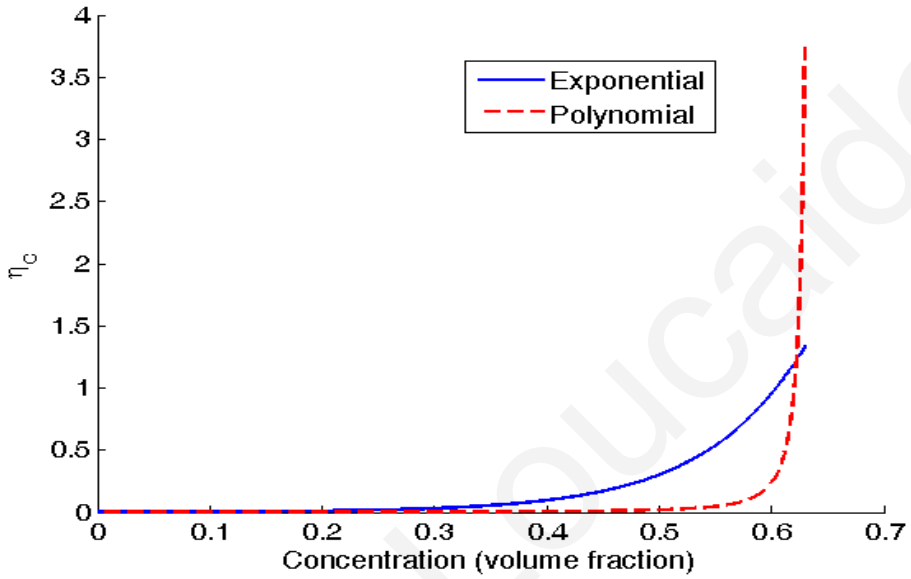

Figure 8.1: The exponential expression for η_c plotted with the polynomial expression.

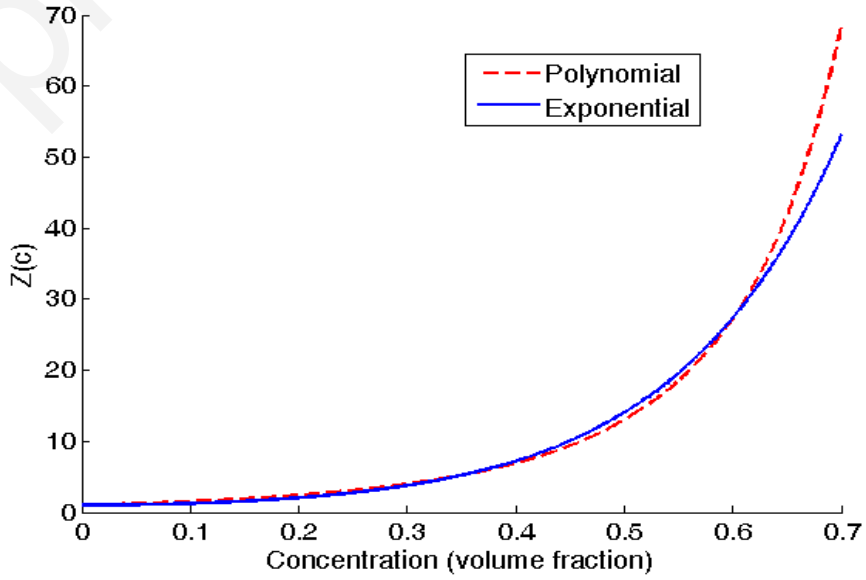

Figure 8.2: The exponential expression for $Z(c)$ plotted with the polynomial expression.

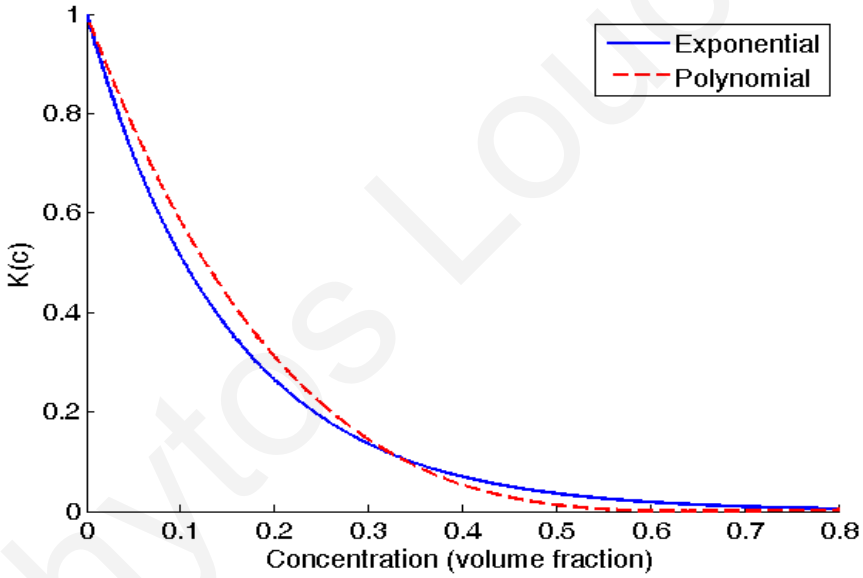

Figure 8.3: The exponential expression for $K(c)$ plotted with the polynomial expression.

8.3 Results

8.3.1 Investigation of the tuning parameter Λ

The theory for the ACEO slip velocity contains a tuning parameter which is experimentally determined. In order to determine its effect, the simulation was run for several values of this parameter, Λ.

The meaning of the particle collection referred to in this chapter is defined as the integral of the concentration/volume fraction over an area of plus or minus 1 μm from the electrode edge and to a height of 1 μm over the electrode edge. This is the focal area of the microscope as stated in (4). This is always plotted as normalised by the initial value of the integral so that the plotted quantity is easier to compare. The evolution of the particle collection for different Λ values is shown in figure 8.4. The differences in the initial rates of increase are small.

However, for the $\Lambda = 0.25$ case the difference in steady state is high. The same plot for the 1 MHz case is shown in figure 8.5. The differences are smaller at this frequency. It can be seen in figures 8.4 and 8.5 that the effect of varying Λ in the vicinity of 0.15 is small. As expected, the effect of varying Λ is much smaller in figure 8.5, because ACEO is weak at such high frequencies and DEP is dominant.

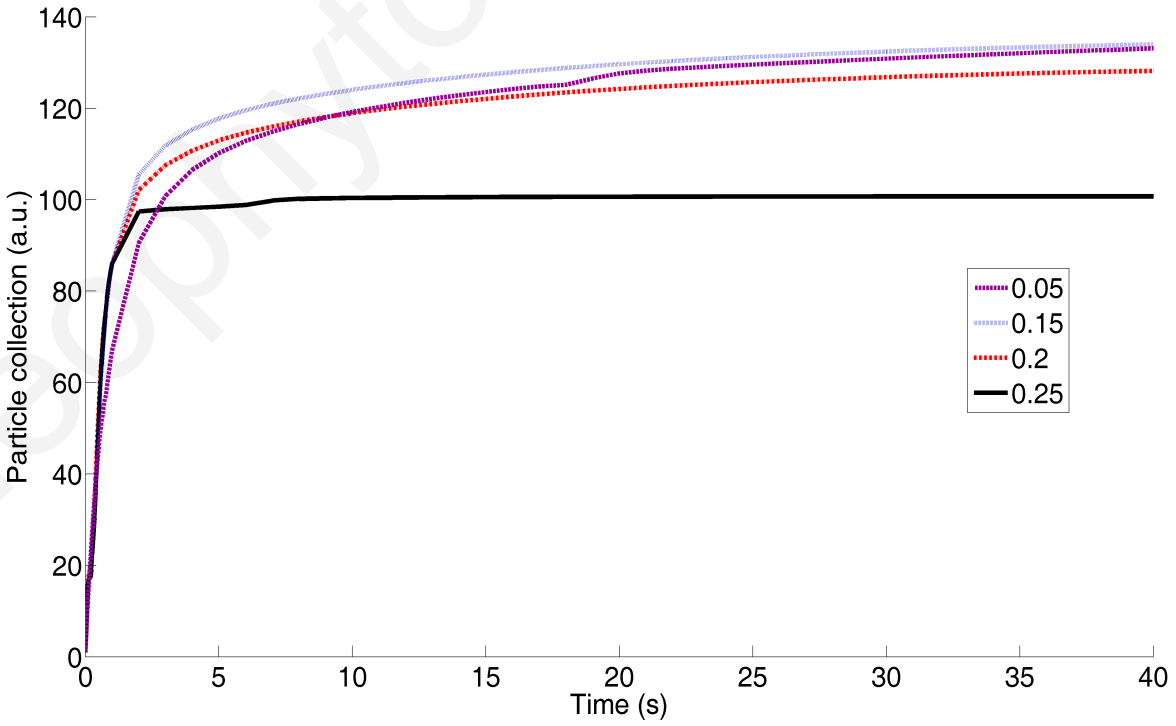

Figure 8.4: The particle collection over the electrode edge for different values of Λ at 200 kHz.

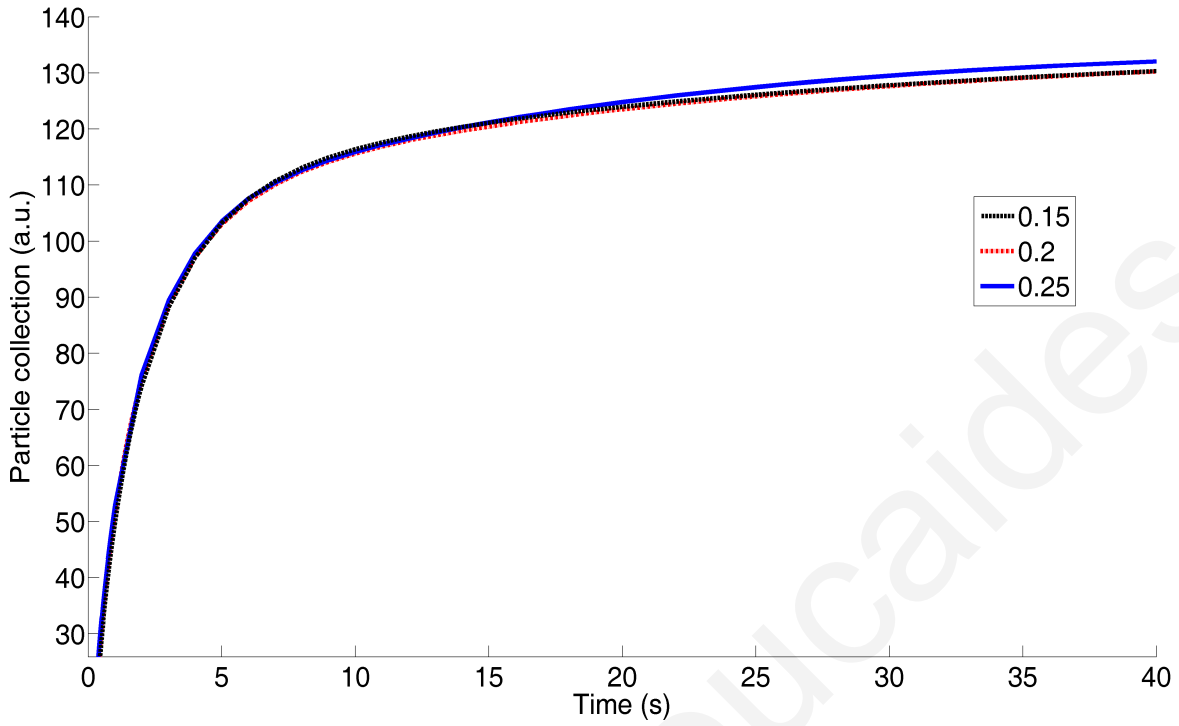

Figure 8.5: The particle collection over the electrode edge for different values of Λ at 1 MHz.

Here, since no ACEO experimental data is available for the system, 0.15 is taken as an estimate[1]. The steady state particle collection for 200 kHz $\Lambda = 0.15$ is shown in figure 8.6. Its form here is such that there is high particle collection at the vicinity of the electrode edge, but there is also significant particle collection over the surface of the electrode towards the electrode centre. This is due to the high ACEO velocity which forces the particles towards the electrode centre.

Figure 8.7 shows the steady state particle collection for 1 MHz $\Lambda = 0.15$. Here it is more confined to the vicinity of the electrode edge. This is due to the fact that ACEO is very small at this frequency and DEP is highly dominant, therefore giving rise to a steady state profile very similar to the one in figures 8.8 and 8.9, the cases without ACEO for 200 kHz $\Lambda = 0$ and 1 MHz $\Lambda = 0$ respectively (where $\Lambda = 0$ is used it is implied that the suspension velocity $\vec{v}_s$ in equation 7.9 is set to zero).

The evolution of the particle collections is shown in figure 8.10, where it can be seen that the steady state and the initial rate decrease with the increase in frequency, due to the reduction in particle polarisability. As can be seen, at lower frequency where ACEO is stronger, collection is significantly disturbed and that particles are dragged away from the electrode edge towards the electrode centre. The particle collection is increased in the region where the electrode intersects the substrate, because this region is shielded from strong ACEO flow. At the electrode edge, it is decreased in both cases.

[1]From this point on it is implied that $\Lambda = 0.15$ unless otherwise stated.

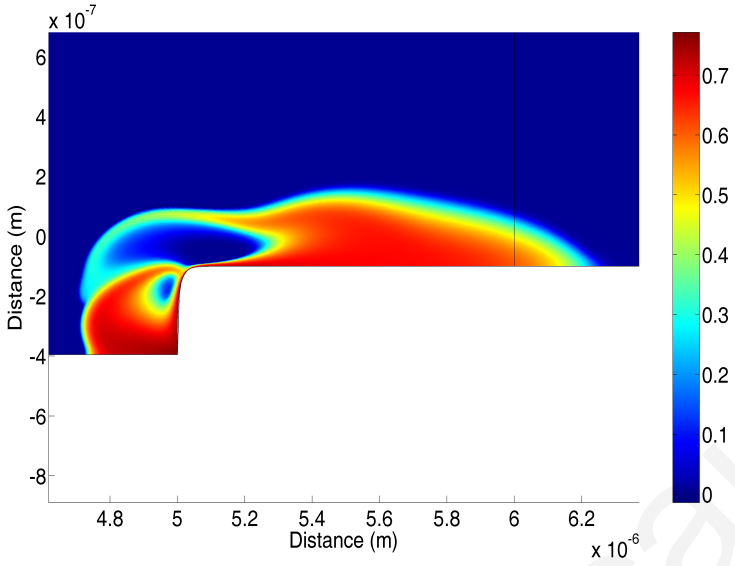

Figure 8.6: The steady state particle collection over the electrode edge for 200 kHz $\Lambda = 0.15$.

It can also be seen that for the case without ACEO the particle collection evolution is much slower than with ACEO. Furthermore, it is clear from figures 8.6 and 8.7 that for the cases where ACEO is not introduced, the frequency change does not affect the collection profile as much as before. Figure 8.11 shows that at 200 kHz the steady state particle collection is much more dependent on Λ than at 1 MHz, which is as expected theoretically, since ACEO is much stronger at this frequency. From the results shown in this section, one can observe that ACEO in this system under the conditions tested always reduces the steady state of the system. The higher the ACEO the higher the reduction in the system steady state trapping.

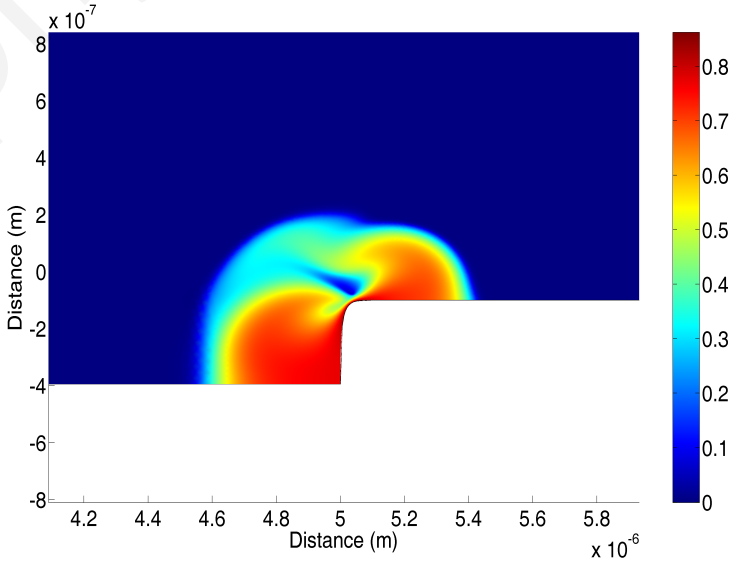

Figure 8.7: The steady state particle collection over the electrode edge for 1 MHz $\Lambda = 0.15$.

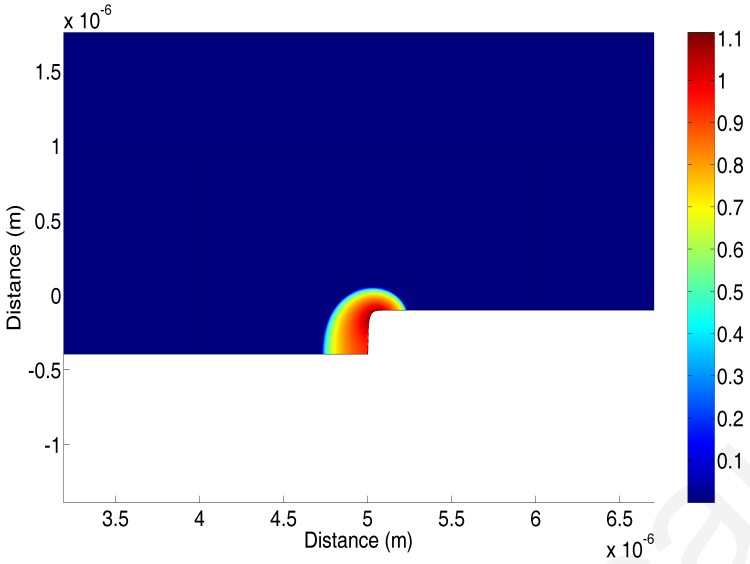

Figure 8.8: The steady state particle collection over the electrode edge for 200 kHz without fluid motion.

In figure 8.12 it is evident that the time to reach steady state is dramatically reduced by ACEO, although the relationship is not monotonic. This is due to the fact that the ACEO fluid velocity is much higher than the DEP-induced velocity in a region that is close to the electrode edge.

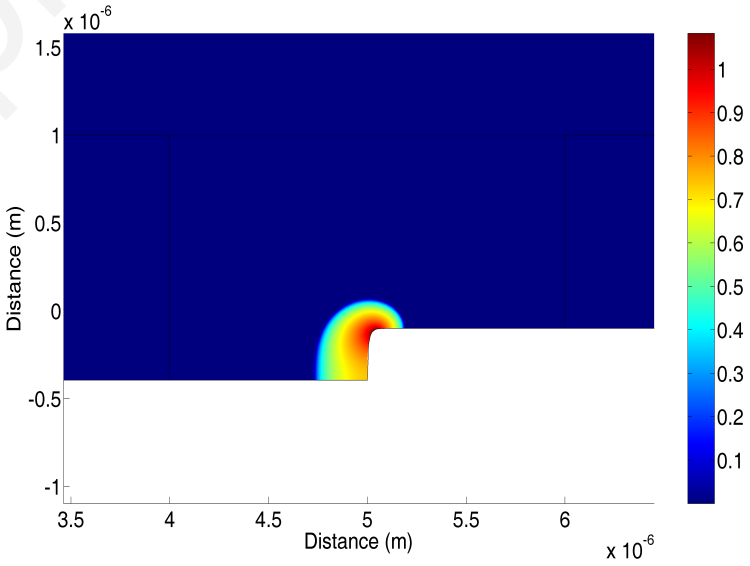

Figure 8.9: The steady state particle collection over the electrode edge for 1 MHz without fluid motion.

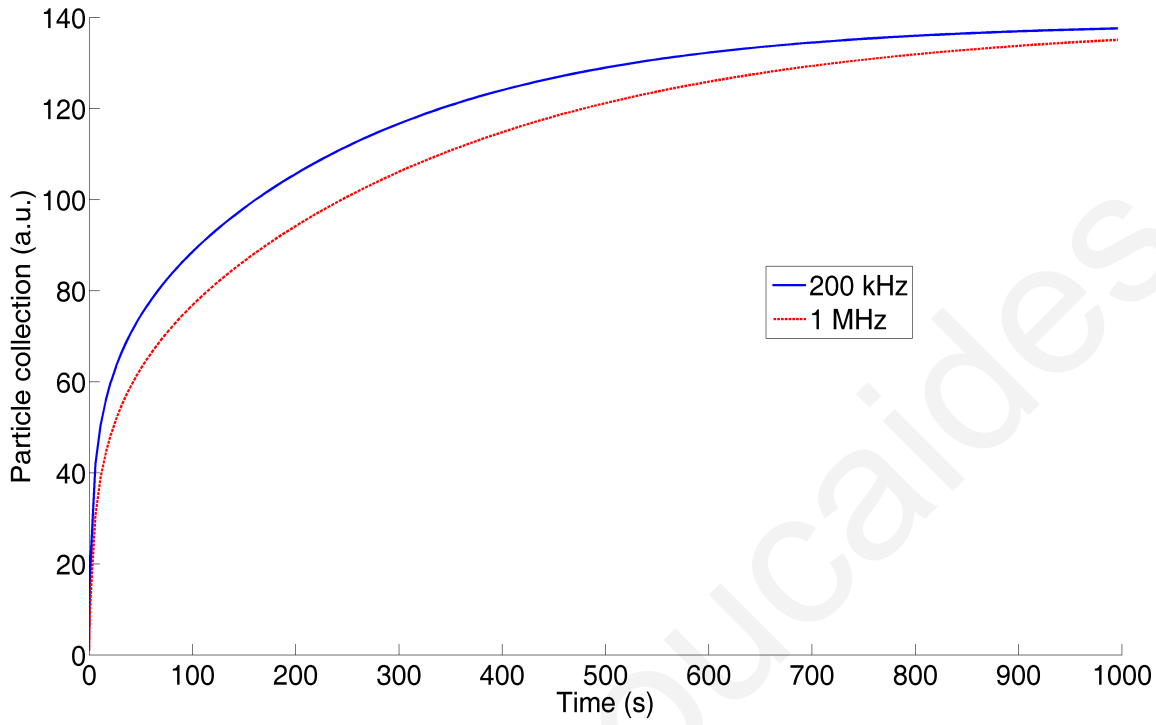

Figure 8.10: The evolution of the particle collection over the electrode edge for 200 kHz and 1 MHz without fluid motion.

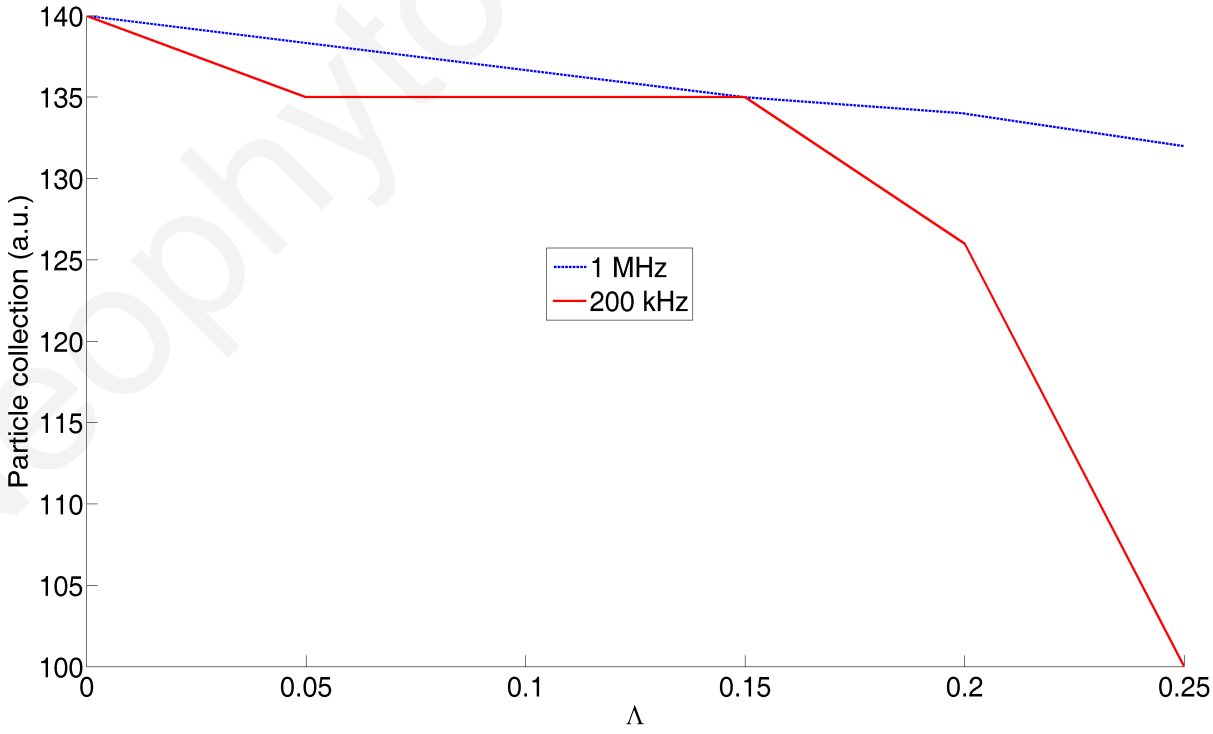

Figure 8.11: The steady state particle collection over the electrode edge for different values of Λ at 200 kHz and 1 MHz.

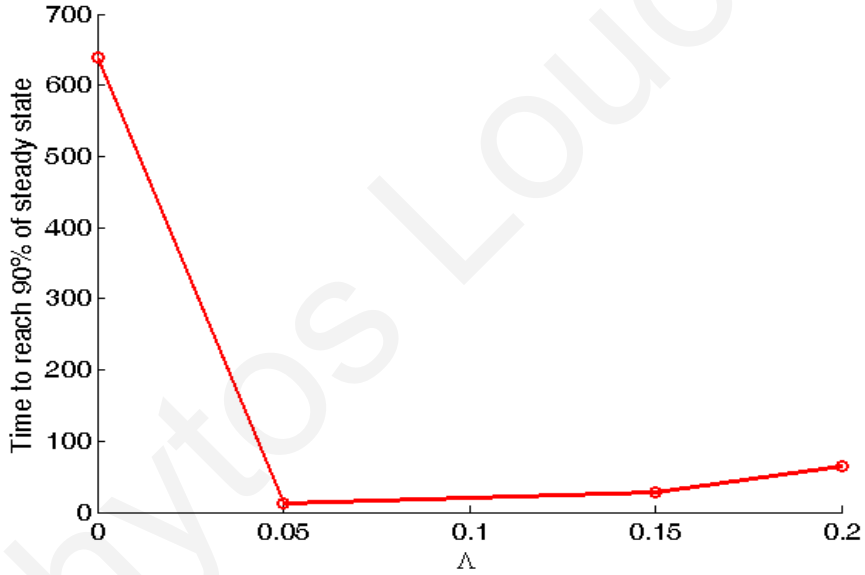

Figure 8.12: The time taken to reach steady state for different values of Λ at 200 kHz.

8.3.2 Investigation of frequency dependence

For the 200 kHz case in figure 8.4 the particle collection steady state is not affected significantly by ACEO. However, what is affected significantly is the initial rate of increase. This becomes much higher with ACEO. As a matter of fact, the analysis of (4) on the initial rate of increase assumes that DEP is the dominant mechanism, which is why it is expected to have a linear relationship with the particle polarisability. However, it is evident here that the initial rate is dominated by ACEO. The dependence of ACEO on frequency is therefore responsible for the non-linearity of the relationship of the initial particle collection rate with the particle polarisability.

The results from figure 8.13 (figure 8.14 is a zoomed version) show that the general form of the particle collection evolution is very similar in terms of the form of the plot and the time scales existent with the fluorescence plots obtained experimentally by (4). In figure 8.15 it can be seen how the steady state particle collection decreases with frequency as also observed experimentally. Direct comparison of the absolute values is not possible, since experimental results are available for the fluorescence and not the particle collection.

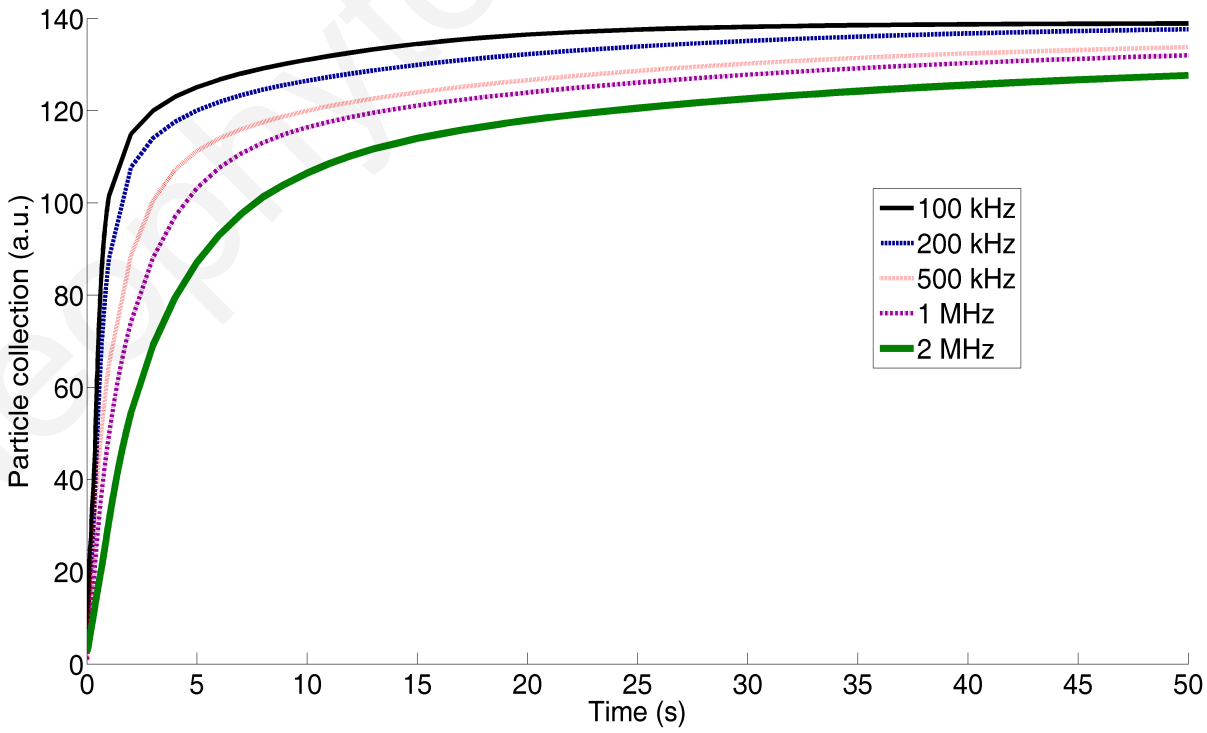

Figure 8.13: The evolution of the particle collection over the electrode edge for all frequencies, $\Lambda = 0.15$.

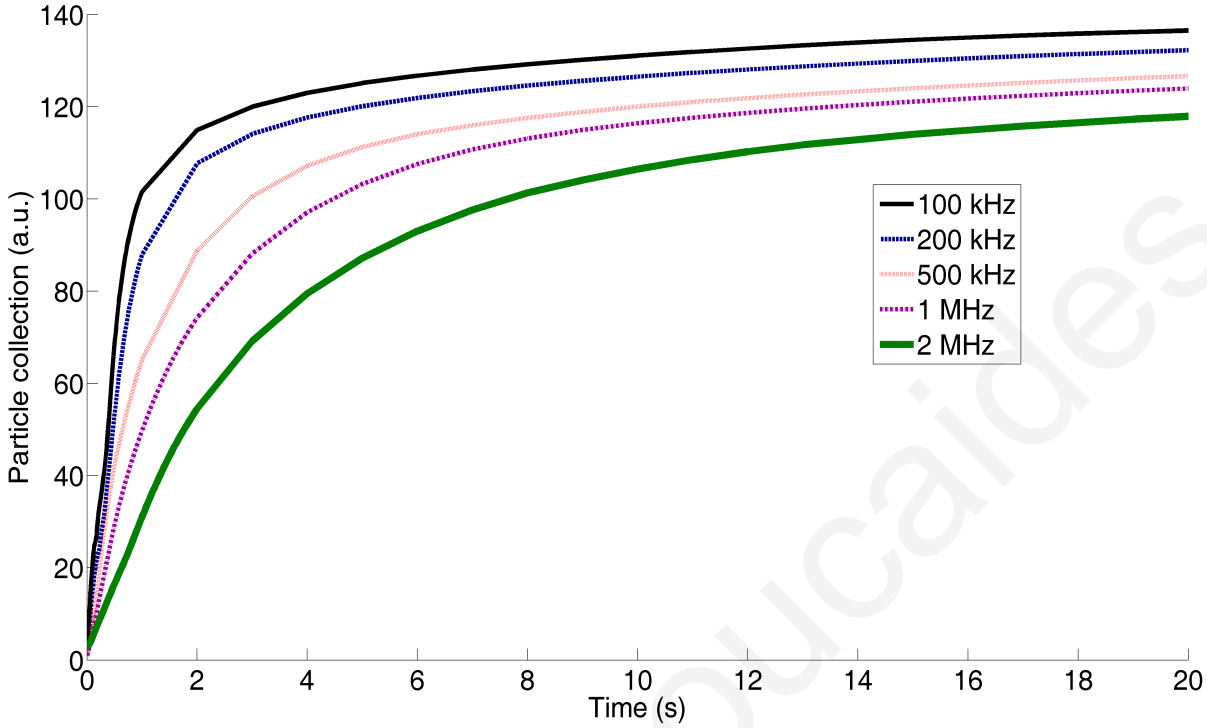

Figure 8.14: The evolution of the particle collection over the electrode edge for all frequencies (zoomed version), $\Lambda = 0.15$.

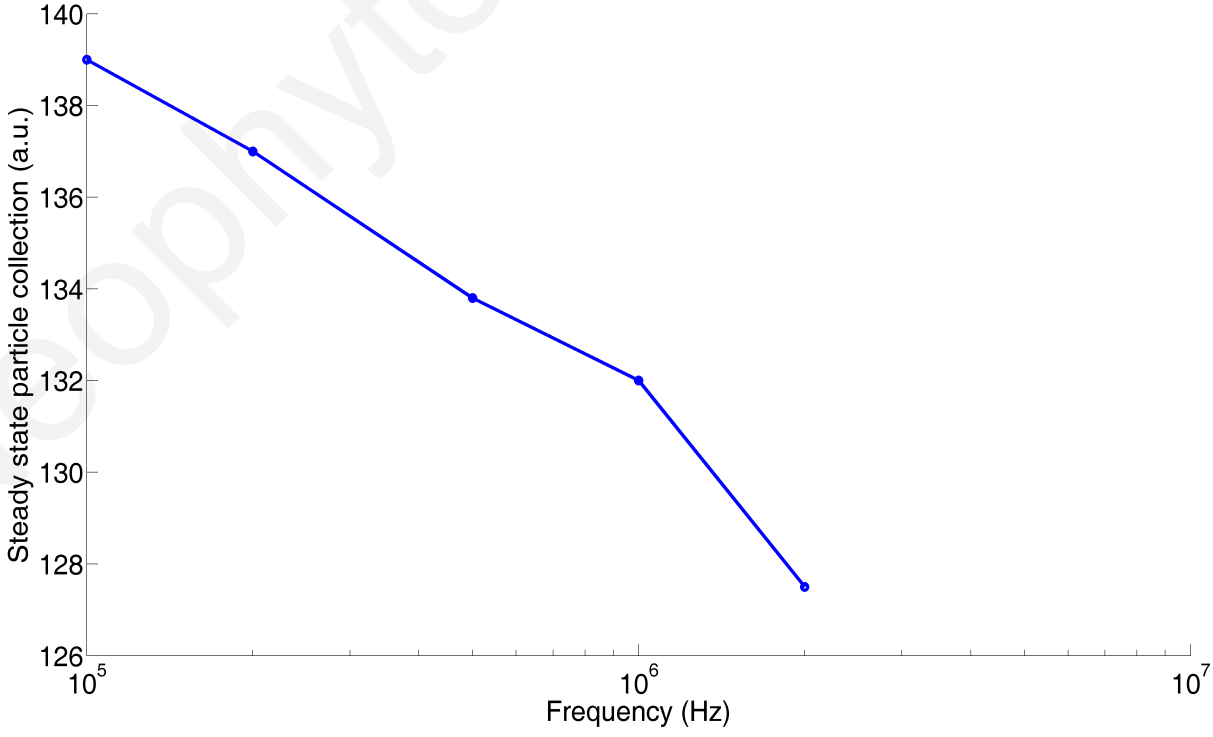

Figure 8.15: Plot of the steady state particle collection vs frequency.

8.3.3 Particle polarisability and initial rate of particle collection

The initial rate, defined as the rate of increase of the particle collection at $t = 0\ s$ (found by dividing the particle collection increase with time for $t = 0.06\ s$, the time instant chosen so that the region used for the calculation is a tangent to the curve at $t = 0\ s$) is plotted with the particle polarisability with and without ACEO in figure 8.16. As predicted by theory, the plot without ACEO is linear. For the plot with ACEO, it is evident that the initial rate is enhanced at all frequencies.

The result from (4) indicates that the enhancement is greater at higher particle polarisability, which resembles the simulation results obtained. Therefore, it is found here that the ACEO fluid motion is a very strong contribution to the departure from the linear relationship predicted by the DEP theory alone. What is further observed here is that the non-linearity is due to enhancement of the process, a fact that has not been verified experimentally but was proposed as a possible explanation by (4). Furthermore, a hypothetical case is also simulated where ACEO is set to zero, but the equations 8.1 are solved for, and the result is plotted in figure 8.16 (no ACEO/with suspension motion). It is evident that some enhancement is still present.

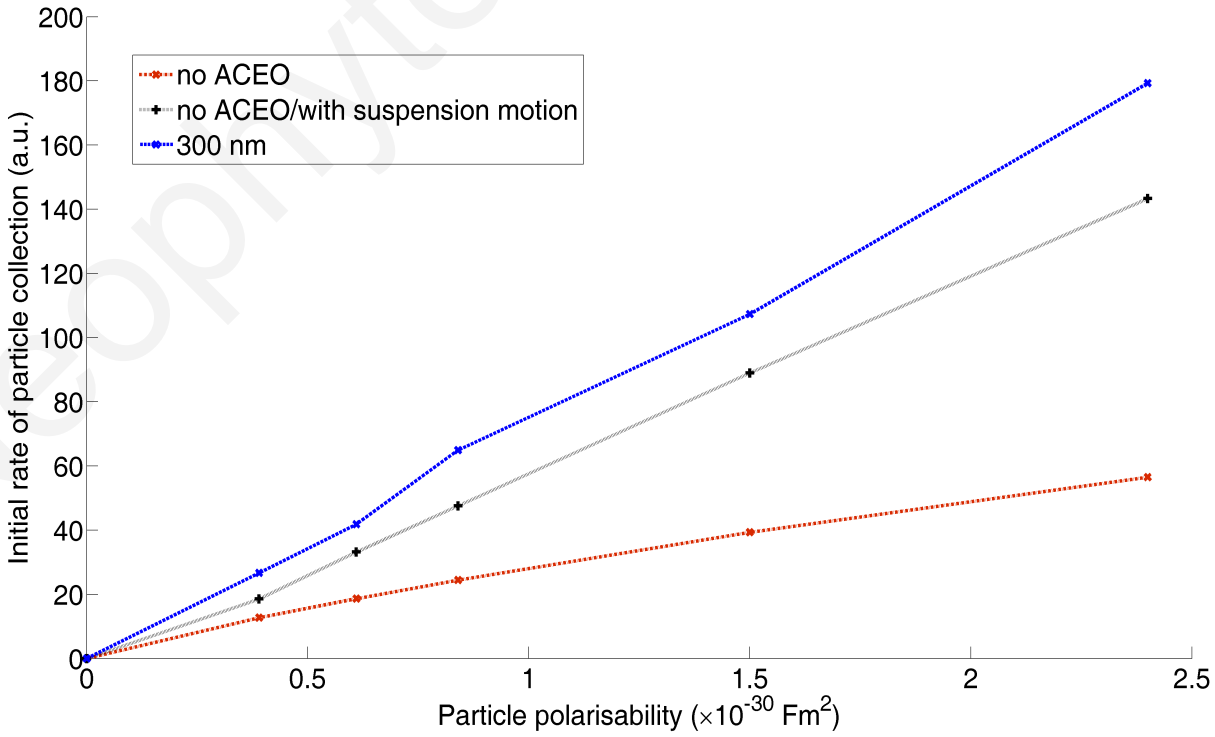

Figure 8.16: The initial rate of particle collection with ACEO, without ACEO and without ACEO but including the suspension motion for $\Lambda = 0.15$.

8.3.4 Investigation of the effect of electrode height

The electrode height is also investigated here as a factor affecting the dynamics of the system. It is a fact that most previous work on the simulation of DEP/ ACEO systems has assumed flat electrodes. While this is geometrically a good approximation, since the electrode height is usually much smaller than the channel height, it is a major source of error for the electrical problem and therefore the DEP and ACEO calculations. The flat electrode theoretically causes an infinite electric field at its edge and so will an electrode of which the edge is a 90^o angle. Instead, a finite height electrode is used throughout this thesis (apart form chapters 3 and 4, where comparison had to be made with simulations which use the flat electrode approximation). The electrode height is typical of real devices and is very important in trapping, as can be seen here, due to the fact that DEP and ACEO calculations are more realistic and also because ACEO velocity is blocked in the regions where the electrode meets the substrate, therefore enhancing trapping at frequencies where ACEO is important.

The simulation for $\Lambda = 0.15$, at 2 MHz is repeated for an electrode height of 400 nm, 350 nm, 300 nm, 200 nm, 100 nm and 50 nm and for $\Lambda = 0.15$, at 200 kHz for an electrode height of 400 nm, 300 nm, 200 nm and 100 nm. It can be seen in figures 8.17 and 8.18 that for the 200 nm, 100 nm and 50 nm electrodes the DEP enhancement and speed of convergence are reduced for the lower frequency, while the enhancement is increased for the higher frequency and the speed of convergence is also increased.

In figure 8.19 the initial rate of increase is plotted for the 100 nm and 300 nm electrode cases, together with the previous case. It is obvious that compared to experimental observations the initial rate dependence on particle polarisability is similar both qualitatively and quantitatively with the quadratic shape observed experimentally, with the 100 nm better fitting the quadratic shape than the 300 nm electrode case (4). In both cases, nevertheless, the initial rate is enhanced. Therefore, it is verified again that the non-linearity is due to enhancement of the process indeed.

In figure 8.20 the steady state particle collection is plotted against the particle polarisability. This is found not to be linear, in contrast to the experimental results by (4) where the fluorescence is found to be linear. This is inconclusive, however, because the fluorescence measured by (4) is not proportional to the particle collection beyond some point where particle layers overlap. Physically, what happens is that the steady state particle collection flattens out at higher particle polarisability, due to the ACEO flow which carries away particles that are further than the distance where the DEP force is smaller than ACEO. That is, even if DEP is stronger, particles away from the electrode edge cannot keep accumulating due to the effect of ACEO.

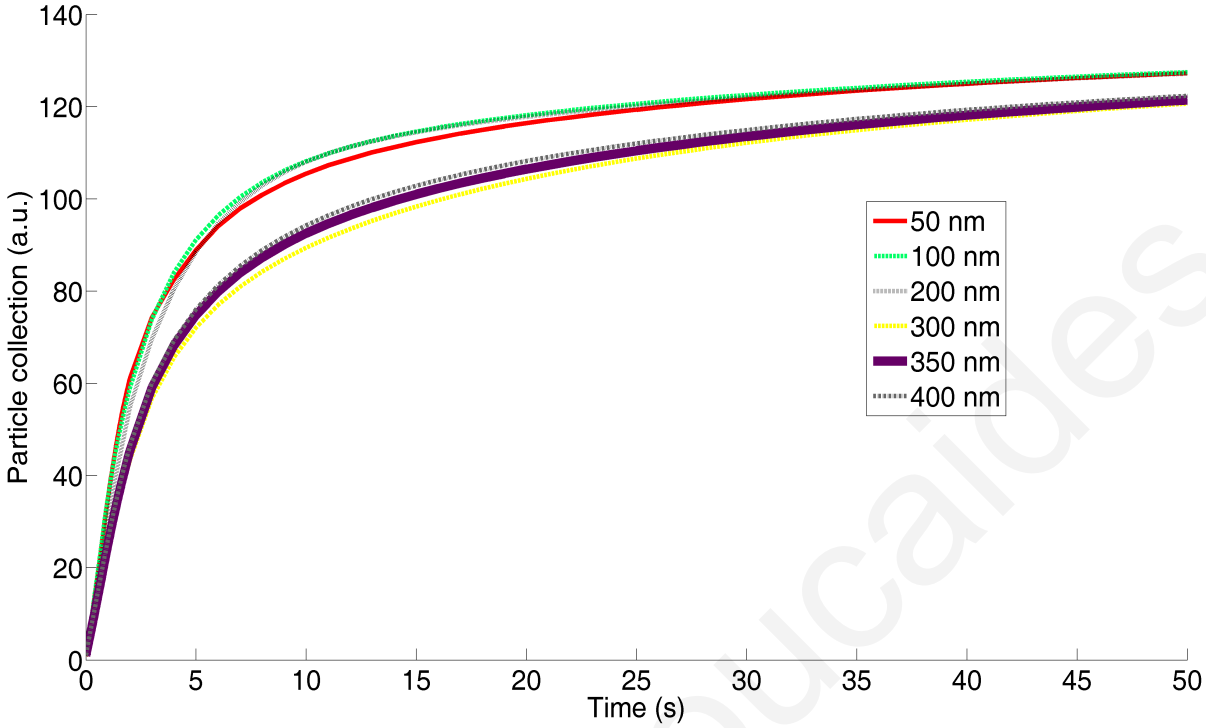

Figure 8.17: The evolution of the particle collection over the electrode edge for $\Lambda = 0.15$ 2 MHz and electrode height of 400 nm, 350 nm, 300 nm, 200 nm, 100 nm and 50 nm.

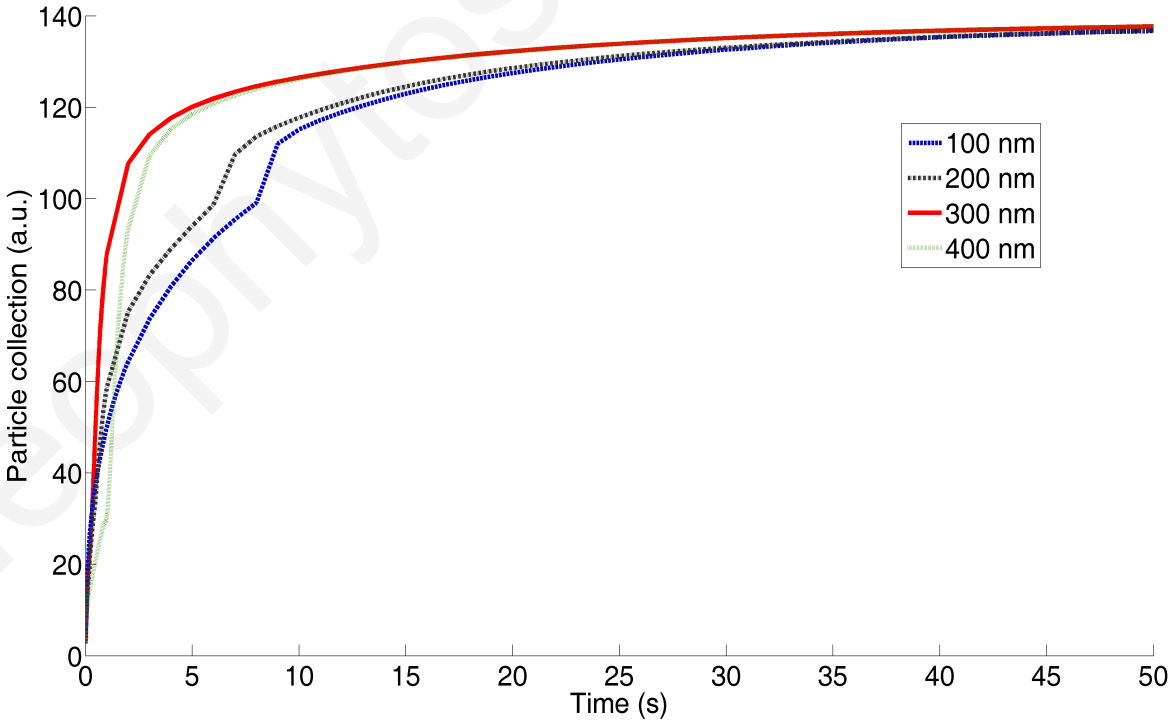

Figure 8.18: The evolution of the particle collection over the electrode edge for $\Lambda = 0.15$ 200 kHz and electrode height of 400 nm, 300 nm, 200 nm and 100 nm (the integral is taken over the whole electrode surface, due to the particle collection extending beyond the focal region at this frequency).

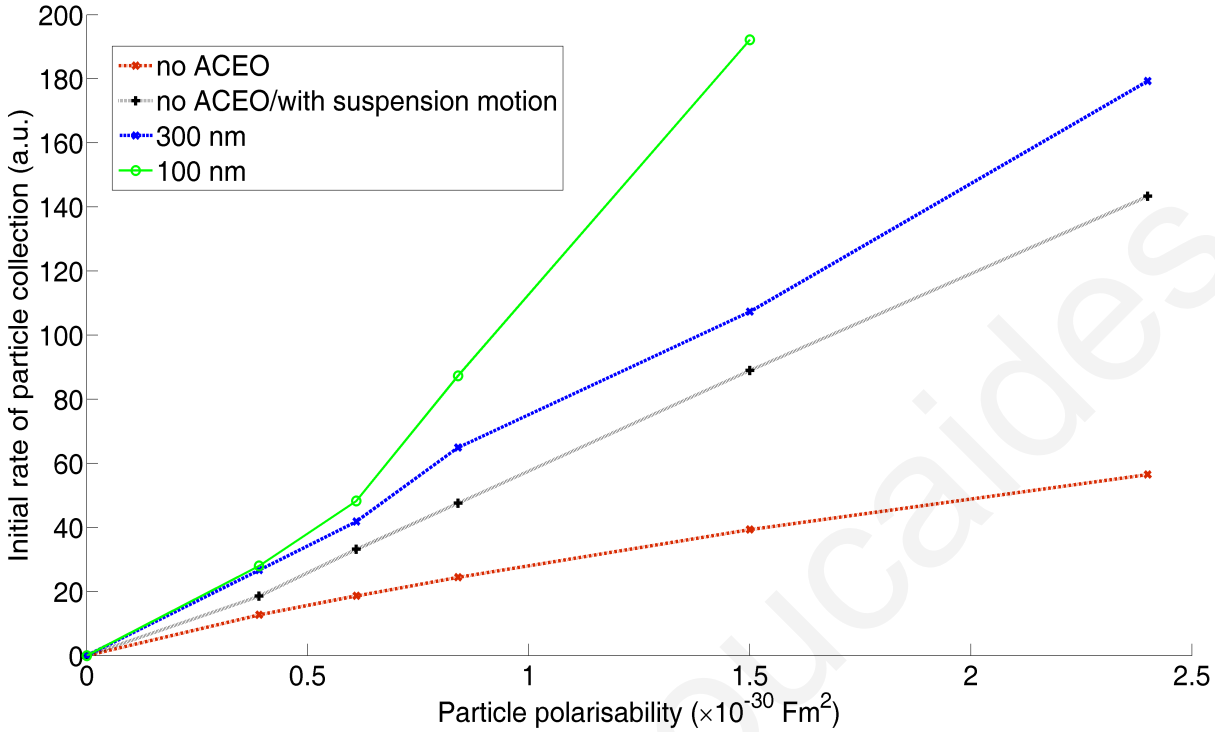

Figure 8.19: The initial rate of particle collection ($\Lambda = 0.15$) and different electrode heights of 100 nm and 300 nm.

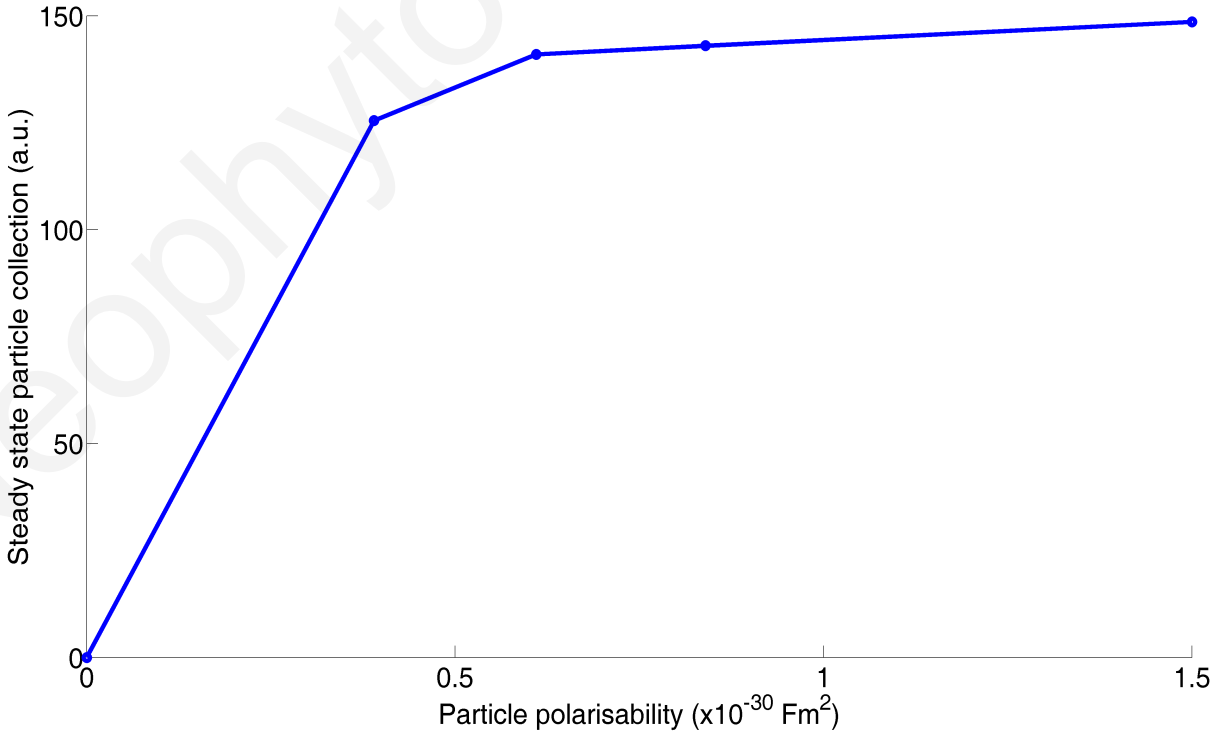

Figure 8.20: Steady state particle collection ($\Lambda = 0.15$) for an electrode height of 100 nm vs the particle polarisability.

8.3.5 Investigation of the effect of particle size

In this section the effect of the DNA particle size is investigated in the range between $3 - 12$ *kbp*. Figure 8.21 depicts the evolution of the collection for the different particle sizes. It can be seen that it increases more slowly for the smaller particles and the steady state particle collection is lower, which is consistent with theoretical and experimental data.

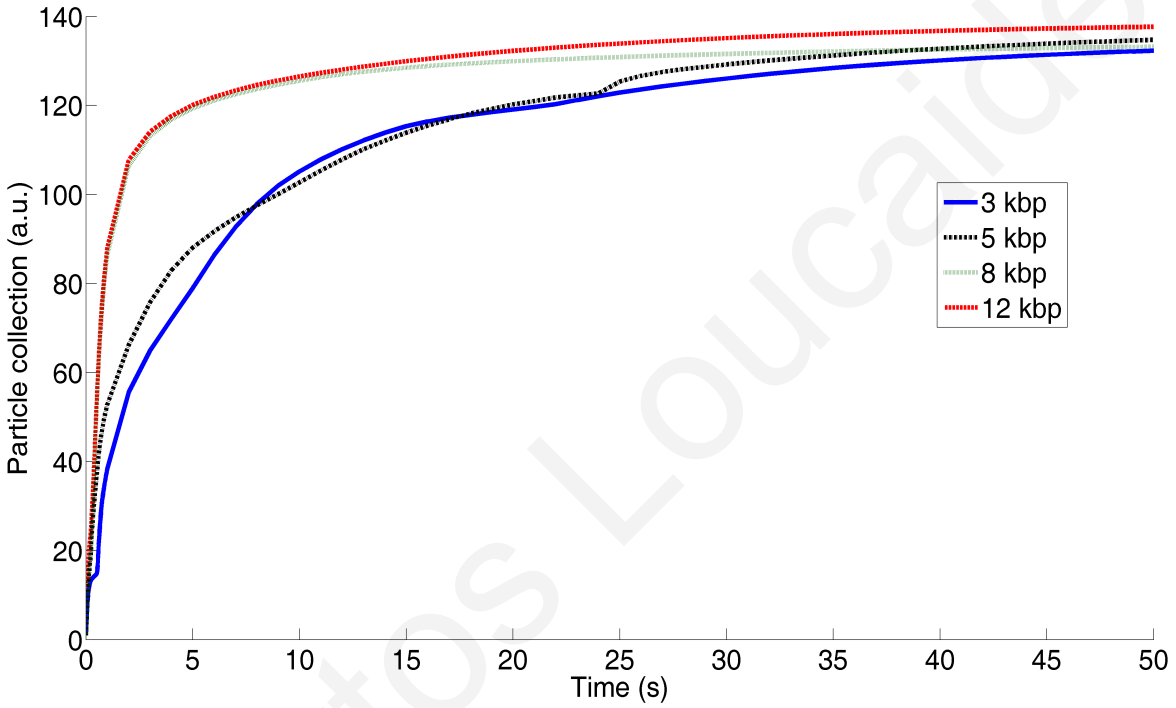

Figure 8.21: The evolution of the particle collection over the electrode edge for 200 kHz and DNA of 3 *kbp*, 5 *kbp*, 8 *kbp* and 12 *kbp* length.

8.3.6 Steric vs non-steric model for 20 *bp* particles

Previous simulations (144) in chapter 6 were performed for much smaller particles of 20 *bp* length due to the properties of the former model, which did not account for the steric particle effect. Here the two models are compared. The focal area was redefined as 200 *nm* from either side of the electrode edge and 300 *nm* height due to the fact that the particle collection is much more localised for the smaller particles, as expected and the larger focal area was too vague. Figure 8.22 reveals the differences between the two models. The new model has a larger steady state particle collection while the old model is approximately the same. This can be explained by the physics of the model: since the new model reduces the velocity of the particles and increases the suspension viscosity where the concentration increases, in regions where the concentration increases the velocity reduces and therefore the particles remain 'attached' to that region.

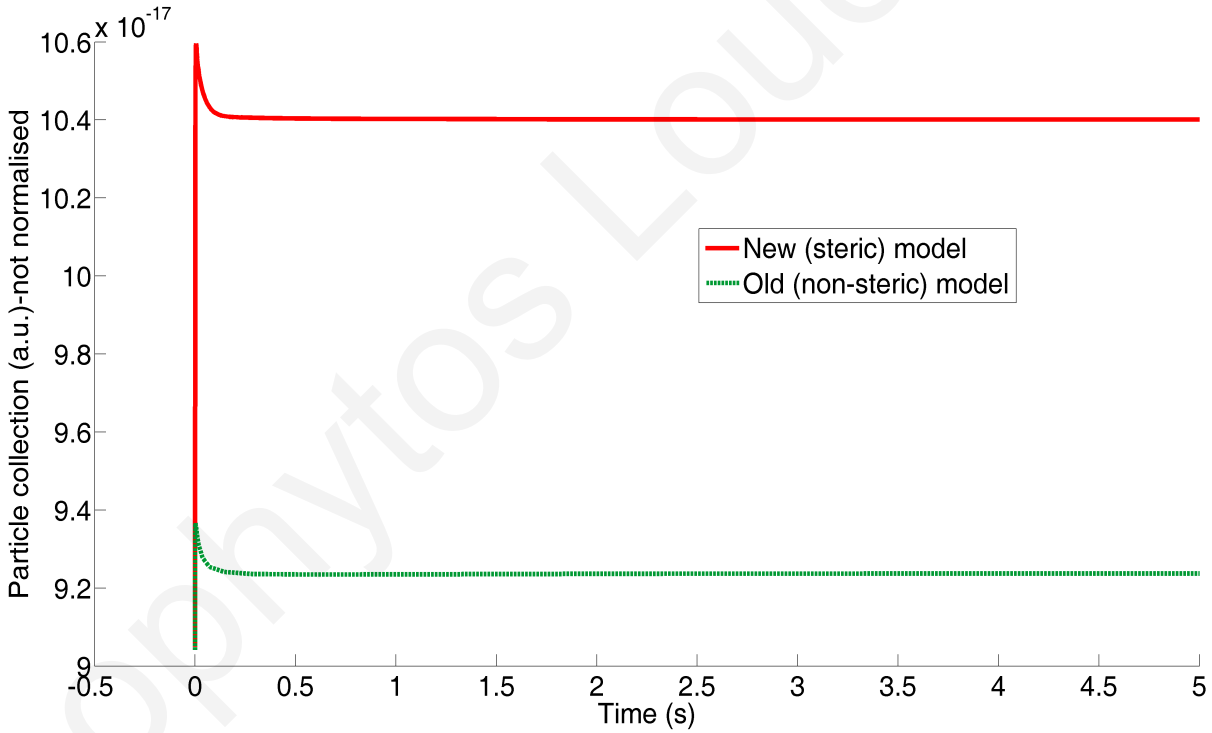

Figure 8.22: The evolution of the particle collection over the electrode edge for 20 *bp* DNA for the cases using the old (non-steric) model and the new (steric) model.

8.3.7 Investigation of the effect of DNA coiling

The DNA molecule used in the simulations above is modelled as a cylinder. However, DNA of such length is expected to exhibit some degree of coiling. In order to investigate the effect of this coiling, the extreme case of an equivalent molecule having the same volume but being spherical is simulated. The result for the concentration is shown in figure 8.23. It can be seen that for the cylindrical DNA the evolution is slower and the steady state concentration is smaller, although to a very small degree.

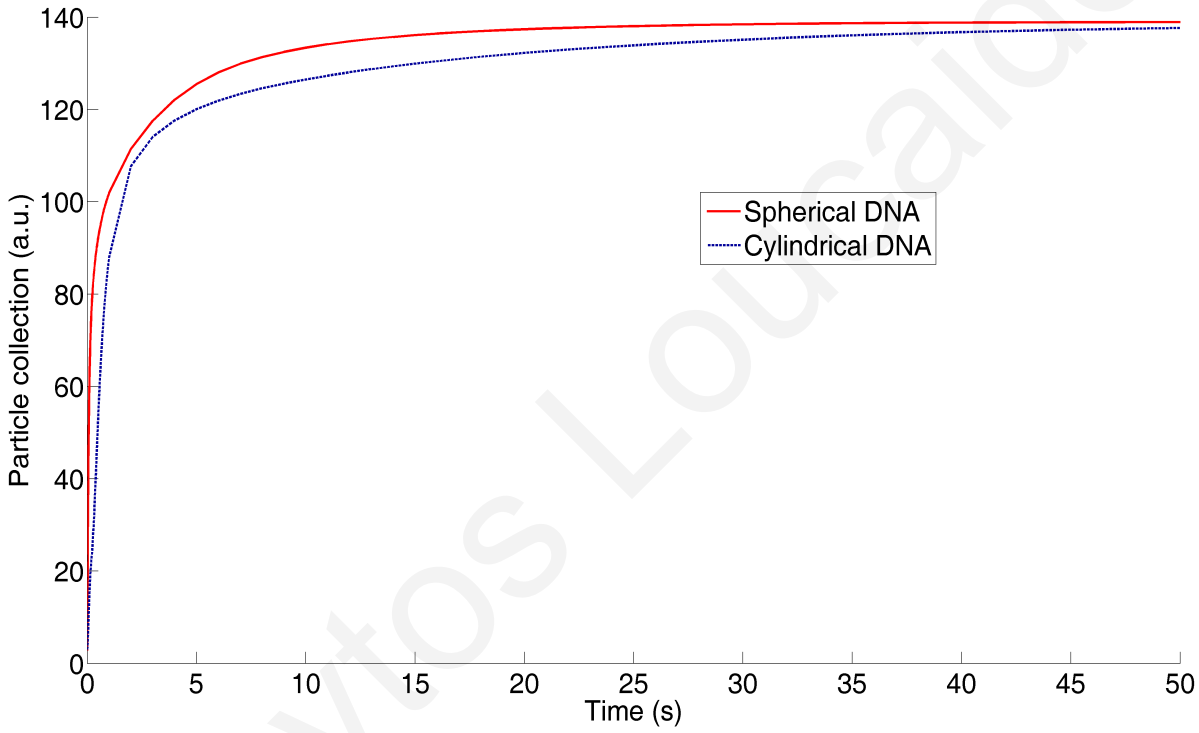

Figure 8.23: The evolution of the particle collection over the electrode edge for the cylindrical and spherical DNA model.

8.3.8 Investigation of the effect of DNA variable density

The DNA molecule is assumed in the simulations to have a density of 1.1 $Kg.m^{-3}$. However, the density of the DNA molecule depends on the environment it is placed in, due to hydration phenomena (148). Therefore, a simulation is repeated for density of 1.7 $Kg.m^{-3}$, so that the effect of this is investigated. It can be seen in figure 8.24 that the effect of this is negligible, since the gravitational force is very small compared to the DEP and ACEO phenomena present in this system. Therefore, this variable is not considered to affect the simulations significantly.

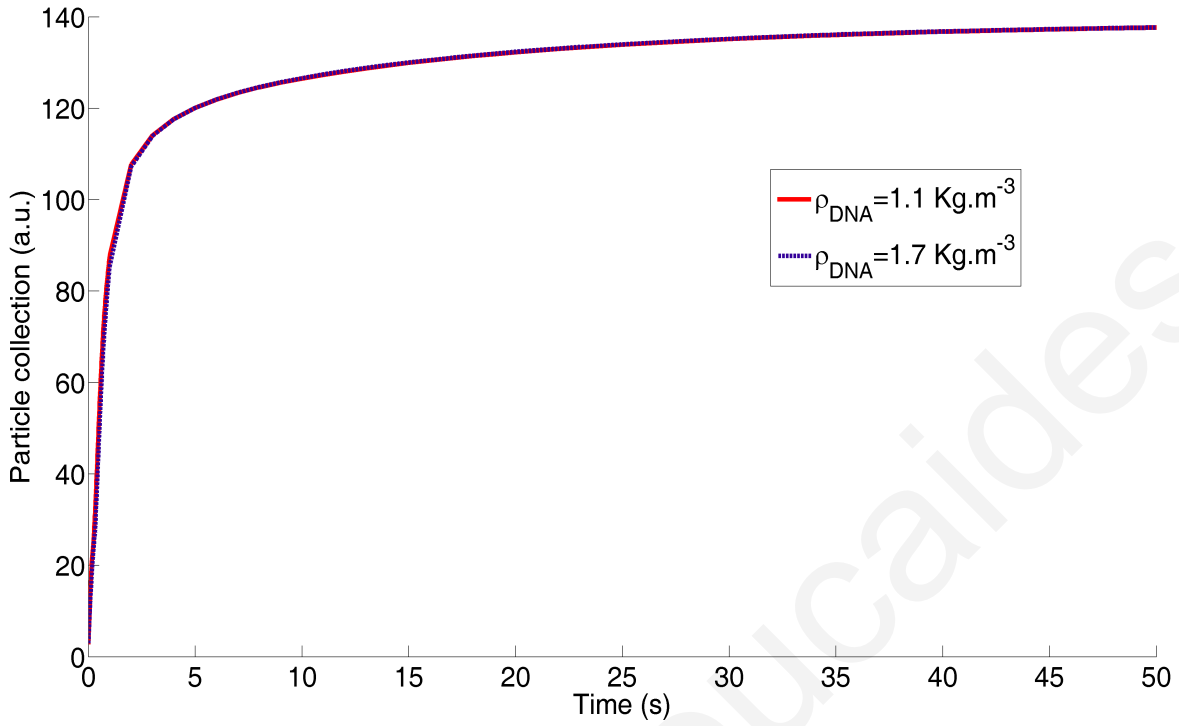

Figure 8.24: The evolution of the particle collection over the electrode edge for two DNA density settings.

8.3.9 The Péclet ratio

The Péclet ratio is the ratio of advection to diffusion in a system and is very important in the analysis of DEP manipulation systems. In the system of interest here, it is found to be:

$$P_{DEP} = \frac{u_{DEP}}{D} \Rightarrow P_{DEP} = \frac{a_m V^2}{4L^2 k_B T} \tag{8.8}$$

Substituting for dsA5 DNA the values are $V = 4.5\ V$, $L = 10\ \mu m$, $a_m = 5 \times 10^{-33}\ F.m^2$ giving $P_{DEP} \approx 0.063$ while for pTA250 DNA $a_m = 2.4 \times 10^{-30}\ F.m^2$ giving $P_{DEP} \approx 30$. Of course, the characteristic length $L = 10\ \mu m$ used here is for the domain bulk and is reduced significantly close to the electrode edges, where $u_{DEP} \approx 10\ \mu m/s$, giving $P_{DEP} \approx 1$ for dsA5 DNA and $P_{DEP} \approx 100$ for pTA250 DNA. Therefore, while for both particles DEP is significant close to the electrode edges, in the domain bulk the dsA5 DNA case is dominated by diffusion while the pTA250 DNA case is dominated by DEP.

8.4 Investigation of the effect of using exponential approximations

As mentioned in section 8.2.2, exponential models are used in the place of the polynomial parameters η_c, $Z(c)$ and $K(c)$. In this section the effect of the exponential models being used instead of the polynomial approximations is investigated. This is done in order to estimate the possible error from this substitution.

8.4.1 Viscosity variation

Another approximation was simulated for the viscosity. This is given by

$$\eta_c = 1 \times 10^{-3} \times e^{|(c)/0.3|^4} \tag{8.9}$$

The result is plotted in figure 8.25.

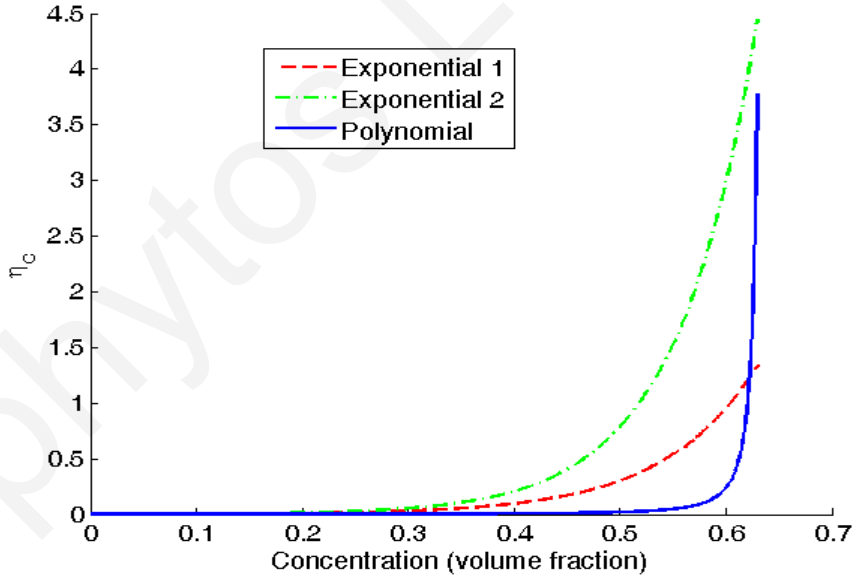

Figure 8.25: The second exponential expression for η_c plotted with the polynomial expression and the first exponential. Exponential 1 was used for the simulations.

It can be seen in figure 8.26 and 8.27 that the effect of this modification is very small, therefore justifying the approximation, since the small deviation from the true value is less than the deviation from the modified exponential model.

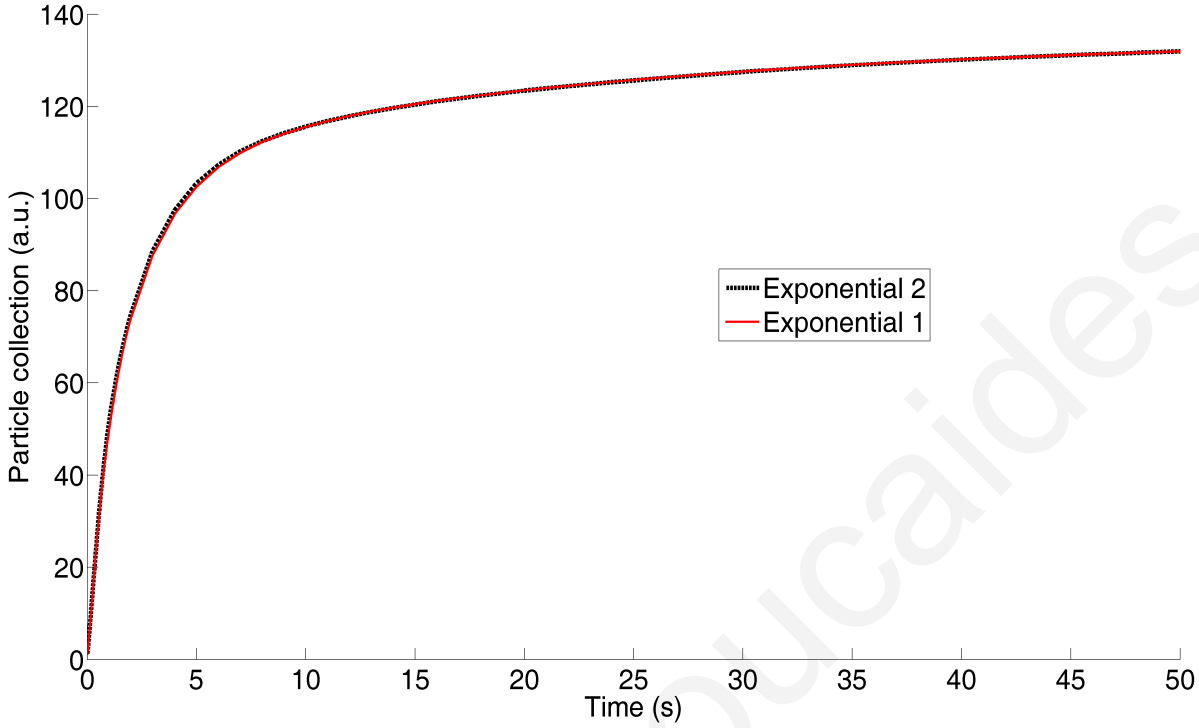

Figure 8.26: Comparison of the particle collection at 1 MHz for the two exponential models of η_c. Exponential 1 was used for the simulations.

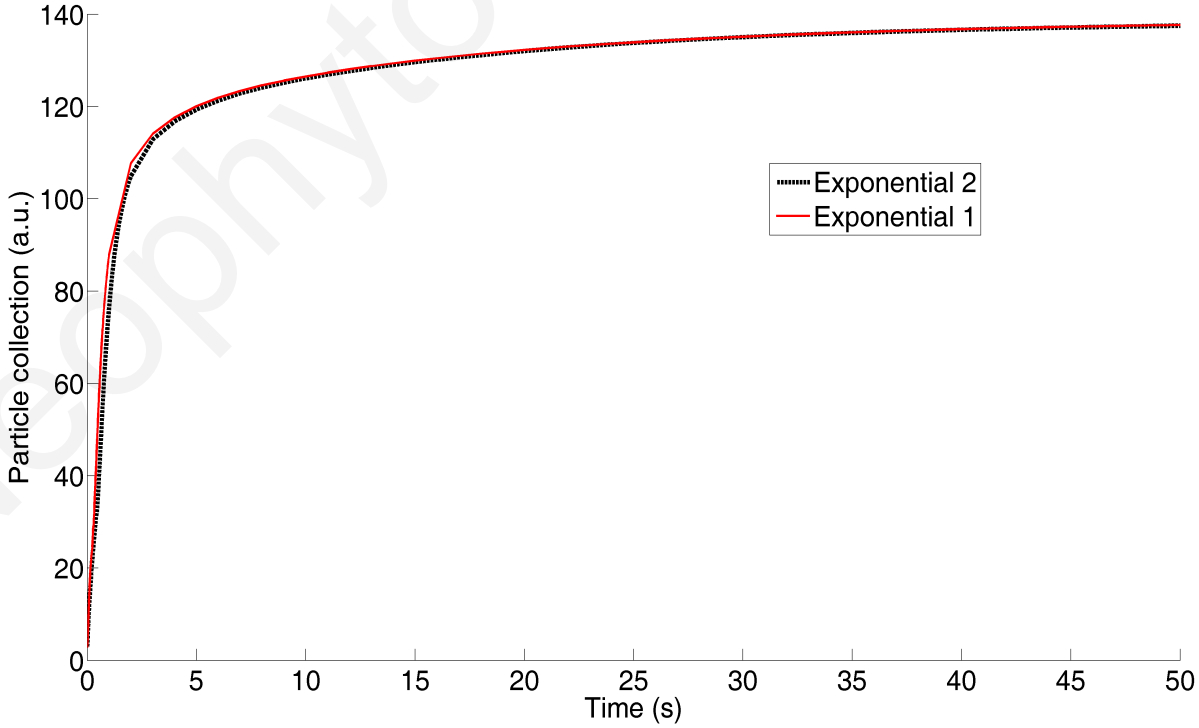

Figure 8.27: Comparison of the particle collection at 200 kHz for the two exponential models of η_c. Exponential 1 was used for the simulations.

8.4.2 Z(c) variation

$Z(c)$ is modified as follows:

$$Z(c) = 0.5 \times (e^{c/0.18} + e^{-c/0.18}) \tag{8.10}$$

The new $Z(c)$ is plotted with the previous ones as shown in figure 8.28. Figure 8.29 shows the effect of this modification. The effect at 1 MHz is minimal, whilst it is more important at 200 kHz. The effect at 200 kHz is more important at the steady state and does not affect the initial rate of increase, as expected since it is more important at high particle collection.

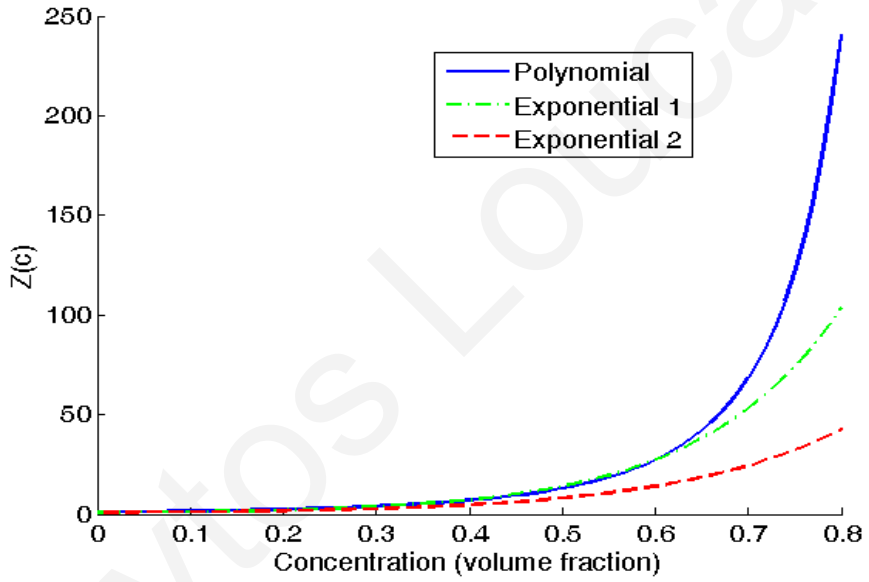

Figure 8.28: The second exponential expression for $Z(c)$ plotted with the polynomial expression and the first exponential. Exponential 1 was used for the simulations.

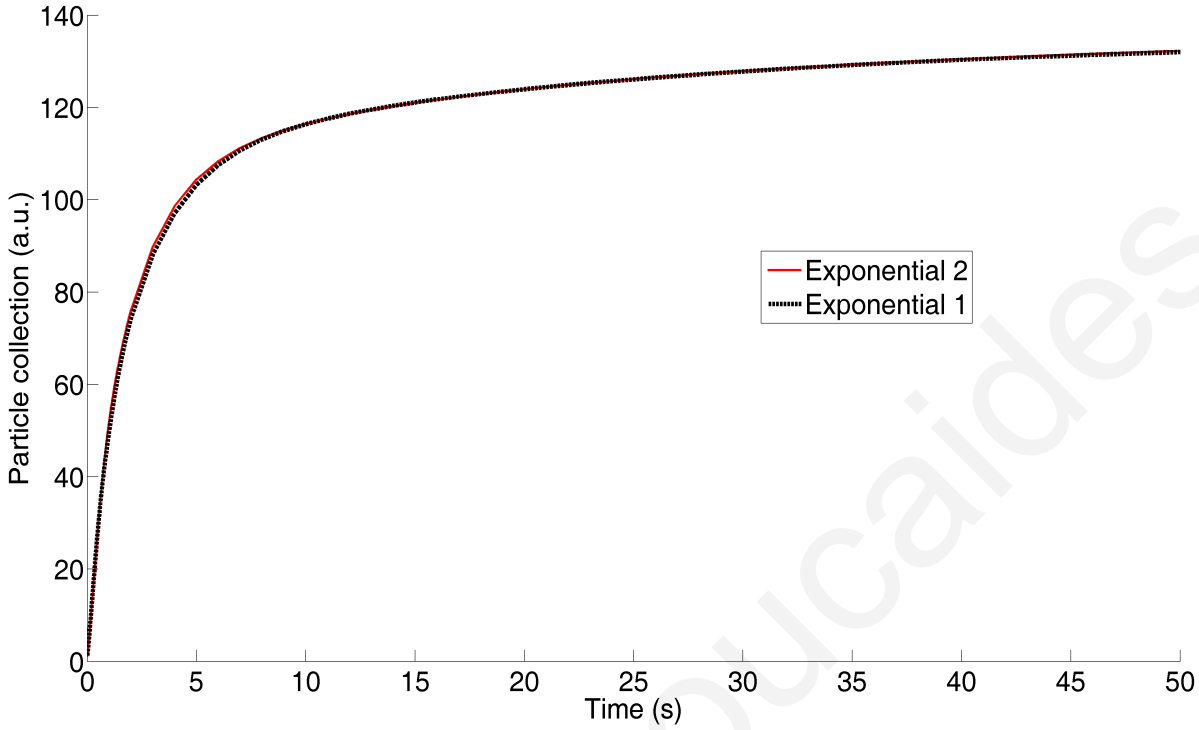

Figure 8.29: Comparison of the particle collection at 1 MHz for the two exponential models of $Z(c)$. Exponential 1 was used for the simulations.

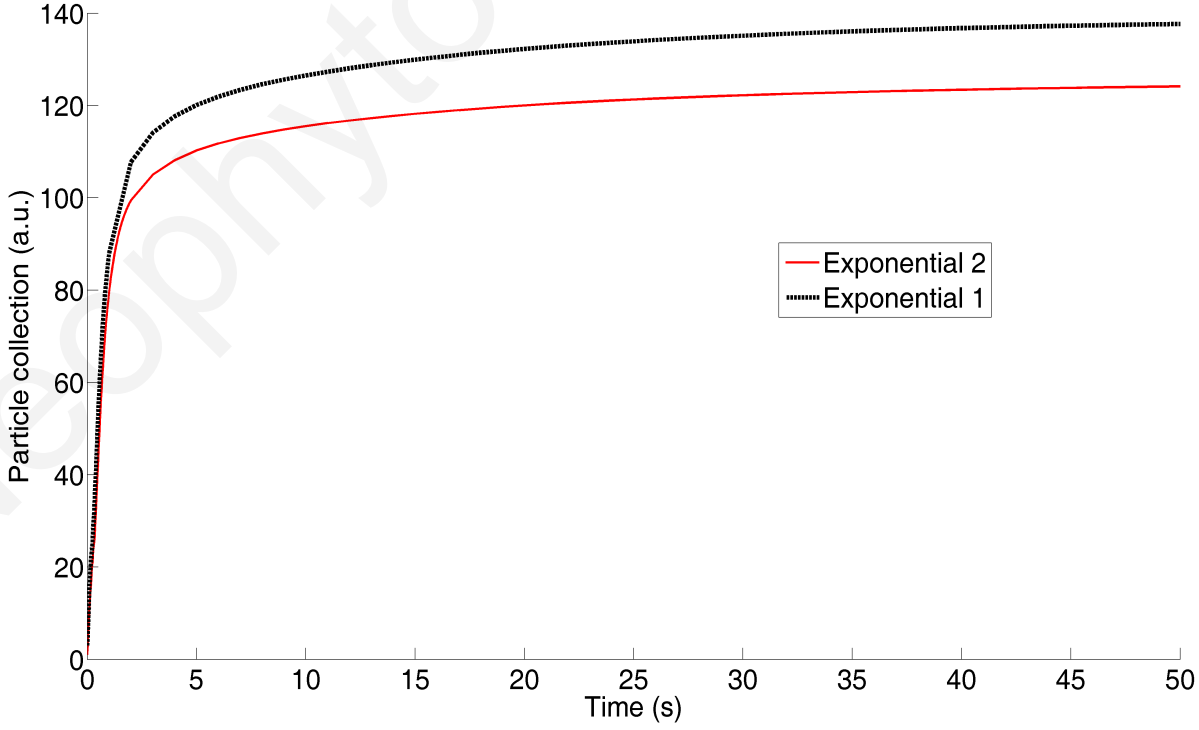

Figure 8.30: Comparison of the particle collection at 200 kHz for the two exponential models of $Z(c)$. Exponential 1 was used for the simulations.

8.4.3 K(c) variation

$K(c)$ is modified as follows:

$$K(c) = e^{-|(c)/0.2|} \tag{8.11}$$

It is evident in figure 8.31 that the effect of this modification on $K(c)$ is minor. The effect on the particle collection can be seen in figures 8.32 for 1 MHz and 8.33 for 200 kHz.

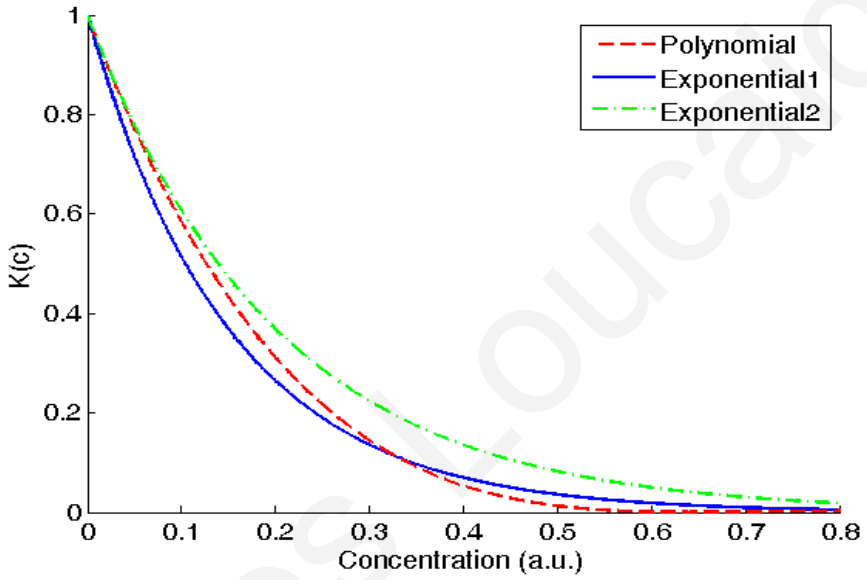

Figure 8.31: The second exponential expression for $K(c)$ plotted with the polynomial expression and the first exponential. Exponential 1 was used for the simulations.

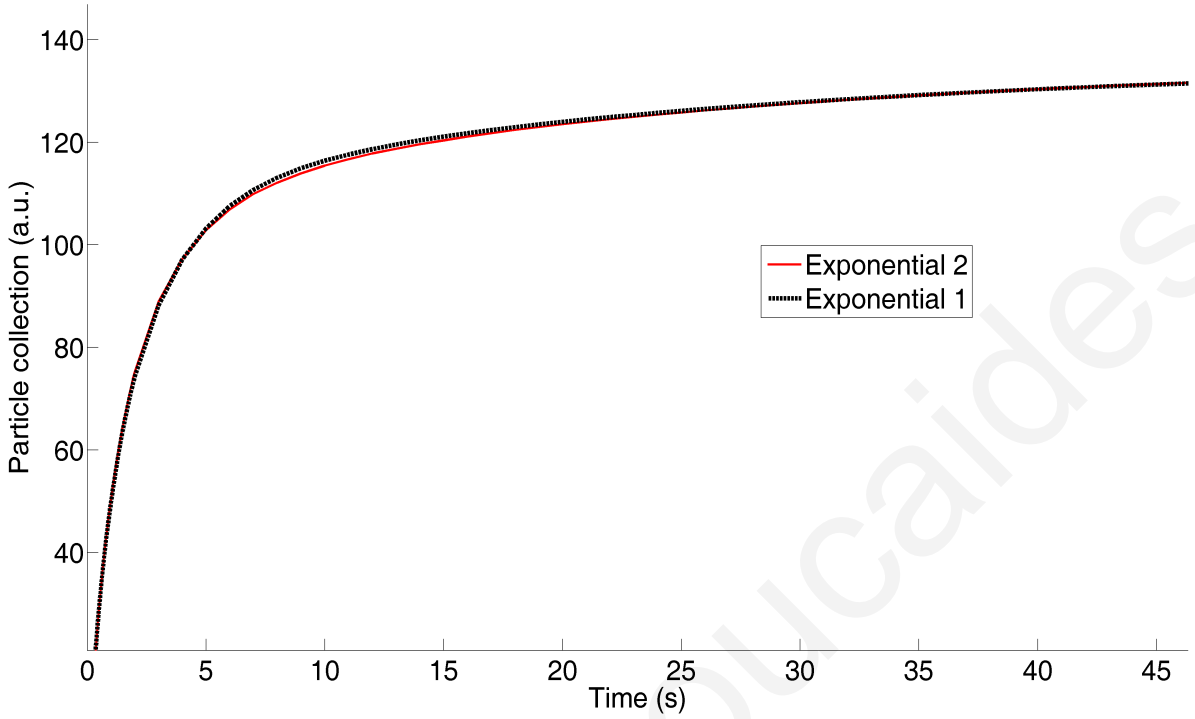

Figure 8.32: Comparison of the particle collection at 1 MHz for the two exponential models of $K(c)$. Exponential 1 was used for the simulations.

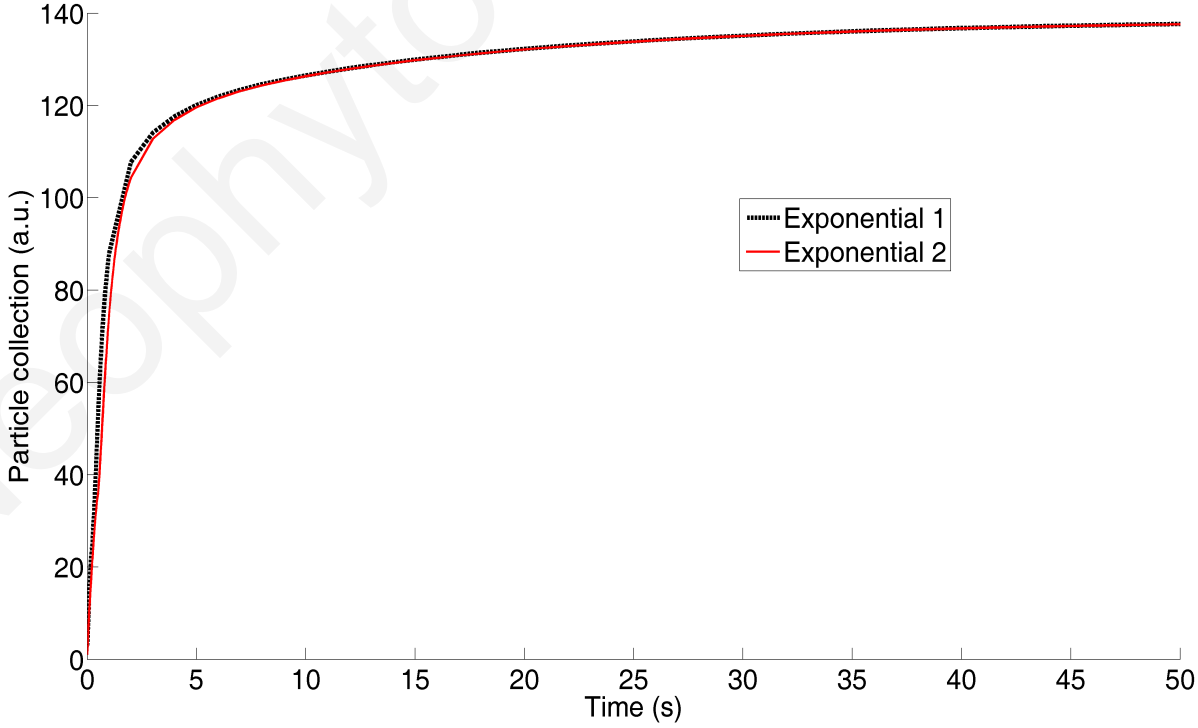

Figure 8.33: Comparison of the particle collection at 200 kHz for the two exponential models of $K(c)$. Exponential 1 was used for the simulations.

8.5 Conclusions

In this section, a model for the collection of DNA on parallel electrode arrays by DEP and ACEO has been introduced that incorporates steric effects in the suspension motion, in addition to the Smoluchowski equation for the particle concentration.

The simulations using this model enable the direct comparison with experimental results, with which good qualitative match in behaviour is observed. The results suggest that the ACEO motion of the fluid is responsible to a significant extent for the non-linearity of the relationship of the particle polarisability and the initial rate of particle collection observed experimentally.

Furthermore, it is found that the non-linearity is due to enhancement of the process speed. Other parameters are also investigated, such as the effect of electrode height, providing interesting design guidelines.

Chapter 9

Conclusions

The main objective of this work was to provide numerical simulations for devices utilising AC Electrokinetics for particle manipulation, in order to aid the analysis and design of such devices. This started with a physical model describing the dynamics of a particle suspended in a fluid under the influence of the Dielectrophoretic force. The electric field distribution was found numerically for a system for which the analytical solution of the electric field and therefore the DEP force, was known, so that the calculations could be verified.

In the next step, a physical model was introduced for the ACEO fluid motion and was also verified. Numerical simulations were then used in order to analyse existing ACEO pumping devices. The analysis performed led to the design of novel systems that can be used for pumping with a configurable direction and introduced the concept of geometric asymmetry formation using electrode excitation grouping. This has numerous applications in lab-on-chip systems where pumping is achieved using ACEO and has already led to the construction of such devices and derivatives of these with many applications.

Furthermore, a physical model was introduced for the Electrothermal fluid motion. This was also solved numerically and verified. The numerical simulations produced were used in order to investigate devices that use Electrothermal fluid motion for biosensor enhancement and specifically the possibility of using combined ACEO with Electrothermal or solely ACEO for the biosensor enhancement. The use of ACEO for this purpose was found to be possible and might be necessary in devices where the electrolyte must be of low conductivity for the sensor to operate.

The DEP and ACEO velocity fields were also analysed simultaneously, so that the particle trapping regions could be identified. A configurable asymmetric system was then proposed in which the trapping points can be varied when the asymmetry is changed. This can be very useful in particle manipulation applications.

It was found, however, that a velocity field analysis did not suffice in the investigation of

particle manipulation devices. Therefore, the Smoluchowski equation was used to simulate the dynamics of the ACEO and DEP motion of the particles together with diffusion. The results showed that the effect of ACEO on the particle concentration is detrimental and that its inclusion in DEP manipulation simulations is essential. However, this model had limitations on the particle size that could be examined. When the particle size became too high, the diffusion embedded in the Smoluchowski equation was not enough to prevent the particle concentration from reaching non-realistic limits.

In order to resolve this limitation, a modification was introduced in the Smoluchowski equation that takes into account the finite particle size. This prevents the simulated concentration from reaching excessively high values and also modifies the system dynamics as the concentration becomes higher. The system was simulated using the particle steric model and very important differences were observed with the non-steric model. In the final step, the physical model was extended to include modifications in the suspension velocity, by using modified Navier-Stokes equations. Therefore, joint DEP and ACEO with the incorporated particle steric effect were simulated and comparison was made to experimental data, where a very similar behaviour is observed.

Furthermore, some modes of operation that were previously unexplained have been investigated. The experimental results exhibited a non-linear relationship of the initial rate of increase of the concentration with the polarisability of the DNA particles, while DEP theory predicted a linear relationship. By including the suspension motion and ACEO it was found that the process is enhanced and that is why the linear relationship is not experimentally observed. Also, many parameters in the device operation were investigated, such as the electrode height, the frequency and the particle size.

9.1 Future Work

While a lot of progress has been made through this work, the accuracy of the simulations can be further developed by introducing more phenomena into the problem.

The first of these phenomena is the effect of the particle concentration on the electric field. The high particle concentration changes the dielectric properties of the suspension and therefore disturbs the solution for the electric field locally. This would render the simulations more accurate and is a recommended addition to the physical model.

The second phenomenon that can be important in the simulation of such a system is the interaction of the particles with the electrode surface. The most important of these is the phenomenon of stiction. This occurs when particles under manipulation come into contact with the electrode or substrate surface and causes them to stick to the electrode

or substrate surfaces and therefore has to be taken into account in order to produce more accurate results.

An important step in the simulation of ACEK manipulation devices is the use of multiscale simulation methods. These can enable the simulation of complete systems such as the ones presented in the thesis, but can also capture the dynamics of particles in a smaller scale region close to the trapping areas, where particle interactions with the surface of the electrodes and with other electrodes are important. Such a model can be realised by using two solution domains, one that includes the complete device and one that includes the much smaller trapping regions. The equations solved in the larger domain can be similar to the model used in the thesis. In the smaller domain that will surround the trapping region, the individual particle dynamics might be simulated using molecular dynamics simulations, therefore giving much more information and accuracy in the solution. Due to the higher detail that can be introduced, individual particle trajectories can be simulated, with the forces on individual particles being modelled.

Another important aspect of the simulation problem is the investigation of the double layer dynamics at high voltages. This investigation is very important in determining a more accurate ACEO model at high voltages and could therefore improve the simulation results. Work on this subject is being published at the time by a number of groups and further developments can be very important.

In the subject of device design, a very promising concept has been introduced, that can be significantly expanded. That is the formation of geometric asymmetries or other grouping by using the electrode excitation, therefore creating devices which are much more flexible in terms of operation modes than fixed-geometry devices. What is even more interesting is the possibility of altering device operation modes by investigating new excitation modes that will exploit device characteristics other than geometry, such as the frequency response.

Furthermore, it is of great importance that manipulation devices are proposed that allow a greater level of particle control, in order for them to be used in practical applications. This can be achieved by careful design that will take into account EHD and DEP in the design process.

Finally, the control of the trapping regions, which should preferably be variable, is of utmost importance in order to achieve true manipulation of micro- and nano-particles and it will no longer suffice to be able to carry particles from one location to another, or trap them in predetermined positions. Novel devices have to be proposed where the trapping regions can be variable and controllable, so that the particles can be moved in predetermined discrete locations with great accuracy.

References

[1] Dimaki M, Bøggild P. DEP of carbon nanotubes using micro-electrodes: a numerical study. Nanotechnology. 2004;15:1095–1102. xvi, 6, 7, 12, 13, 63, 70

[2] Green NG, Ramos A, Gonzalez A, Morgan H, Castellanos A. Fluid flow induced by nonuniform ac electric fields in electrolytes on microelectrodes, III. Observation of streamlines and numerical simulation. Physical Review E. 2002 August;66:026305–11. xvii, 8, 22, 23, 27, 29, 68

[3] Ramos A, Gonzalez A, Castellanos A, Green NG, Morgan H. Pumping of liquids with AC voltages applied to asymmetric pairs of microelectrodes. Physical Review E. 2003;67(056302). xvii, 6, 23, 27, 30, 33, 34, 35

[4] Bakewell DJ, Morgan H. Dielectrophoresis of DNA: time and frequency dependent collections on microelectrodes. IEEE Trans NanoBioscience. 2006 March;5(1):139–146. xxii, 8, 62, 65, 66, 68, 73, 79, 82, 88, 90, 91

[5] Pohl HA. Dielectrophoresis. Cambridge University Press; 1978. 3, 10

[6] Pohl HA. Some Effects of Non-uniform Fields on Dielectrics. J Appl Phys. 1958;29:1182–1188. 3

[7] Chen CS, Pohl HA. Biological dielectrophoresis: the behavior of lone cells in a nonuniform electric field. Annals of the New York Academy of Sciences. 1974;238:176–85. 3

[8] Jones T. Electromechanics of Particles. Cambridge University Press; 2005. 3

[9] Sauer FA, Schlogl RW. Interactions between Electromagnetic Fields and Cells. Chiabrera A, editor. Springer; 1 edition; 1985. 3

[10] Sher L. Dielectrophoresis in Lossy Dielectric Media. Nature. 1968;220:695 – 696. 3

[11] Jones TB. Dielectrophoretic force calculation. Journal of Electrostatics. 1979;6:69–82. 3

[12] Sigurdson M, Meinhart C, Liu X, Wang D. Biosensor performance enhancement through ac electrokinetics. MicroTAS conference. 2003;. 4, 6, 39

[13] Green NG, Ramos A, Gonzalez A, Castellanos A, Morgan H. Electric field induced fluid flow on microelectrodes: the effect of illumination. J Phys D. 2000;33:13–17. 4, 7

[14] Washizu M, Kurosawa O. Electrostatic manipulation of DNA in microfabricated structures. Industry Applications, IEEE Transactions on. 1990;26(6):1165 – 1172. 4

[15] Washizu M, Nanba T, Masuda S. Handling biological cells using a fluid integrated circuit. Industry Applications, IEEE Transactions on. 1990;26(2):352–358. 4

[16] Pethig R. Dielectric properties of body tissues. Clin Phys Physiol Meas. 1987;8:5–12. 4

[17] Mark GH, Talary MS, Pethig R. Separation of viable and non-viable yeast using dielectrophoresis. J Biotechnology. 1994;32:29–37. 4

[18] Becker FF, Wang XB, Huang Y, Pethig R, Vykoukal J, Gascoyne PRC. The removal of human leukaemia cells from blood using interdigitated microelectrodes. J Phys D: Appl Phys. 1994;27:2659–2662. 4

[19] Wang XB, Huang Y, Holzel R, Burt JPH, Pethig R. Theoretical and experimental investigations of the interdependence of the dielectric, dielectrophoretic and electrorotational behaviour of colloidal particles. J Phys D: Appl Phys. 1993;26:312–322. 4

[20] Xiao-Bo Wang RP, Jones TB. Relationship of dielectrophoretic and electrorotational behaviour exhibited by polarized particles. J Phys D: Appl Phys. 1992;25:905–912. 4

[21] Green NG, Morgan H. Dielectrophoretic trapping of single sub-micrometre scale bioparticles. J Phys D. 1998;31:2205–2210. 4

[22] Menachery A, Pethig R. Controlling cell destruction using dielectrophoretic forces. IEE Proc Nanobiotechnol. 2005;152(4):145–149. 4

[23] Bennett D, Khusid B, James CD, Chalambos PC, Okandan M, Jacqmin D, et al. Combined field-induced dielectrophoresis and phase separation for manipulating particles in microfluidics. Applied Physics Letters. 2003;83:4866–4868. 4, 78

[24] Chan RHM, Fung CKM, Li WJ. Rapid assembly of carbon nanotubes for nanosensing by DEP force. Nanotechnology. 2004;15:672–677. 4, 6

[25] Ghallab Y, Badawy W. Sensing methods for dielectrophoresis phenomenon: from bulky instruments to lab-on-a-chip. Circuits and Systems Magazine IEEE. 2004;4(3). 4

[26] Boote J, Evans S. Dielectrophoretic manipulation and electrical characterization of gold nanowires. Nanotechnology. 2005;16:1500–1505. 4

[27] Hughes MP. AC electrokinetics: applications for nanotechnology. Nanotechnology. 2000;11:124–132. 4

[28] Hoettges KF, McDonnell M, Hughes MP. Use of combined dielectrophoretic/electrohydrodynamic forces for biosensor enhancement. J Phys D. 2003;36:101–104. 4, 53

[29] Fixe F, Branz HM, Louro N, Chu V, Prazeres DMF, Conde JP. Electric-field assisted immobilization and hybridization of DNA oligomers on thin-film microchip. Nanotechnology. 2005;16:2061–2071. 4

[30] Gascoyne PRC, Wang XB, Huang Y, Becker FF. Dielectrophoretic separation of cancer cells from blood. Industry Applications, IEEE Transactions on. 1997;33(3):670–678. 4

[31] Germishuizen W, Walti C, Wirtz R, Johnston M, Pepper M, Davies A, et al. Selective DEP manipulation of surface-immobilized DNA molecules. Nanotechnology. 2003;14:896–902. 4, 5

[32] Masuda S, Washidu M, Nanda T. Novel method of cell fusion in field constriction area in fluid integration circuit. IEEE Trans Indust Appl. 1989;25:732–737. 4

[33] Ruthe HJ, Adler J. Fusion of bacterial spheroplasts by electric fields. Biochim Biophys Acta. 1985 September;819(1):105–113. 4

[34] Zimmermann U, Vienken J. Electric field-induced cell-to-cell fusion. Journal of Membrane Biology. 1982 December;67(1):165 – 182. 4

[35] Groth I, Jacob HE, Kunkel W, Berg H. Electrofusion of Penicillium protoplasts after dielectrophoresis. Journal of basic microbiology. 1987;27(6):341–344. 4

[36] Green NG, Morgan H. Dielectrophoretic separation of nano-particles. J Phys D. 1997;30:L41. 4

[37] Morgan H, Hughes MP, Green NG. Separation of Submicron Bioparticles by Dielectrophoresis. Biophys J. 1999 July;77(1):516–525. 4

[38] Green NG, Morgan H. Dielectrophoresis of submicron latex spheres. 1. Experimental results. J Phys Chem. 1999;103:41–50. 4

[39] Markx GH, Dyda PA, Pethig R. Dielectrophoretic separation of bacteria using a conductivity gradient. J Biotechnol. 1996;51:175–180. 4

[40] Suehiro J, Zhou G, Hara M. Fabrication of a carbon nano-tubes-based gas sensor using dielectrophoresis and its application for ammonia detection by impedance spectroscopy. J Phys D Applied Physics. 2003;36:109–114. 4, 6

[41] Burke P. Nanodielectrophoresis: Electronic Nanotweezers. Encyclopedia of Nanoscience and Nanotechnology. 2003;10:1–19. 5

[42] Huang Y, J Yang XW, Beckerand F, Gascoyne P. The removal of human breast cancer cells from hematopoietic CD34+ stem cells by DEP field flow fractionation. Journal of hematotherapy and stem cell research. 1999;8:481–490. 5

[43] Huang Y, Wang XB, Becker FF, Gascoyne PR. Introducing dielectrophoresis as a new force field for field-flow fractionation. Biophysical Journal. 1997;73:1118–1129. 5

[44] Berzyadin A, Dekker C, Schmid G. Electrostatic trapping of single conducting nanoparticles between nanoelectrodes. Appl Phys Lett. 1997;71:1273–1275. 5

[45] Yang J, Huang Y, Wang XB, Becker FF, Gascoyne PRC. Differential Analysis of Human Leukocytes by Dielectrophoretic Field-Flow-Fractionation. Biophys Journal. 2000 May;78(5):2680–2689. 5

[46] Gascoyne PRC, Vykoukal JV. Dielectrophoresis-Based Sample Handling in General-Purpose Programmable Diagnostic Instruments. Proceedings of the IEEE. 2004;92(1). 5

[47] Fuhr G, Schnelle T, Wagner B. Travelling wave-driven microfabricated electrohydrodynamic pumps for liquids. J Micromech Microeng. 1994;4:217–226. 5, 8

[48] Huang Y, Wang XB, Tame JA, Pethig R. Electrokinetic behaviour of colloidal particles in travelling electric fields: studies using yeast cells. J Phys D: Appl Phys. 1993;26:1528–1535. 5

[49] Wang XB, Huang Y, Becker FF, Gascoyne PRC. A unified theory of dielectrophoresis and travelling wave dielectrophoresis. J Phys D: Appl Phys. 1994;27:1571–1574. 5

[50] Jones TB, Washizu M. Multipolar dielectrophoretic and electrorotation theory. Journal of Electrostatics. 1996;37:121–134. 5

[51] Bakewell DJ, Ermolina I, Morgan H, Milner J, Feldman Y. Dielectric relaxation measurements of 12 kbp plasmid DNA. Biochimica et Biophysica Acta. 2000 September;1493:151–158. 5, 63

[52] Tegenfeldt JO, Prinz C, Cao H, Huang R, Austin R, Chou S, et al. Micro- and nanofluidics for DNA analysis. Anal Bioanal Chem. 2004;378:1678–1692. 5, 7

[53] Srivastava A, Metaxas A, So P, Matsudaira P, Ehrlich D, Georghiou G. Numerical Simulation Of DNA Sample Preconcentration In Microdevice Electrophoresis. Electrophoresis. 2005;26:1130–1143. 5

[54] Asbury C, van der Engh G. Trapping of DNA in Nonuniform Oscillating Electric Fields. Biophysical Journal. 1998;74:1024–1030. 5

[55] Asbury C, Dierks A, van der Engh G. Trapping of DNA by DEP. Electrophoresis. 2002;23:2658–2666. 5

[56] Moeller R, Fritzsche W. Chip-based electrical detection of DNA. IEE Proc Nanobiotechnol. 2005;152(1):47–51. 5, 62

[57] Mehrvar M, Abdi M. Recent Developments, Characteristics, and Potential Applications of Electrochemical Biosensors. Analytical Science. 2005;20:1113–1126. 5

[58] Tuukkanen S, Toppari JJ, Kuzyk A, Hirviniemi L, Hytonen VP, Ihalainen T, et al. Carbon Nanotubes as Electrodes for Dielectrophoresis of DNA. Nano Letters. 2006;6:1339–1343. 5

[59] Dimaki M, Bøggild P. Frequency dependence of the structure and electrical behaviour of carbon nanotube networks assembled by dielectrophoresis. Nanotechnology. 2005;16:759–763. 6

[60] Dimaki M, Boggild P. Single- and multiwalled carbon nanotubes and bundles assembled on microelectrodes. Journal of Nanoengineering and Nanosystems. 2005;219:1–7. 6

[61] Lin H, Tsai L, Chi P, Chen C. Positioning of extended individual DNA molecules on electrodes by non-uniform AC electric fields. Nanotechnology. 2005;16(11):2738–2742. 6

[62] Zheng L, Li S, Burke PJ. Manipulating nanoparticles in solution with electrically contacted nanotubes using dielectrophoresis. Langmuir. 2004;20:8612–8619. 6

[63] Zheng L, Burke PJ, Brody JP. Electronic manipulation of DNA and proteins for potential nano-bio circuit assembly. Microarrays and Combinatorial Techniques: Design, Fabrication, and Analysis II, Proceedings of the SPIE. 2004;5331:126–135. 6

[64] Wong PK, Wang T, Deval JH, Ho C. Electrokinetics in Micro Devices for Biotechnology Applications. IEEE/ASME Trans Mechatronics. 2004;9(2):366–376. 6

[65] Asokan S, Jawerth L, Carroll R, Cheney R, Washburn S, Superfine R. Two-Dimensional Manipulation and Orientation of Ac-tin-Myosin Systems with DEP. Nano Letters. 2003;3(4):431–437. 6

[66] Becker FF, Wang X, Huang Y, Pethig R, Vykoukal J, R P C Gascoyne PRC. Separation of human breast cancer cells from blood by differential dielectric affinity. Proc Natl Acad Sci. 1995;92:860–864. 6

[67] Bakewell D, Morgan H. Measuring the frequency dependent polarizability of colloidal particles from DEP collection data. IEEE Transactions on Dielectrics and Electrical Insulation. 2001;8(3):56–571. 6

[68] Drummond T, Hill M, Barton J. Electrochemical DNA sensors. Nature Biotechnology. 2003;21:1192–1199. 6

[69] Gao H, Kong Y, Cui D. Spontaneous Insertion of DNA Oligonucleotides into Carbon Nanotubes. Nano Letters. 2003;3:471–473. 6

[70] Gao H, Kong Y. Simulation of DNA-carbon nanotube interactions. Annu Rev Mater Res. 2004;34:123–150. 6

[71] Guiducci C, Stagni C, Zuccheri G, andv L Benini AB, Samori B, Riccò B. DNA detection by integrable electronics. Biosensors and Bioelectronics. 2004;19:781–787. 6

[72] Fritz J, Cooper EB, Gaudet S, Sorger PK, , Manalis SR. Electronic detection of DNA by its intrinsic molecular charge. Proceedings of the National Academy of Sciences. 2002;99:14142–14146. 6

[73] Muller T, Gerardino AM, Schelle T, Shirley SG, Bordoni F, Gasperis GD, et al. Trapping of micrometre and sub-micrometre particles by high-frequency electric fields and hydrodynamic forces. J Phys D. 1996;29:340–350. 6

[74] Ho C. Fluidics- The Link Between Micro And Nano Sciences And Technologies. MEMs 2001 conference keynote presentation. 2001;. 6

[75] Kuzyk A. Dielectrophoresis of nanoscale dsDNA and its electrical conductivity. University Of Jyväaskylä Department of Physics; 2005. 6

[76] Ramos A, Morgan H, Green NG, Castellanos A. AC Electric-Field-Induced Fluid Flow in Microelectrodes. Journal of Colloid and Interface Science. 1999 September;217(2):420–422. 6, 21, 22, 30

[77] Ajdari A. Pumping liquids using asymmetric electrode arrays. Physical Review E. 2000 January;61(1):R45–R48. 6, 30

[78] Zhou H, Lee W, Robert T. Lateral separation of colloids or cells by dielectrophoresis augmented by AC electroosmosis. Journal of colloid and interface science. 2005;285(1):179–191. 6, 53

[79] Islam N, Lian M, Wu J. Enhancing microcantilever capability with integrated AC electroosmotic trapping. Microfluidics and Nanofluidics. 2006 November;3(3):369–375. 6

[80] Wu J. Biased AC electro-osmosis for on-chip bioparticle processing. IEEE Transactions on Nanotechnology,. 2006 March;5(2):84 – 89. 6, 30

[81] Garcia-Sanchez P, Ramos A, Green N, Morgan H. Experiments on AC electrokinetic pumping of liquids using arrays of microelectrodes. Dielectrics and Electrical Insulation, IEEE Transactions on. 2006 June;13(3):670– 677. 6, 30, 31

[82] Loucaides N, Ramos A, Georghiou GE. Novel systems for configurable AC electroosmotic pumping. Microfluidics and Nanofluidics. 2007 December;3(6):709–714. 6, 31, 53, 57, 70

[83] Huang SH, Hsueh HJ, Hung KY. Configurable AC electroosmotic generated in-plane microvortices and pumping flow in microchannels. Microfluidics and Nanofluidics;Online first. 6

[84] Studer V, Pépin A, Chen Y, Ajdari A. An integrated AC electrokinetic pump in a microfluidic loop for fast and tunable flow control. The Analyst. 2004;129,:944–949. 6, 30, 31

[85] Brown ABD, Smith CG, Rennie AR. Pumping of water with ac electric fields applied to asymmetric pairs of microelectrodes. Phys Rev E. 2001 January;63:016305. 6, 30, 33

[86] Melcher JR. Continuum Electromechanics. Cambridge, MA: The MIT Press; 1981. 7

[87] Lian M, Wu J. Microfluidic flow reversal at low frequency by AC electrothermal effect. Microfluidics and Nanofluidics;. 7

[88] Castellanos A, Ramos A, Gonzales A, Green N, Morgan H. Electrohydrodynamics and dielectrophoresis in microsystems: scaling laws. J Phys D: Appl Phys. 2003;36:2584–2597. 7

[89] Gonzalez A, Ramos A, Morgan H, Green N, Castellanos A. Electrothermal flows generated by alternating and rotating electric fields in microsystems. Journal of Fluid Mechanics. 2006;564:415–433. 7

[90] Ramos A, Morgan H, Green NG, Castellanos A. AC electrokinetics: a review of forces in microelectrode structures. J Phys D. 1998;31:2338–2353. 7, 30, 38, 42, 43

[91] Toner M, Irimia D. Blood-on-Chip. Annual Review of Biomedical Engineering. 2005 August;7:77–103. 7

[92] A computer-aided analysis of dielectrophoretic force calculations. Fifth International Conference on Dielectric Materials, Measurements and Applications; 1988. 7

[93] Kadaksham J. Direct numerical simulations and experimental investigation of dielectrophoresis. New Jersey Institute of Technology; 2005. 7

[94] Kadaksham J, Singh P, Aubry N. Dielectrophoresis of nano particles. Electrophoresis. 2004;25:3625–3632. 7

[95] Gascoyne PRC, Becker FF, Wang XB. Numerical analysis of the influence of experimental conditions on the accuracy of dielectric parameters derived from electrorotation measurements. Bioelectrochemistry and Bioenergetics. 1995 March;36(11):115–125. 7

[96] Oh J, Hart R, Capurro J, Noh HM. Comprehensive analysis of particle motion under non-uniform AC electric fields in a microchannel. Lab Chip. 2009;9:62 – 78. 7

[97] Song CX, Liu G, Li H, Han X. Simulation of an extruded quadrupolar dielectrophoretic trap using meshfree approach. Engineering Analysis with Boundary Elements. 2006;30:994–1005. 7

[98] Hughes MP. Numerical simulation of dielectrophoretic ratchet structures. J Phys D: Appl Phys. 2004;37:1275–1280. 7

[99] Salonen E, Terama E, Vattulainen, Karttunen M. Dielectrophoresis of nanocolloids: A molecular dynamics study. The European Physical Journal E: Soft Matter and Biological Physics;Online. 7

[100] Lian M, Islam N, Wu J. AC electrothermal manipulation of conductive fluids and particles for lab-chip applications. IET Nanobiotechnology. 2007;1(3):36–43. 7

[101] Sigurdson M, Wang D, Meinhart C. Electrothermal Stirring for Heterogeneous Immunoassays. Lab on a Chip. 2005;5:1366 – 1373. 7, 43, 44, 47, 49, 50, 60

[102] Perch-Nielsen IR, Green NG, Wolff A. Numerical simulation of travelling wave induced electrothermal fluid flows. Journal Of Physics D: Applied Physics. 2004;37:2323–2330. 7

[103] Yang CK, Chang JS, Chao SD, , Wu KC. Two dimensional simulation on immunoassay for a biosensor with applying electrothermal effect. Appl Phys Lett. 2007;91:113904. 7

[104] Wood JA, Zhang B, Tomkins MR, Docoslis A. Numerical investigation of AC electrokinetic virus trapping inside high ionic strength media. Microfluidics and Nanofluidics Online first;. 7, 53

[105] Green NG, Ramos A, González A, Morgan H, Castellanos A. Fluid flow induced by nonuniform ac electric fields in electrolytes on microelectrodes. I. Experimental measurements. Phys Rev E. 2000 April;61(4):4011–4018. 8, 70

[106] González A, Ramos A, Green NG, Castellanos A, Morgan H. Fluid flow induced by non uniform ac electric fields in electrolytes on microelectrodes. II. A linear double-layer analysis. Phys Rev E. 2000 April;61(4):4019–4028. 8, 70

[107] Lian M, Islam N, Wu J. Particle Line Assembly/Patterning by Microfluidic AC Electroosmosis. J Phys: Conf Ser. 2006;34:589–594. 8

[108] Islam N, Wu J. Microfluidic transport by AC electroosmosis. J Phys: Conf Ser. 2006;34:356–361. 8

[109] Yang H, Jiang H, Ramos A, García-Sánchez P. AC electrokinetic pumping on symmetric electrode arrays. Microfluidics and Nanofluidics;Online first. 8

[110] Lastochkin D, Zhou R, Wang P, Ben Y, Chang H. Electrokinetic micropump and micromixer design based on ac faradaic polarization. Journal of Applied Physics. 2004 August;96(3):1730–1733. 8, 30

[111] Urbanski JP, Thorsen T, Levitan JA, Bazant MZ. Fast AC electroosmotic micropumps with non-planar electrodes. Applied Physics Letters. 2006 October;89:143508. 8, 30

[112] Bazant MZ, Ben Y. Theoretical prediction of fast 3D AC electroosmotic pumps. Lab on a Chip. 2006;6:1455 – 1461. 8, 30

[113] Olesen LH, Bruus H, Ajdari A. AC electrokinetic micropumps: the effect of geometrical confinement, Faradaic current injection, and nonlinear surface capacitance. Phys Rev E. 2006;73(5):056313. 8, 31

[114] Soni G, Squires TM, Meinhart CD. Simulation of Highly Nonlinear Electrokinetics Using a Weak Formulation. In: Proceedings of the COMSOL Conference 2008 Boston; 2008. . 8

[115] Ramos A, Morgan H, Green NG, González A, Castellanos A. Pumping of liquids with traveling-wave electroosmosis. Journal of Applied Physics. 2005 April;97:084906. 8, 30

[116] Kilic MS, Bazant MZ, Ajdari A. Steric effects in the dynamics of electrolytes at large applied voltages. I. Double-layer charging. Phys Rev E. 2007;75:021502. 8

[117] Kilic MS, Bazant MZ, Ajdari A. Steric effects in the dynamics of electrolytes at large applied voltages: II. Modified Nernst-Planck equations. Phys Rev E. 2007;75:021503. 8

[118] Garcia-Sanchez P, Ramos A. Flow Reversal in Traveling-Wave Electrokinetics: an Analysis of Forces due to Ionic Concentration Gradients. Langmuir. 2009,;25(9):4988–4997. 8

[119] Green NG, Ramos A, Morgan H. AC electrokinetics: a survey of sub-micrometre particle dynamics. J Phys D: Appl Phys. 2000;33:632–641. 8

[120] Green N. Particle movement in microelectrode structures in AC electric fields, under the influence of dielectrophoresis and electrohydrodynamics. Nanotech conference. 2003;1:63 – 66. 8

[121] Green NG, Ramos A, Morgan H. Numerical solution of the dielectrophoretic and travelling wave forces for interdigitated electrode arrays using the finite element method. Journal of Electrostatics. 2002;56:235–254. 8

[122] Hughes MP. Nanoelectromechanics in Engineering and Biology. CRC Press; 2003. 8, 11, 12, 14

[123] Morgan H, Holmes D, Green NG. 3D focusing of nanoparticles in microfluidic channels. Nanobiotechnology, IEE Proceedings. 2003;150(2):76 – 81. 8

[124] Kumar A, Qiu Z, Acrivos A, Khusid B, Jacqmin D. Combined negative dielectrophoresis and phase separation in non-dilute suspensions subject to a high-gradient ac electric field. Phys Rev E. 2004 August;69:021402. 8, 58, 70, 78

[125] Nicotra OE, Magna AL, Coffa S. A mean field approach to many-particles effects in dielectrophoresis. Appl Phys Lett. 2008;93:193902. 8, 70

[126] Petrone G, Cammarata G. Recent advances in modelling and simulation. Petrone G, Cammarata G, editors. I-Tech Education and Publishing; 2008. 8

[127] Loucaides N, Georghiou GE, Charalambous CD. Manipulation of nanoparticles by electronic methods: Model development and control problem formulation. The 3rd International Symposium on Nanomanufacturing. 2005 November;1:69–73. 16, 58, 62, 64, 70

[128] Risken H. The Fokker-Planck Equation. Springer; 1989. 16, 64, 70

[129] Bockris J, Reddy A. Modern Electrochemistry: An Introduction to an Interdisciplinary Area. 1st ed. Springer; 1973. 20, 21

[130] Bown MR, Meinhart CD. AC electroosmotic flow in a DNA concentrator. Microfluidics and Nanofluidics Journal. 2006 November;2(6):513–523. 30, 36

[131] Cahill BP, Heyderman L, Gobrecht J, Stemmer A. Electro-osmotic streaming on application of traveling-wave electric fields. Physical Review E. 2004;70:036305. 30

[132] Wu J, Ben Y, Chang H. Particle detection by electrical impedance spectroscopy with asymmetric polarization AC electroosmotic trapping. Journal of Microfluidics and Nanofluidics. 2005 April;1(2):161–167. 30, 49

[133] Gitlin I, Stroock AD, Whitesides GM, Ajdari A. Pumping based on transverse electrokinetic effects. Applied Physics Letters. 2003 August;83(7):1486–1488. 37

[134] Loucaides N, Georghiou GE, Kyprianou A, Charalambous CD, Doumanides C. Combined AC electroosmotic and Electrothermal stirring for biosensor enhancement. In: The 4th International Symposium on Nanomanufacturing; 2006. . 44

[135] Myszka DG, He X, Dembo M, Morton TA, Goldstein B. Extending the Range of Rate Constants Available from BIACORE-Interpreting Mass Transport-Influenced Binding Data. Biophys J. 1998 August;75(2):583–594. 46

[136] Tuval I, Mezic I, Bottausci F, Zhang Y, MacDonald N, Piro O. Control of Particles in Microelectrode Devices. Phys Rev Lett. 2005;95:236002. 52

[137] Skytte T, Skafte-Pedersen P, Pedersen M. Particle manipulation in microfluidics by AC electroosmosis and dielectrophoresis; 2006. 52, 55

[138] Hoettges KF, Hughes MP, Cotton A, Hopkins NAE, McDonnell MB. Optimizing particle collection for enhanced surface-based biosensors. Engineering in Medicine and Biology Magazine, IEEE. 2003 December;22(6):68 – 74. 53

[139] Docoslis A, Espinoza LAT, Zhang B, Cheng L, Israel BA, Alexandridis P, et al. Using Nonuniform Electric Fields To Accelerate the Transport of Viruses to Surfaces from Media of Physiological Ionic Strength. Langmuir. 2007;23(7):3840 – 3848. 53

[140] Loucaides N, Ramos A, Georghiou GE. Trapping and manipulation of nanoparticles by using jointly dielectrophoresis and AC electroosmosis. J Phys: Conf Ser. 2008;100:052015–052020. 53

[141] Bakewell D, Morgan H. Quantifying DEP collections of sub-micron particles on microelectrodes. Meas Sci Technol. 2004;15:254–266. 62, 63, 65

[142] Morgan H, Green N. AC Electrokinetics: Colloids and Nanoparticles. Pethig R, editor. Microtechnologies Microsystems. Research Studies Press; 2003. 62

[143] Stellwagen E, Stellwagen NC. Determining the electrophoretic mobility and translational diffusion coefficients of DNA molecules in free solution. Electrophoresis. 2002;23:2794–2803. 63, 64

[144] Loucaides N, Georghiou GE, Charalambous CD. Numerical simulation of the Dielectrophoretic concentration of DNA and the effect of AC electroosmosis. J Phys: Conf Ser. 2007 May;61:718–723. 63, 70, 95

[145] Loucaides N, Ramos A, Georghiou GE, Doumanides C. Simulation of the concentration of DNA under Dielectrophoresis taking into account steric effects. In: Electronic Proceedings. The 5th International Symposium on Nanomanufacturing; 2008. . 70

[146] Loucaides NG, Ramos A, Georghiou GE. Micro- and Nano-particle manipulation by Dielectrophoresis: Devices for particle trapping and the influence of steric effects. Physica Status Solidi (c). 2008;5(12):3794 – 3797. 71

[147] Russel WB, Saville DA, Schowalter WR. Colloidal Dispersions. Cambridge University Press; 1992. 71

[148] Takahashi T, Kaga K, Akahane Y, Yamashita T, Miyakawa Y, Mayumi M. Isolation of dane particles containing a dna strand by metrizamide density gradient. J Med Microbiol. 1980;13:163–166. 96

Appendix A

Formulation of the weak form

In order to solve

$$\nabla^2 u = -\frac{\rho}{\epsilon} = 0 \tag{A.1}$$

with the boundary condition

$$\sigma \nabla u_{ep}.\vec{n} \quad = \quad \frac{u_{ep} - V_{applied}}{Z_{DL}} \tag{A.2}$$

the following transformation to the Comsol^{TM}Weak form is required.

$$\nabla^2 u = -\frac{\rho}{\epsilon} = 0 \Rightarrow \int \nu.\nabla.\nabla u dA = \int \nu.0 dA \Rightarrow \int \nu.\nabla u.\vec{n} ds - \int \nabla \nu.\nabla u dA = 0 \tag{A.3}$$

where $\vec{n}$ the normal vector to the surface and ν a test function. In equation A.3 the integral under ds gives the boundary term and the integral under dA gives the domain term. Therefore the domain term under a test function $\nu = u_{test}$ becomes $-(ux_{test} * ux + uy_{test} * uy)$. The boundary term becomes $u_{test}.(ux * \vec{x} + uy * \vec{y}).\vec{n}$

For a problem given by

$$\nabla^2\phi = F \tag{A.4}$$

with boundary conditions $\phi = k$ and $\vec{n}.\nabla\phi = G + \frac{\partial R}{\partial u}.\mu$ the weak formulation is

$$0 = \int (\nabla\nu.\nabla\phi + \nu.F)dA + \int \nu(G + \frac{\partial R}{\partial u}.\mu)ds \tag{A.5}$$

with the term under dA being the domain term, the term under ds the boundary term and $k = \phi$ as a constraint on the boundary. As derived from above, the homogeneous Neumann condition $\vec{n}.\nabla\phi = 0$ need not be actively imposed in the weak form of Galerkin-type residual minimisation methods (which is why it is called a natural boundary condition for the finite element method).

Appendix B

Publications from this thesis

[1] Loucaides N, Georghiou GE, Charalambous CD. Manipulation of nanoparticles by electronic methods: Model development and control problem formulation. The 3rd International Symposium on Nanomanufacturing. 2005 November;1:69-73.

[2] Loucaides N, Georghiou GE, Charalambous CD. Numerical simulation of the Dielectrophoretic concentration of DNA and the effect of AC electroosmosis. J Phys: Conf Ser. 2007 May;61:718-723.

[3] Loucaides N, Ramos A, Georghiou GE. Novel systems for configurable AC electroosmotic pumping. Microfluidics and Nanofluidics. 2007 December;3(6):709-714.

[4] Loucaides N, Georghiou GE, Kyprianou A, Charalambous CD, Doumanides C. Combined AC electroosmotic and Electrothermal stirring for biosensor enhancement. In: The 4th International Symposium on Nanomanufacturing; 2006.

[5] Loucaides N, Ramos A, Georghiou GE. Trapping and manipulation of nanoparticles by using jointly dielectrophoresis and AC electroosmosis. J Phys: Conf Ser. 2008;100:052015-052020.

[6] Loucaides N, Ramos A, Georghiou GE, Doumanides C. Simulation of the concentration of DNA under Dielectrophoresis taking into account steric effects. The 5th International Symposium on Nanomanufacturing; 2008. Electronic Proceedings.

[7] Loucaides NG, Ramos A, Georghiou GE. Micro- and Nano-particle manipulation by Dielectrophoresis: Devices for particle trapping and the influence of steric effects. Physica Status Solidi. 2008;5(12):3794-3797.